UNCERTAINTY ANALYSIS OF
COORDINATE MEASURING MACHINE (CMM) MEASUREMENTS

A THESIS SUBMITTED TO
THE GRADUATE SCHOOL OF NATURAL AND APPLIED SCIENCES
OF
MIDDLE EAST TECHNICAL UNIVERSITY

BY

AHMET SÖZAK

IN PARTIAL FULFILLMENT OF THE REQUIREMENTS
FOR
THE DEGREEE OF MASTER OF SCIENCE
IN
MECHANICAL ENGINEERING

SEPTEMBER 2007

Approval of the Thesis

"UNCERTAINTY ANALYSIS OF
COORDINATE MEASURING MACHINE (CMM) MEASUREMENTS"

Submitted by **AHMET SÖZAK** in partial fulfilment of the requirements for the degree of **Master of Science in Mechanical Engineering** by,

Prof. Dr. Canan Özgen

Dean, Graduate School of **Natural and Applied Sciences**   _____

Prof. Dr. Kemal İder

Head of Department, **Mechanical Engineering**   _____

Asst. Prof. Dr. İlhan Konukseven

Supervisor, **Mechanical Engineering, METU**   _____

Asst. Prof. Dr. Melik Dölen

Co - Supervisor, **Mechanical Engineering, METU**   _____

Examining Committee Members

Prof. Dr. Metin Akkök (*)
Mechanical Engineering, METU   _____

Asst. Prof. Dr. İlhan Konukseven (**)
Mechanical Engineering, METU   _____

Asst. Prof. Dr. Melik Dölen
Mechanical Engineering, METU   _____

Asst. Prof. Dr. Buğra Koku
Mechanical Engineering, METU   _____

Tolga Ziya Sander (M.S.)
MGEO, ASELSAN   _____

Date: 05.09.2007

(*)   Head of Examining Committee
(**)   Supervisor

I hereby declare that all information in this document has been obtained and presented in accordance with academic rules and ethical conduct. I also declare that, as required by these rules and conduct, I have fully cited and referenced all material and results that are not original to this work.

Name, Last name : Ahmet SÖZAK

Signature   :

ABSTRACT

UNCERTAINTY ANALYSIS OF COORDINATE MEASURING MACHINE (CMM) MEASUREMENTS

Sözak, Ahmet

M.S., Department of Mechanical Engineering

Supervisor: Asst. Prof. Dr. İlhan Konukseven

Co-Supervisor: Asst. Prof. Dr. Melik Dölen

September 2007, 156 pages

In this thesis, the measurement uncertainty of Coordinate Measuring Machine (CMM) is analysed and software is designed to simulate this. Analysis begins with the inspection of the measurement process and structure of the CMMs. After that, error sources are defined with respect to their effects on the measurement and then an error model is constructed to compensate these effects. In other words, systematic part of geometric, kinematic and thermal errors are compensated with error modelling. Kinematic and geometric error model is specific for the structure of CMM under inspection. Also, a common orthogonal kinematic model is formed and with using the laser error data of the CMM and error maps of the machine volume is obtained. Afterwards, the models are compared with each other by taking the difference and ratio.

The definition and compensation of the systematic errors leave the uncertainty of measurements for analysing. Measurement uncertainty consists of the uncompensated systematic errors and random errors. The other aim of the thesis is to quantify these uncertainties with using the different methods and to inspect the success of these methods. Uncertainty budgeting, comparison, statistical evaluation by designing an experiments and simulation methods are examined and applied to the CMM under inspection. In addition, Virtual CMM software is designed to

simulate the task specific measurement uncertainty of circle, sphere and plane without using the repeated measurements.

Finally, the performance of the software, highly depending on the mathematical modelling of machine volume, is tested by using actual measurements.

Keywords: Precision Engineering, Dimensional Measurement Uncertainty, Coordinate Measuring Machine, Kinematic and Geometric Error Modelling, Simulation.

ÖZ

KOORDİNAT ÖLÇME CİHAZI İLE YAPILAN ÖLÇÜMLERİN BELİRSİZLİK ANALİZİ

Sözak, Ahmet

Y.Lisans, Makina Mühendisliği Bölümü

Tez Yöneticisi: Y.Doç. Dr. İlhan Konukseven

Ortak Tez Yöneticisi: Y.Doç.Dr. Melik Dölen

Eylül 2007, 156 sayfa

Bu tezde, koordinat ölçme cihazlarında yapılan ölçümlerin belirsizlikleri analiz edilmiş ve bu belirsizliklerin benzetimine imkan veren bir simulasyon yazılımı tasarlanmıştır. Söz konusu analize cihazın ölçüm işleminin ve yapısının incelenmesi ile başlanmıştır Sonrasında ölçümü etkileyecek hata kaynakları tespit edilmiş, sistematik hataların bir bölümü modellenmiş ve ayrılmıştır. Bu sayede ölçüm belirsizliği sistematik olan kinematik, geometrik ve ısıl hatalardan ayrılmış olmuştur. Uygulanan kinematik ve geometrik hata modeli cihazın yapısına bağlıdır. Ayrıca cihazın yapısına bağlı olmayan ortak bir model oluşturulmuş ve modelde lazer hata verileri kullanılarak makina hacminin hata haritası çıkarılmıştır. Sonrasında ise oluşturulan iki model, sonuçların farkına ve oranına bakılarak karşılaştırılmıştır.

Tanımlanan sistematik hataların telafi edilmesi analiz için geriye ölçüm belirsizliğini bırakmıştır. Ölçüm belirsizliği telafi edilemeyen sistematik ve rasgele hatalardan kaynaklanmaktadır. Bu tezin diğer bir amacıda bahsedilen belirsizliğin farklı yöntemler kullanılarak miktarlanması ve bu yöntemlerin başarısının incelenmesidir. Bu kapsamda belirsizlik bütçeleme, karşılaştırma, deney tasarlanarak istatistik ile değerlendirme ve benzeşim yöntemleri

incelenmiş ve mevcut bir cihaza uygulanmıştır. Bununla birlikte, tekrarlanan ölçümler gerektirmeden daire, düzlem ve küre ölçümleri gibi işe özel ölçüm belirsizliklerini benzeştirmek için sanal koordinat ölçme cihazı yazılımı tasarlamıştır. Son olarak performansı cihazın matematiksel modellemesi bağlı olarak değişen bu yazılım gerçek ölçümler ile karşılaştırılarak test edilmiştir.

Anahtar Kelimeler: Doğruluk Mühendisliği, Boyutsal Ölçüm Belirsizliği, Koordinat Ölçme Cihazı, Kinematik ve Geometrik Hata Modellemesi, Simülasyon

ACKNOWLEDGEMENTS

I would like to express my sincere gratitude to my supervisor Asst. Prof. Dr. İlhan Konukseven and co-supervisor Asst. Prof. Dr. Melik Dölen for their supervisions, guidance and encouragements throughout this study.

I would like to also express my thanks to my friends and my colleagues for their precious support and fellowship.

Finally, I would like to thank my family for their love, support and patience over the years. This thesis is dedicated to them.

TABLE OF CONTENTS

LIST OF FIGURES

LIST OF TABLES

CHAPTER 1

INTRODUCTION

Coordinate measuring machines, (CMMs) are the most advanced dimensional measuring instruments on the market today. Therefore, measurement process of CMMs is significant and essential part for production control in modern manufacturing because they are used to measure three dimensional sizes, positions and forms of the machined parts. The CMMs are indispensable instruments especially in the automobile industry for developing new automobiles, evaluation of mechanical parts and molds. Actually, their unlimited versatility allows them to be used for an infinite number of measurements. However, the flexibility of CMM's can also make them difficult to implement. The big question is how the measurement uncertainty of CMM's can be estimated. Measurement uncertainty was a relatively obscure term only a few years ago. Now, it becomes very important, with increased attention coming from various quality standards.

The uncertainty of measurement made on complex instruments like CMM's is a difficult task, because there are many uncertainty contributors. Consequently, it is not possible to cover all of the details, and cover every single contribution. Indeed, fully understanding the measurement process is required to determine all the contributors that will influence the measured results. Therefore, CMMs have been widely investigated by researchers and different methods have been created in order to analysis the measurement uncertainty. The methods of mathematical modelling (simulation), comparison and performance tests are applied to determination of measurement uncertainty.

The method of mathematical modelling involves the calibration of CMM geometric errors to build a theoretical model and predict the uncertainty for any measurement done according to the model's assumptions. A comparison method involves the inspection of a calibrated artifact identical to the piece under

measurement and the measurement uncertainty statement has a specific application. Performance tests designate artifacts and a criterion to determine the measurement errors. A two-point length measurement uncertainty may be established as a performance parameter [1].

Performance tests are largely applied for the inspection of parts and in the purchasing selection of a suitable CMM. According to known standards, gauges like a ring, a length bar, a step gauge, and a ball plate have been used to determine the volumetric errors, inspect hardware and estimate the CMM measurement uncertainty. The best known standards are the American ANSI/ASME B89.4.1 [2], the German VDI/VDE 2617 [3], the British BS 6808 [4], the Japanese JIS B7440 [5], the ISO10360 [6], and the manufacturers association CMMA [7].

These performance test methods recommend different test methodologies and distinct ways of determining a performance parameter. Some standards indicate the maximum range of measured lengths as the performance parameter, and others establish the standard deviation of results. The measurement uncertainty may be established using information acquired by performance tests and may be carried out by $A + B/L$-type statement, describing uncertainty of a two-point measurement. Other methodologies were developed to estimate task-specific uncertainties according to the ISO Guide to the Expression of Uncertainty in Measurement [8] and to an established inspection plan [9,10,11].

Numerous studies about the development of coordinate measuring uncertainty have been conducted in the past. These studies mainly concentrated on the accuracy improvement by developing hardware, software, and operating strategies. The issues of acquisition and computational correction of the equipment specific deviation behaviour of a CMM have been examined. In addition, the study of the error compensation issue of a CMM has been reported in many papers.

The purpose of thesis is to analyse the measurement uncertainty of CMMs which means determining the uncertainty sources, estimating and quantifying the measurement uncertainty of CMM with using the different techniques. In addition, to attain this goal, error sources of CMM shall be designated and required compensation of these errors must be done by modelling the entire machine volume. Therefore, the error modelling of CMM under inspection is another aim of the thesis. Analysis of measurement uncertainty by using different methods naturally leads to a

review of various national and international standards regarding CMM performance evaluation. Afterwards, the advantages and disadvantages of these methods can be evaluated absolutely. Finally, a simulation software, known as Virtual CMM, is designed for analysing the uncertainty of task specific measurements on CMM. This software is an application of simulation method and mimics the real measurements. The advantages of Virtual CMM are eliminating the time wasting with repeated measurements and providing successful solution including thermal effects for different type of CMMs.

CHAPTER 2

EXPLANATION OF MEASUREMENT UNCERTAINTY AND PROCESS

In this chapter, some definitions in "Guidance to Expression of Uncertainty in Measurement" (GUM) [8] will be explained.

2.1. Measurement Error and Uncertainty

The difference between *measurement error* and *measurement uncertainty* shall be explained clearly to evaluate the measurement results correctly. The term measurement error means the difference between the "true value" and the value found by a measurement (measurand). According to the GUM, measurement errors are distinguished as random and systematic errors [8]. Figure 1 indicates the difference between the measurement uncertainty and error, clearly.
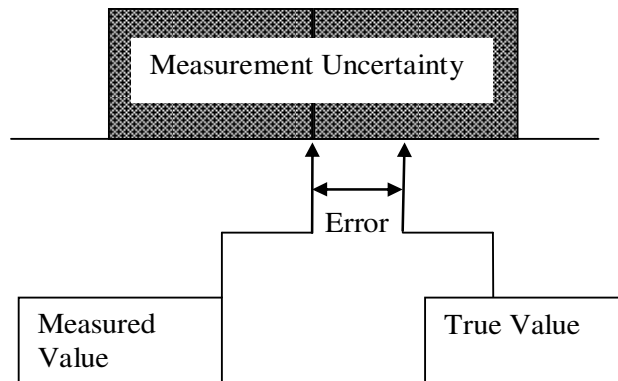
Figure 1: Measurement Error and Measurement Uncertainty

2.1.1. Random Error

Random error in measurement typically arises from unpredictable variations of influence quantities. These random effects under apparently equal condition at a given position give rise to variations in repeated observations of the measurand. Although it is not possible to compensate for the random error of a measurement result, it can usually be reduced by increasing the number of observations and only be expressed statistically.

2.1.2. Systematic Error

Systematic error, like random error, can not be eliminated but it can be reduced. If a systematic error arises from a recognized effect of an influence quantity on a measurement result, hereafter termed a *systematic effect*, the effect can be quantified and *a correction* or *correction factor* can be applied to compensate for the effect. Recognized systematic errors can generally be correlated with position along an axis. If the relative accompanying random error is small enough, systematic error can be corrected .

Systematic errors can often be compensated to a certain degree using calibration techniques. Random errors cannot be compensated for without real time measurement and feedback into correction loop. Thus when evaluating the error budget for a machine two distinct sub-budgets based on systematic and random errors should be kept.

2.1.3. Measurement Uncertainty

The lack of exact knowledge of the value of the measurand explains the uncertainty of the result of a measurement. The result of a measurement after correction for recognized systematic effects is still only an estimate of the measurand's value due to the uncertainty arising from random effects and from imperfect correction of the result for systematic effects.

In general, there are many sources of uncertainty in a measurement and details can be seen in GUM. Uncertainty components in two categories are based on their

methods of evaluation, Type A and B. The uncertainty of a correction for a known systematic effect may be obtained in some cases by Type A evaluation while in other cases by a Type B evaluation. Type A standard uncertainty is obtained from a probability density function derived from an observed frequency distribution. Figure 2 illustrates a typical type A distribution.
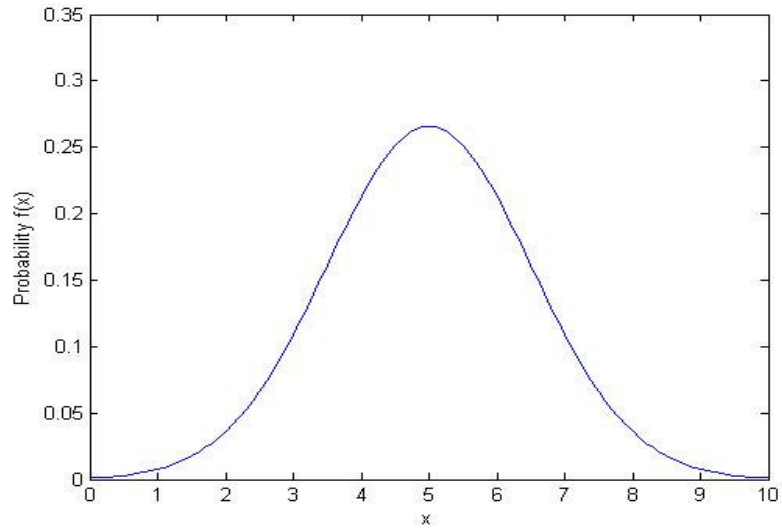
Figure 2: Type A Uncertainty

$$f(x) = \frac{1}{\sigma\sqrt{2\pi}} \times \exp(\frac{-z^2}{2}) \tag{2.1}$$

$$z = \frac{x - \mu}{\sigma} \tag{2.2}$$

$$\sigma = \sqrt{\frac{1}{n-1}\sum_{i=1}^{N}(x_i - \mu)} \tag{2.3}$$

$$u(x) = \frac{\sigma}{\sqrt{n}} \tag{2.4}$$

where

$\mu =$ Mean of Repeated Measurements

$n =$ Number of Repeated Measurements

$\sigma =$ Standard Deviation

$u =$ Uncertainty

Type B standard uncertainty is obtained from an assumed probability density function based on degree of belief that an event will occur or calibration certificates. Figure 3 indicates a rectangular distribution of Type B uncertainty.
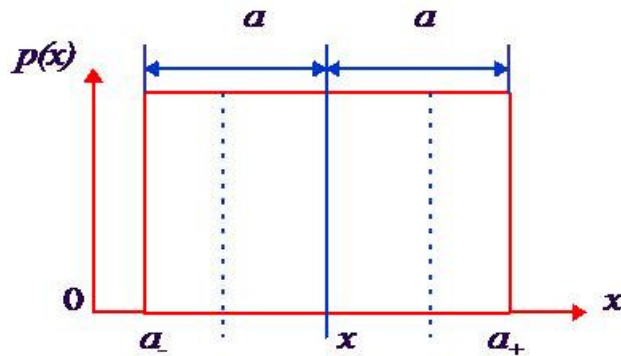
Figure 3: Type B Uncertainty (Rectangular Distribution)

$$u(x) = \frac{a_+ - a_-}{2\sqrt{3}}, \qquad u(x) = \frac{a}{\sqrt{3}} \tag{2.5}$$

For most measurements typically performed by CMMs, the true value, and hence the measurement error, is unknown. To overcome this difficulty in the special case of a CMM performance evaluation, well-calibrated dimensional artifacts are used, *e.g. ring gauge, length and ball bars*. The uncertainty of the calibrated artifact shall be sufficiently small that the calibrated value may be considered as the true value. The calibration of artifacts has to be done with more precise machines than CMM. Many national and international standards impose a constraint on the uncertainty of artifacts used in CMM evaluations, permitting the uncertainty of the artifact calibration to be ignored. Hence the difference between the CMM measurement and the calibrated value can be considered as the measurement error.

John A. Bosch describes the *measurement uncertainty* as the collection of (all possible) measurement errors [1]. **The measurement uncertainty is positioned**

about the measured value and **is usually centered symmetrically** (as shown in Figure 1).

The uncertainty of a measurement includes all factors which influence its result. The estimation of the magnitude of the uncertainty sources and their affect on the measurement result is required for this task.

This process may utilize many sources of information including analysis of

- *repeated measurements,*
- *data provided in calibration reports,*
- *uncertainties assigned to reference data taken from handbooks,*
- *manufacturer's specifications*
- *environmental condition*
- *machine structure*
- *general knowledge of behavior and property of relevant materials and instruments* [8].

The uncertainty sources mentioned just above are common for all machines. The sources special for CMMs will be explained later in detail.

2.1.3.1.Combined Standard Uncertainty

The combined standard uncertainty, denoted by u_c can be thought of as representing one standard deviation of the measurement uncertainty resulting from combining all known sources of uncertainties in a root sum of squares (RSS) manner. GUM method is the quantification of all uncertainty sources by assigning them a variance, the square root of which is the standard deviation of that uncertainty source. This is denoted by $u(x_i)$ where the quantity x_i is the i th source of uncertainty.

$$Y = f(X_1, X_2, ... X_N) \tag{2.6}$$

$$u^2{}_c = \sum_{i=1}^{N} (\frac{\partial f}{\partial x_i})^2 \times u^2(x_i) + 2\sum_{i=1}^{N-1} \sum_{j=i+1}^{N} \frac{\partial f}{\partial x_i} \frac{\partial f}{\partial x_j} u(x_i, x_j) \tag{2.7}$$

The quantity $u(x_i, x_j)$ is the covariance of x_i and x_j .It is a measure of the correlation between these two uncertainty sources.

The classification of uncertainty into categories A and B is based on the method of assessing the uncertainty source and not on whether the source is "random" or "systematic."

2.1.3.2. Expanded Uncertainty and Confidence Intervals

According to the GUM [8], expanded uncertainty quantity defines an interval about the result of measurement. This interval may be expected to cover a large fraction of the distribution of values that could reasonably be attributed to the measurand. It is used to describe an interval in which the true value can be expected to lie with a *specified level of confidence* (p). *Coverage factor* (k) defines the interval. It is a numerical factor used as a multiplier of the combined standard uncertainty in order to obtain an expanded uncertainty [1].

The concept of measurement uncertainty is incomplete without an associated level of confidence. A given value of measurement uncertainty corresponds to some level of confidence in the measurement result. For example, the measurement uncertainty associated with a specific measurement having a 90% level of confidence implies statistically that a measurement has a nine-out-of-ten chance of differing from the true value by no more than the measurement uncertainty. This value of measurement uncertainty will be smaller than that assigned if a 99% level of confidence is used. A schematic of the relationship between measurement confidence and measurement uncertainty is shown in Figure 4 [1].

$$U_p = k_p \times u_c \tag{2.8}$$
$$y - U_p \leq Y \leq y + U_p \tag{2.9}$$
$$u_c \rightarrow \text{Combined Standard Uncertainty}$$
$$U_{95\%} \rightarrow \text{Expanded Uncertainty } (k_{95\%} = 2)$$
$$U_{99\%} \rightarrow \text{Expanded Uncertainty } (k_{99\%} = 3)$$

For example, if u_c is assumed to represent a normal (Gaussian) uncertainty distribution, then a 99.7% confidence interval corresponds to using an expanded uncertainty obtained with $k_p = 3$ in equation (2.8), *i.e.,* three standard deviations. A confidence interval can be expressed mathematically as in equation (2.9). "y" is the result of a measurement and *"U"* is the expanded measurement uncertainty for the

particular level of confidence *(p)* (which might be 90%, or 95%, or 99%, etc.), and "Y" is the measurand (the quantity of interest). Most expanded uncertainties are reported using a coverage factor of two or three, *i.e.,* k = 2 or 3. Figure 4 illustrates the coverage effect of this factors [1].
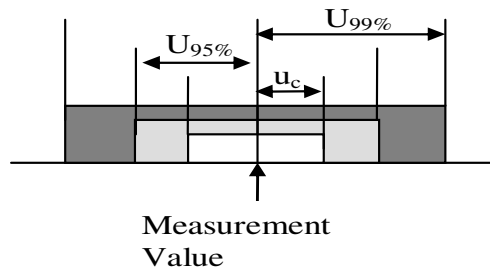
Figure 4: Combined and Expanded Uncertainty [1]

2.2. Summary

In this chapter, the difference between measurement error and measurement uncertainty is explained according to the general terms of GUM. Afterwards, the procedure of the evaluation of uncertainty in measurements is mentioned to guide the uncertainty analysis of CMM measurements.

CHAPTER 3

MECHANICAL STRUCTURE OF CMM'S

Understanding the measurement process and structure of CMM's is very helpful in evaluating the error and uncertainty components. Therefore, this chapter covers the fundamentals of CMM's. In the following sections, the concept of coordinate metrology is introduced. Finally, a general discussion of hardware elements, various design configurations and their characteristics are necessary to clarify the error sources and to evaluate the uncertainty contributors.

3.1. Measurement Process of Coordinate Measuring Machines

The basic function of coordinate metrology consists of the measurement of the actual shape of a workpiece, its comparison with the desired shape, and the evaluation of the metrological information, such as size, form, location, and orientation.

CMMs give physical representations of a three dimensional rectilinear Cartesian Coordinate System. The actual shape of the workpiece is obtained by probing the surface at discrete measuring points. Every measuring point is expressed in terms of its measured coordinates. However, it is not possible to evaluate the parameters of workpieces (e.g. diameter, distance, and angle) directly from the coordinates of measured points. Therefore, an analytical model of the workpiece is used to evaluate the parameters. This model consists of ideal geometric elements. Such elements may be determined by applying an appropriate geometric element best fit algorithm to the measured data set [1].

The measurement procedure of a CMM can be defined as:

- Generating the measured data sets by point to point probing of the actual workpiece.
- Calculating the relevant geometric elements in terms of parameters specifying size, form, location and orientation.
- Evaluating the workpiece features in terms of the drawing.

Probe head is attached to the three carriages of a CMM forming a Cartesian reference coordinate system. The displacement along a coordinate path is determined with displacement sensors. Sensors cover the measurement volume of the CMM and obtain the measured point by using a spatial reference point on the probe head. This reference point can be the mid-point of the probe tip.

The measurement steps of a CMM;

- Calibration of the stylus with respect to the probe head reference point using a calibrated ball.
- Determination of the part position (part-related coordinate system) in the measuring machine-related coordinate system.
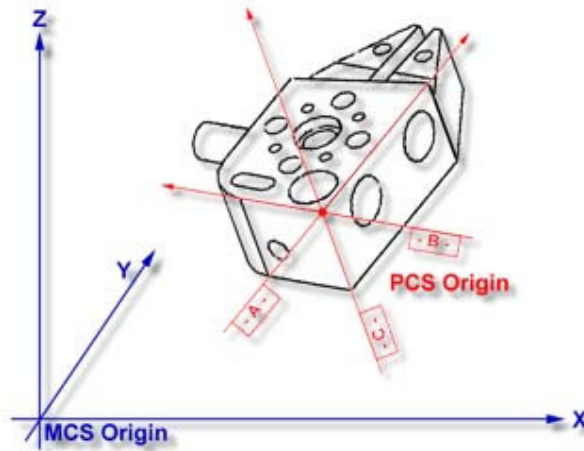
Figure 5: Coordinate Systems

- Measurement of the surface points on the part in the measuring machine coordinate system.
- Evaluation of the geometric parameters of the workpiece.

- Representation of the measurement results after coordinate transformation into the part coordinate system.
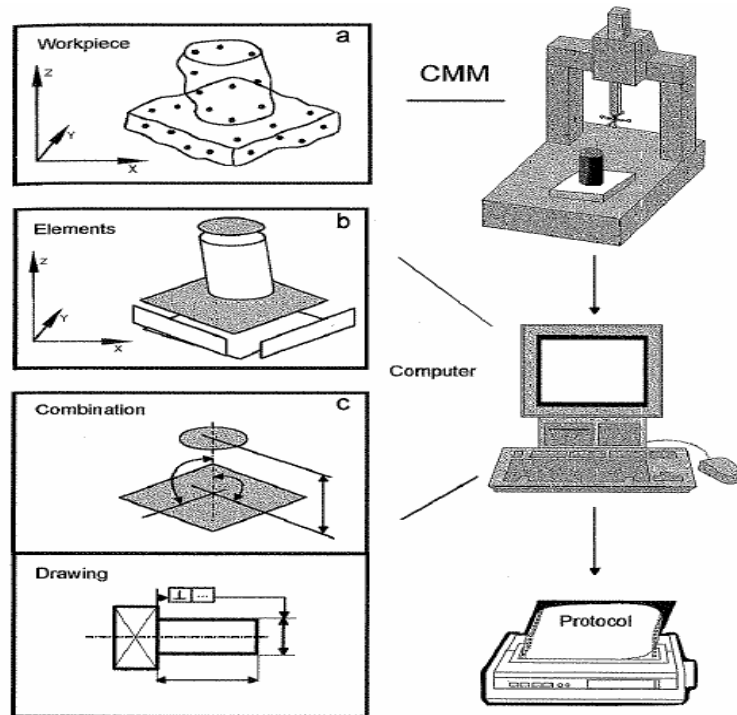
Figure 6: Process of CMM Measurement [1]

3.2. Hardware Components of CMMs

The basic components of a typical CMM are presented, including structural elements, supporting bearings, drive systems, feedback elements, probe head and control systems.

This section deals with technical characteristics of the above hardware components and their influences on a CMM's performance.

3.2.1. Structural Elements

From the perspective at design , the structural elements are significant part of design procedure, because they affect overall performance of the machine.

Structural elements serve as the backbone of a CMM. The machine base, table to support the part to be measured, machine columns, guide ways, and probe shaft are essential structure elements. Some of the desired properties of structural elements are;

- Dimensional stability
- Infinite stiffness
- Weightlessness
- High damping capacity
- Low coefficient of thermal expansion
- High thermal conductivity

No material is capable of satisfying all the above listed properties. At the design process, knowing the desirable properties and their influence is very significant because it really helps in the selection of materials for the structural elements.

Dimensional stability is one of the most important properties of the structural elements. Lack of dimensional stability will adversely affect CMM performance even with error compensated machines. Aging and stress-relieving techniques are used for obtaining dimensional stability. Granite is considered as the most suitable material for structural elements of CMMs [1].

To achieve high performance with sufficient accuracy, the dynamic characteristics of the structural elements become very important. The stiffness-to-weight ratio is the key measure of the dynamic characteristics of the structural elements. Analytical tools such as finite element methods are applied for lighter weight and better stiffness of structural elements. The damping characteristics of the overall measuring system are also a concern for good dynamic performance. It can be enhanced with using the servo control system or active vibration cancellation technique [16].

Furthermore, coefficient of thermal expansion and thermal conductivity influence the accuracy of CMMs. It is desirable to have low thermal expansion and high thermal conductivity. Aluminium has a larger coefficient of thermal expansion compared with granite or steel but it still can be a better choice for CMM structural elements because of its extremely high thermal conductivity. An aluminium structure can quickly achieve its thermal stability when it is disturbed by a temperature change [1].

3.2.2. Bearing Systems

Bearing systems for CMMs are very important because they are part of the structure and can affect measurement accuracy. They can also influence the characteristics of the drive systems. In general, there are two classes of bearing systems in use for CMM applications. These are;

- Non-Contact Air Bearings
- Hard contact Bearings

Among many design criteria for bearing systems, the dynamic stiffness, load carrying capability, damping, and frictional effects are given first consideration. Aerostatic air bearings utilize a thin film of air under pressure to provide the support of a load. The low viscosity of air requires a very close gap of around 5 mm.
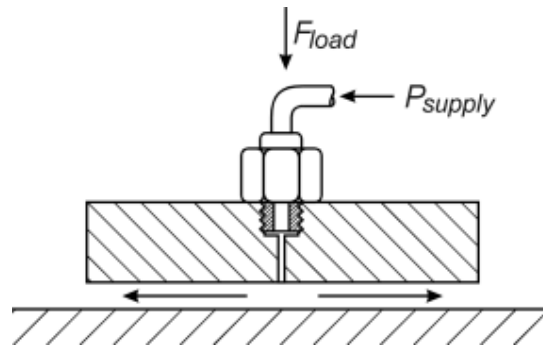
Figure 7: Aerostatic Bearing

Air bearings have the following characteristics and advantages:

- Minimal friction and high accuracy over a wide speed range
- No oil or grease lubrication
- No contamination
- No wear

Precautions must be taken as air pressure variation can cause CMM geometric errors to change. Sudden loss of air pressure will cause catastrophic failure and can damage the way surfaces and bearings.

The CMM under inspection uses air bearings to obtain precise motion on all axes and therefore, it consists of all advantages and disadvantages mentioned here.

3.2.3. Drive Systems

The demand for high performance CMM requires fast drive systems and stiff transmission linkages. CMM drive systems play a significant role in direct computer controlled machines. The purpose of a drive system is only to move the probe, not to provide positional information. This is provided by the displacement transducers.

There are many different types of drive systems in use, such as rack and pinion, belt, friction, leadscrew, and linear motor. The users of CMMs can benefit from an understanding of the need and performance characteristics of different drive systems [1].

3.2.3.1.Rack and Pinion Drive

One simple solution for generating linear motion is the use of rack and pinion drives. This drive system finds application where long length of travel is desired. Form errors and backlash in gear limit the accuracy of CMM's. However, it is a cheap solution for cost effective design [1].

3.2.3.2.Belt Drive

A belt drive system consists of a belt, multi-stage speed reducer, and a servo motor. The belt offers a quiet transmission of power to the moving axes. It prevents

high frequency motor oscillations from entering the measure structure. The moving axes can be driven at high accelerations and speeds with belt drives. Disadvantages are its elasticity, limiting its use for high-precision scanning operations [1].

3.2.3.3. Friction Drive

Friction drive has been used for certain CMMs. It consists of a driving wheel, a flat or round bar, and a supporting back-up roller. The driving wheel can be driven directly by a motor or through a speed reducer. A constant preload is applied to the driving wheel so that it maintains a smooth contact with the bar.

The advantages of friction drives include;

- their simplicity in design,
- low friction force
- minimum backlash and deadband due to elastic deformation
- high positioning accuracy.

These characteristics are important conditions for designing high dynamic and stable drive systems. Some of the undesirable properties are their low drive force capability, relatively low stiffness and damping, and minimum transmission gain.

Figure 8: Precision Friction Drive Systems [37]

The CMM under inspection has friction drive systems for the motion of X, Y and Z Axis.

3.2.4. *Displacement Sensors*

When a probe touches the workpiece, its position is actually determined by displacement sensors fixed along each of the three linear axes of the CMM. Therefore, the displacement transducers become a critical feedback element in the measurement process [1].

In principle, optical linear scales consist of a scale element and an electro-optic read head. One of them is fixed to the moving slide of the CMM. Relative motions between these two components generate the positioning signal.
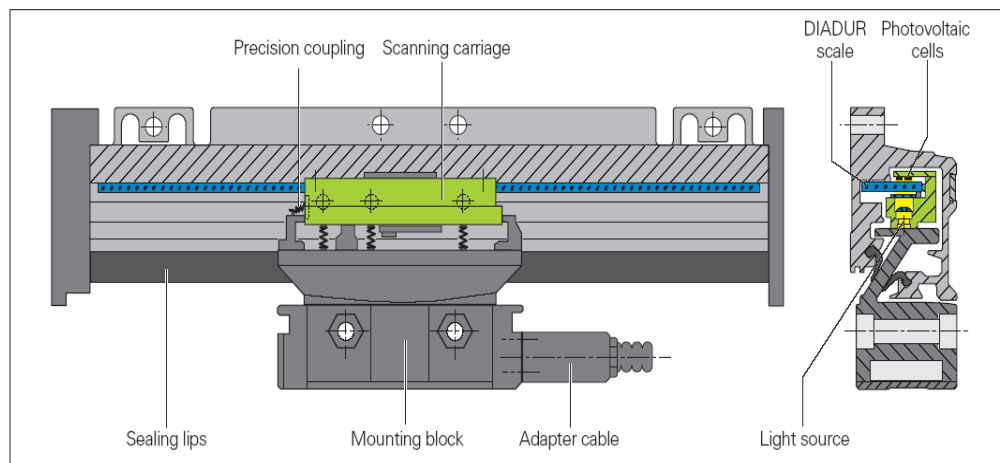
Figure 9: General Structure of Displacement Transducer [38]

Among the optical scales, there are three general types;
1) Photo Transmission Scale
2) Photo Reflection Scale
3) Interferential Scale

Linear scales with optical scanning incorporate measuring standards made of periodic structures are known as graduations. These graduations are applied to a carrier substrate of glass or steel. The scale substrate for large measuring lengths is a steel tape. The precision graduations are manufactured in different photolithographic processes. At the most popular manufacturer who's name is Dr. J. Heidenhain, graduations are fabricated from:

• extremely hard chrome lines on glass,

• matte-etched lines on gold-plated steel tape, or

• three-dimensional structures on glass or steel substrates.

3.2.4.1.Photo Transmission Scale

The scale is typically made of glass and is a precision lined grating with a line pitch of 50 to 100 lines per mm. The read head contains a light source, a collimating lens for conditioning the light beam, a scanning reticle with the index gratings, and photocells [1]. When the read head is moved relative to the scale, the lines of the scale coincide alternately with lines or spaces in the index grating. The periodic fluctuation of light intensity is converted by photo cells into electrical signals. Figure 10 indicates the measurement principle of the photo transmission scale.
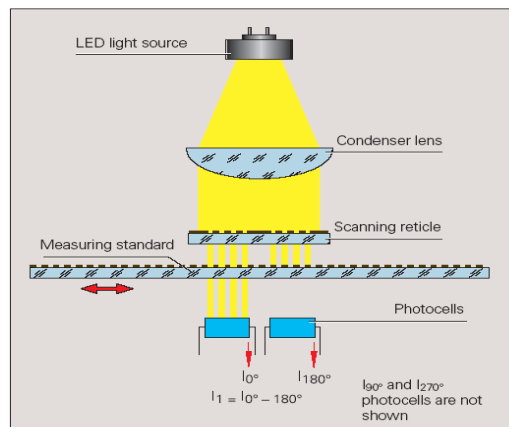
Figure 10: Principle of Transmission Scale [38]

3.2.4.2. Photo Reflection Scale

Different from the glass scale (transmission scale), the reflection scale is made of steel [1]. The interference pattern for the reflection scale is established with alternative reflective lines and diffusely reflective gaps. Figure 11 illustrates the measurement principle of the photo reflection scale .
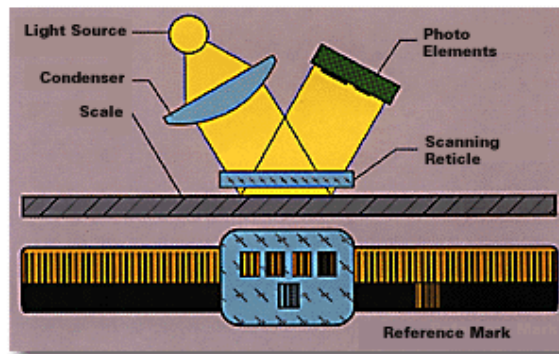
Figure 11: Principle of Reflection Scale [38]

3.2.4.3. Interferential Scale

This type of displacement transducer uses grating scales. The scale is a precision lined grating with a line pitch of 100 or more lines per mm [38]. The lines are read by a photo electric head that detects the interference fringes created by light reflected from the scale and a reference grating on the read head as indicated in Figure 12.

C   Grating period.

ψ Phase shift of the light wave when passing through the scanning reticle.

Ω Phase shift of the light wave due to motion of the scale.
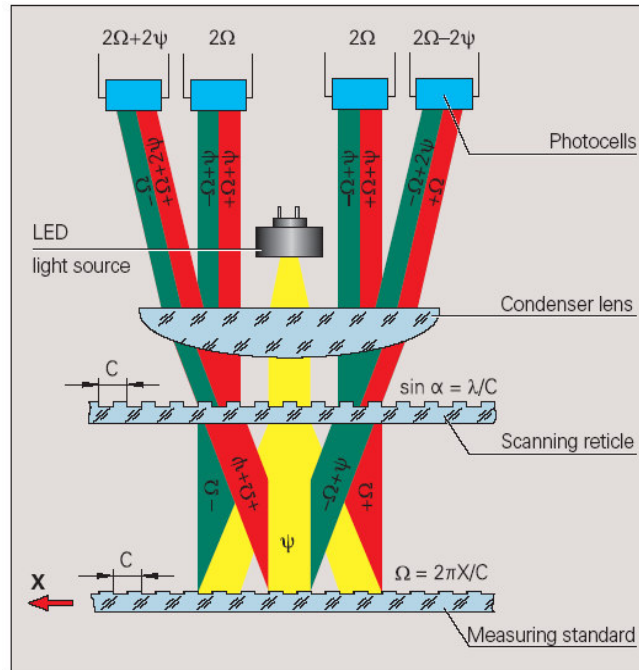
Figure 12: Principle of Interferential Scale [38]

3.2.5. Probe Head

Probe that takes the point on workpiece is one of the important part of CMM . When a probe touches the workpiece, contact is made or broken within probe. This generates an impulse to the control system for reading the position of all three slide data from the displacement transducers. The switching signal is produced by opening and closing of a *mechanical contact*. This electromechanical principle is prone to higher measuring uncertainties. These uncertainties are dependent on the preload and the measuring direction. To overcome this problem, *piezo sensor switching* probes are used. They generate the trigger signal and are sensitive to tension and compression. In addition, the motorized probe head makes the measurement very flexible, but this adds uncertainty to the measurement [1].

CMM under inspection has the probe system indicated at Figure 13, this system uses piezo sensors (strain) and specifications of probe can be seen in Appendices.

Figure 13: Renishaw TP7M Probe System

3.3. Structure Types of CMM's

Slocum explains the properties of the different types of CMMs in his book "Precision Machine Design" [16]. This research can guide about the error sources unique to the structure and is summarized in this section .

The fixed table cantilever coordinate arm measuring machine shown in Figure 14 has the following characteristics:

- Table deflects under the part's weight.
- Cantilever design can have a low natural frequency and large Abbe errors can occur.
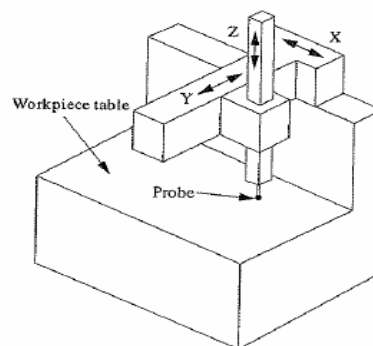
Figure 14: Fixed table cantilever coordinate arm measuring machine [16]

Moving bridge CMM's, such as shown in Figure 15, could be built larger than cantilever machines. Characteristic problems of this type of CMM are;

- The structure deforms under the weight of the part.
- Problems with the outer leg "walking" because the bridge cannot be driven through the center of gravity without the addition of a costly overhead drive system suspended above the Y axis, or a second (slave) actuator on the outer leg [16].
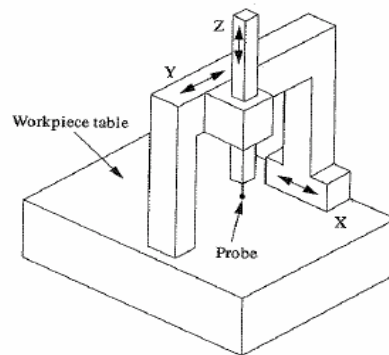
Figure 15: Moving Bridge CMM [16]

To increase the work volume, the column CMM is evolved as shown in Figure 16. The vertical axis was isolated from the planer axes to reduce the effect of Abbe errors. The open table design is allowed for larger parts to be put on the table. Characteristics problem of this type of CMM are defined by A.H. Slocum as below;

- Table deformations still affect accuracy.
- The open C section prone to thermal gradients. Thermal gradients cause the column to arch back and induce large Abbe errors.
- Accuracy is a function of the weight of the part and how it deforms the machine.
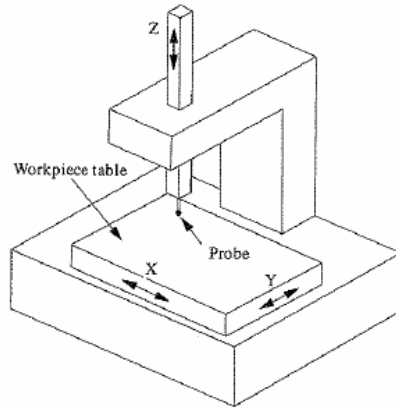
Figure 16: Column Type CMM [16]

The moving ram horizontal arm CMM shown in Figure 17 can probe deep into horizontal recesses in parts [16]. Characteristic problems of this type of CMM are;

- The part weight is a problem for accuracy.
- Cantilever design causes to lower natural frequencies and is vulnerable to large Abbe errors.
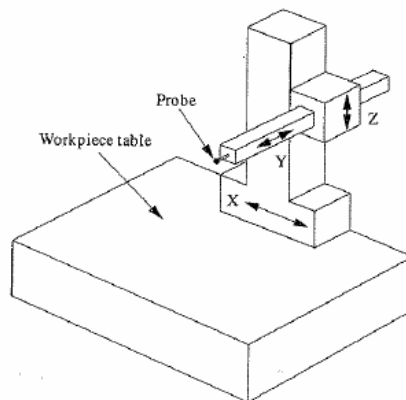
Figure 17: Moving Ram Horizontal Arm CMM [16]

All designs discussed as part-weight limited because the parts are in close physical contact with the measuring frame. The weight of the part causes static deflections in the structure, which decreases accuracy. This leads to the evolution of the gantry type CMM shown in Figure 18. Gantry-type CMMs have the following characteristics [16];

- The weight of the part is not a problem for the accuracy.
- Requires massive construction to minimize bending deformations in beams supporting the axes.
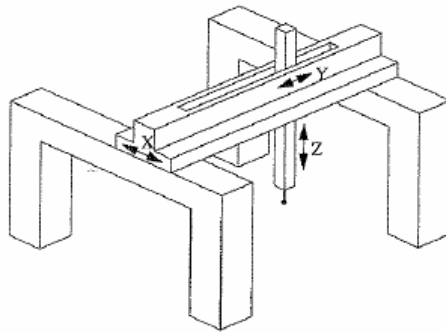
Figure 18: Gantry Type CMM [16]

3.4 CMM used in this study

To understand the CMM inspected, the summation of its measurement process is required and mentioned briefly as below.

First of all, it is a moving bridge type CMM so that it contains all properties of this type of structure. It has an S (Slave) Axis scale to obtain high precision. Software compensates the outer leg walking with using the reading from S axis scale. Actually, the hardware of this CMM is mentioned at the middle part of this chapter. After partial explanation of the machine hardware, it becomes better to mention

complete process flow of machine. The principle of operation of all drive systems is identical and each has a similar mechanical/pneumatic arrangement.

Each drive system comprises of a precision dc servo-motor, a gearbox assembly, a reaction arm, a diaphragm unit, a drive roller, a reaction roller, round drive bar and associated brackets, air bearings and fixings.

The drive roller is in permanent contact with the axis drive bar at all times. When the electrical supply to the motor is switched on a solenoid valve in the air supply line is energized. And this allows air to flow into the diaphragm unit. This unit reacts against the reaction arm and forces the reaction roller against the axis drive bar. Under these conditions, the drive bar is effectively clamped between the drive and reaction rollers. And then carriage bridge or reference spindle is driven to the reset position. When the electrical supply to the motor is switched off, the solenoid valve is de-energized. After that, the air supply to the diaphragm unit is cut off, the reaction arm retracts the reaction roller and the drive is disengaged.

The motors are driven by computer generated drive signals. The instantaneous position of each axis is monitored by photoelectric reader heads which scan a grating imposed on a glass and steel scale. The scanned positional information is relayed to the computer to complete the position feedback loop.

The structure of CMM under inspection can be seen at Figure 72. A **LK** Model CMM used for analysis of measurement uncertainty. The properties of CMM;

X Axis: 1000 mm

Y Axis: 900 mm

Z Axis: 600 mm

Certificate Accuracy: 1.2μm+ L/400 (L = Distance)

Probe: Renishaw TP7M Enhanced Performance

The probe and linear sensors properties of CMM used in this study can be seen in appendices.

3.5 Summary

In this chapter, the reason of the explanation of CMM structures and hardware is to clarify the sources of error and uncertainty because properties of structure and hardware highly effect the measurement characteristics of the machine. Therefore, the relevance of structure to the measurement is significant part of uncertainty

analysis. On the other hand, measurement process is another factor that effects the uncertainty. Finally, the properties of CMM used for the error modelling and application of uncertainty analysis methods are mentioned at the last section of the chapter.

CHAPTER 4

KINEMATIC AND GEOMETRIC ERROR MODELLING AND COMPENSATION OF A COORDINATE MEASURING MACHINE

In this chapter, the error sources of CMM measurements will be explained and classified with respect to the impact on the measurements. Afterwards, kinematic and geometric models of defined errors will be constructed for two types deviation sense and evaluation methods.

4.1. Error Description

Inaccuracy of CMM measurement occurs when an error exists in the relative position between measured point and the probe. These errors cause a deterioration of the machine performance, therefore they have to be detected and eliminated to maintain high performance of a machine.

It shall be reminded that for most CMMs, the machine frame, composed of three orthogonal linear axes, generates the geometry of a Cartesian Coordinate System. The purpose of this system is to provide pure one-dimensional motion along each axis and these axes are to be perpendicular to one another. However, in reality, a carriage moving over a linear guideway will not move purely in one dimension, but will undergo extraneous motion.

Errors occurring in a machine such as this CMM can be categorized according to their sources and may have systematic and random components.

For example;

- Flatness errors of guideways due to manufacturing
- Defective bearings
- Incorrect graduation or calibration of the machine displacement sensors
- Incorrect adjustment of the machine components (e.g. links) with respect to each other
- Elastic deformation of the components and bearings when the mass is displaced during the carriage movements.

28

These errors prevent the machine from reaching the exact position specified by the controller and are the **major** contributors to the CMM inaccuracy and performance deterioration. The researches show that these errors account for almost 70% of the machine error [18]. There are other sources of errors that also contribute to the machine inaccuracy. However, they have a **minor** role, such as the stiffness error, or have a high frequency response, like the dynamics and drives controllers errors [23]. The magnitude of these errors is comparatively minor, therefore they will not be considered in the study of error definition.

Errors can be eliminated to a greater extent by using standard methods of calibration and error correction. In general, calibration methods of CMMs fall into three categories:

1. Methods based on measuring the 21 source errors requiring the use of expensive instruments. (e.g. Laser interferometer)

2. Methods based on measuring certain artifacts, which are used as references for calibration.

3. Methods based on kinematic references (e.g. the magnetic ball bar).

4.2. Types of errors

Error in a CMM reading, whether it is a random or a systematic error, can originate from different sources. Errors can include the thermal error, dynamic including controller errors, or software induced. Structure dependent errors can be divided into categories based on different criteria, as follows.

4.2.1. Geometric error

Alexander H. Slocum has defined geometric error as *errors in form of individual machine components* [16]. Geometric errors are concerned with the accuracy of surfaces which move relative to each other, such as components of linear and rotary axes. They affect the machine repeatability and kinematic accuracy. It is also the direct measured error produced partially by other sources such as the thermal error.

Many factors affect geometric errors including;

- Surface Straightness

29

- Surface Roughness
- Bearing Preload

Straightness error can be considered the deviation from true-straight line motion. In addition, surface roughness is a characterization of the profile of the surface and often has an effect on the smoothness of a bearing's motion. However, hydrostatic and aerostatic bearings are insensitive to the effects of surface finish when they are considerably less than the bearing clearance [16].

4.2.2. Kinematic error

Kinematic errors can be defined as *errors in an axis's trajectory that are caused by misaligned or improperly sized components*. These errors appear in the inability of the CMM to reach the exact specified position by the controller. Position of machine slides, gears, couplers, motors, etc. affect these errors. For example, kinematic errors include orthogonality and parallelism of axes with respect to their ideal location and each other. The other form of the kinematic error is translational errors in the spatial position of axes. Therefore, this type of error is a function of *motion direction*. Actually, Kinematic and geometric errors are inter-related.

4.2.3. Stiffness error

This error can originate from sources which are the lack of stiffness, weight of components in the structure, and configuration of components. External loads include gravity loads, and axis acceleration loads cause this dynamic error due to the lack of stiffness.

4.2.4. Thermal errors

If the machine has a thermally uncontrolled environment, thermal effects have been the largest single source of dimensional errors and non-repeatability. Thermal error variation has a complex nonlinear nature which makes it difficult to handle. Error causes due to temperature [1];
- Uniform temperature variations in the components of the CMM. They cause only length variations of the scales.

- Non-uniform temperature variations giving rise to temperature gradients with in a cross-section of the CMM components. Similar to the bimetal effect, they cause deformations (bending) of the guideways and thus change the alignment of the machine components with respect to each other.

"The following heat transfer mechanisms are responsible for the temperature distribution within a CMM.

- Heat transfer due to air currents (blowers and coolers, fans of motor and control units and of air conditioning equipment)
- Exchange of heat radiation with the environment (outer walls, ceiling, floor, neighbouring instrument, lighting, and personnel)
- Heat transmission by the workpiece, its fixture, and foundation , as well as by inside heat sources (drives, electronic components, bearings)

What happens with the heat introduced ultimately depends on the capability of the machine components to conduct heat and thus to compensate for the temperature gradients. Due to the heat capacity of the individual components, this happens with delay. " (Bosch, 1995)

4.3. Theory of Error Modelling

Modelling a CMM is important to establish a generalized framework. Modelling facilitates a systematic approach to the analysis of errors and the subsequent assessment of their influence on the overall accuracy of a multi-axis machine.

Historically, accuracy was achieved by mechanically reducing these rigid body errors by carefully manufacturing and assembling the CMM structure. Since the 1980's, an alternative approach known as error mapping , which provides a correction for these errors, has been commercially available. Error mapping can be meant as accuracy enhancement or computer accuracy. In this method, each of the rigid body errors is measured. After that, with the use of a computer, errors are mathematically combined to determine the locating error of the CMM stylus at each point in the work zone. N.A. Barakat (2000) stated two compensation techniques in which this error is accounted for

- by either moving the CMM stylus to the correct position (active compensation), which is done in real time during the measurement process,
- or by mathematically correcting the measurement coordinates (Passive Compensation) which can be done after all the measurement points are taken [18].

For rigid body kinematics description, the main assumption is that the moving carriage remains rigid during its motion, *i.e.,* it does not bend or otherwise distort. The motion of the carriage can be given by specifying its six degrees of freedom which include three translational motions (scale and two mutually orthogonal straightnesses), and three rotational motions (roll, pitch, and yaw).

A schematic of six error components of the CMM's X-axis carriage system is given in Figure 19.
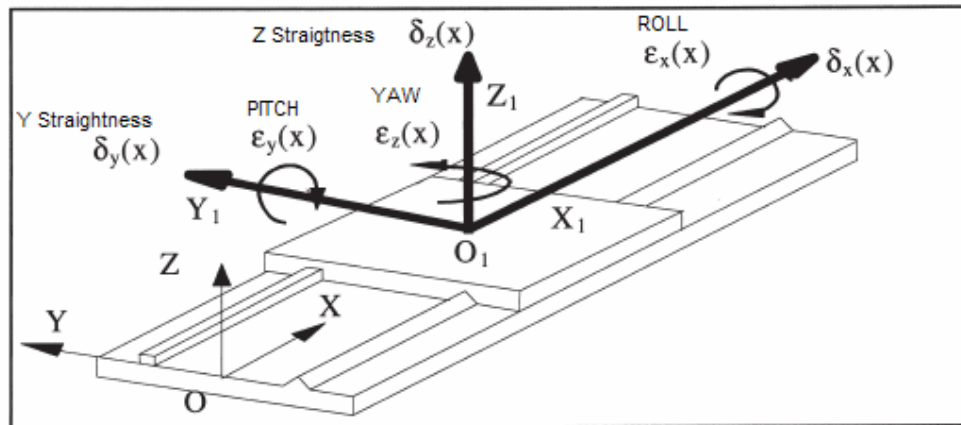
Figure 19: X-Axis Carriage (Joint) Motion with Error [19]

A summary of the symbols used is as follows:

OXYZ	Reference coordinate system
$O_1X_1Y_1Z_1$	Carriage coordinate system
X	Desired direction of motion
$\varepsilon_x(x)$	Rotational error about X-axis (roll)

32

$\varepsilon_y(x)$ Rotational error about Y-axis (pitch)

$\varepsilon_z(x)$ Rotational error about Z-axis (yaw)

$\delta_x(x)$ Translational (scale) error along X axis

$\delta_y(x)$ Translational (horizontal straightness) error along Y axis

$\delta_z(x)$ Translational (vertical straightness) error along Z axis

       Each of these parameters is a function of the position of the carriage along the axis. In addition, there are three out of squareness values of the axis pairs (X-Y, Z-X, Z-Y). Since a CMM has three independent axes, there are a total of 21 parameters which describe the CMM probe location error in the rigid body model. These errors are often referred to as the 21 parametric errors of the CMM.

	Number of error components
Linear positioning errors (scale error)	3
Straightness errors	6
Angular errors	9
Orthogonality (squareness) errors of machine axes	3
	Total=21 error components

4.3.1. *Homogeneous Transformation Matrix (HTM)*

       Multi-axis machines are typically composed of a sequence of elements (linkages) connected by joints that provide either rotational or translational motion. With the assumption of Rigid Body Kinematics, each axis of a machine tool relative to each other and to the reference frame can be modelled by using a Homogeneous Transformation Matrix (HTM). A Homogeneous Transformation Matrix in 3 dimensional space is a 4×4 matrix[16]. It can be used to represent one coordinate system with respect to another or reference coordinate system. A general homogeneous transformation matrix with null perspective transformation is in the following form:

$$T = \begin{bmatrix} R_{3\times3} & P_{3\times1} \\ f_{1\times3} & 1\times1 \end{bmatrix} = \begin{bmatrix} \text{Rotation Matrix} & \text{Position Vector} \\ \text{Perspective Transformation} & \text{Scaling} \end{bmatrix} \qquad (3.1)$$

$$T = \begin{bmatrix} n_x & s_x & a_x & P_x \\ n_y & s_y & a_y & P_y \\ n_z & s_z & a_z & P_z \\ 0 & 0 & 0 & 1 \end{bmatrix} = \begin{bmatrix} n & s & a & p \\ 0 & 0 & 0 & 1 \end{bmatrix} \qquad (3.2)$$

Where n, s, a represent orientation (direction cosines) of a coordinate system with respect to another coordinate system. "p" represents the position vector of the origin of a coordinate system with respect to another coordinate system. If the coordinate frame is embedded in an object, it is possible to describe its relative position and orientation with respect to another object or coordinate system in space using HTM [19]. The compound displacement, resulting from kinematically related components, is then obtained by matrix multiplication. A homogeneous transformation matrix describes the pure translation of an ideal carriage for the X-axis in the following form:

$$T_{ideal} = \begin{bmatrix} 1 & 0 & 0 & x+a \\ 0 & 1 & 0 & b \\ 0 & 0 & 1 & c \\ 0 & 0 & 0 & 1 \end{bmatrix} \qquad (3.3)$$

where, x denotes variable position of the carriage coordinate system origin with respect to the reference coordinate system. a, b, and c represent constant offsets of the origin of the carriage coordinate system ($O_1X_1Y_1Z_1$) origin with respect to the reference coordinate system (OXYZ) in x, y and z directions, respectively. In reality, any single degree of freedom carriage has error motions in six degrees of freedom (Figure 19). The total error motion of the carriage is a combination of rotational and translational errors. The homogeneous transformation matrix of rotational and translational errors is given below with the assumption of small angular errors:

X axis rotated about θ_x.

$$T_1 = \begin{bmatrix} 1 & 0 & 0 & 0 \\ 0 & \cos\theta_x & -\sin\theta_x & 0 \\ 0 & \sin\theta_x & \cos\theta_x & 0 \\ 0 & 0 & 0 & 1 \end{bmatrix}$$

(3.4)

Y axis rotated about θ_y.

$$T_2 = \begin{bmatrix} \cos\theta_y & 0 & \sin\theta & 0 \\ 0 & 1 & 0 & 0 \\ -\sin\theta_y & 0 & \cos\theta_y & 0 \\ 0 & 0 & 0 & 1 \end{bmatrix}$$

(3.5)

Z axis rotated about θ_z.

$$T_3 = \begin{bmatrix} \cos\theta_z & -\sin\theta_z & 0 & 0 \\ \sin\theta_z & \cos\theta_z & 0 & 0 \\ 0 & 0 & 1 & 0 \\ 0 & 0 & 0 & 1 \end{bmatrix}$$

(3.6)

$T_{rot} = T_1 \times T_2 \times T_3$

$$T_{rot} = \begin{bmatrix} \cos\theta_y \times \cos\theta_z & -\cos\theta_y \times \sin\theta_z & \sin\theta_y & 0 \\ \sin\theta_x \times \sin\theta_y \times \cos\theta_z + \cos\theta_x \times \sin\theta_z & -\sin\theta_x \times \sin\theta_y \times \sin\theta_z + \cos\theta_x \times \cos\theta_z & -\cos\theta_y \times \sin\theta_x & 0 \\ -\cos\theta_x \times \sin\theta_y \times \cos\theta_z + \sin\theta_x \times \sin\theta_z & \cos\theta_x \times \sin\theta_y \times \sin\theta_z + \sin\theta_x \times \cos\theta_z & \cos\theta_x \times \cos\theta_y & 0 \\ 0 & 0 & 0 & 1 \end{bmatrix}$$

(3.7)

Since θ is too small; $\cos\theta \cong 1$; $\sin\theta \cong \theta \cong \varepsilon$ (3.8)

$$T_{rot} = \begin{bmatrix} 1 & -\varepsilon_z & \varepsilon_y & 0 \\ \varepsilon_z & 1 & -\varepsilon_x & 0 \\ -\varepsilon_y & \varepsilon_x & 1 & 0 \\ 0 & 0 & 0 & 1 \end{bmatrix}$$

(3.9)

$$T_{trans} = \begin{bmatrix} 1 & 0 & 0 & \delta_x \\ 0 & 1 & 0 & \delta_y \\ 0 & 0 & 1 & \delta_z \\ 0 & 0 & 0 & 1 \end{bmatrix}$$

(3.10)

where, ε_x , ε_y and ε_z are rotational errors about x, y and z axes respectively.

δx, δy and δz represent translational errors along X, Y and Z axes, respectively. The resultant HTM describing the error in position of the carriage with respect to its ideal position is (neglecting higher order terms):

$$T_{total} = T_{rot} \times T_{trans} \tag{3.11}$$

$$T_{total} = \begin{bmatrix} 1 & -\varepsilon_z & \varepsilon_y & \delta_x \\ \varepsilon_z & 1 & -\varepsilon_x & \delta_y \\ -\varepsilon_y & \varepsilon_x & 1 & \delta_z \\ 0 & 0 & 0 & 1 \end{bmatrix} \tag{3.12}$$

T_{total} could be used as total error (translation and rotation) of each elements of CMM. The links and joints of the CMM are modelled as Homogeneous Transformation Matrices (HTMs). Matrices S_i and J_i can be used to model link (i) and joint (i), respectively.

The errors in the S_i matrix are assumed to be independent from position and treated as constant. These are ε_{xi}, ε_{yi} and ε_{zi} which are the angular errors of the ith link and δ_{xi}, δ_{yi} and δ_{zi} which are the dimensional errors of the ith link.

$$S_i = \begin{bmatrix} 1 & -\varepsilon_{zi} & \varepsilon_{yi} & a_i + \delta_{xi} \\ \varepsilon_{zi} & 1 & -\varepsilon_{xi} & b_i + \delta_{yi} \\ -\varepsilon_{yi} & \varepsilon_{xi} & 1 & c_i + \delta_{zi} \\ 0 & 0 & 0 & 1 \end{bmatrix} \tag{3.13}$$
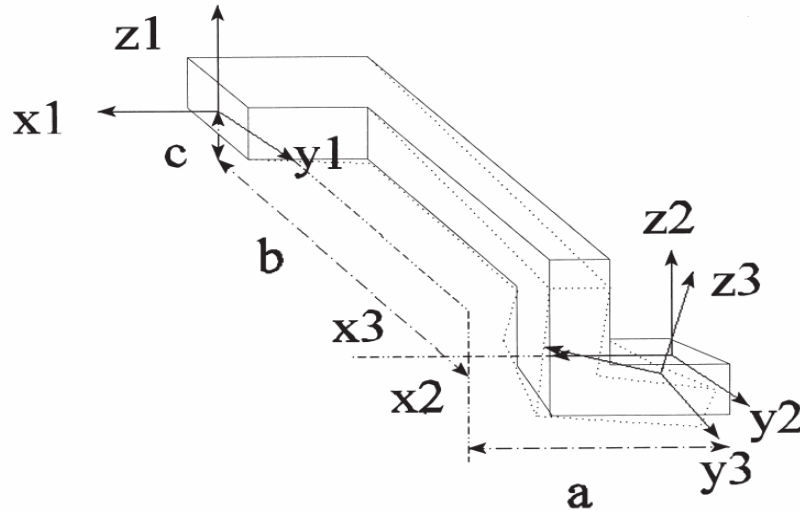
Figure 20: Solid Link with Error [28]

36

On the other hand, errors in the J_i matrix are position dependent. These are ε_{xi} (x)(roll), ε_{yi} (x)(pitch) and ε_{zi} (x)(yaw) which are the angular errors of the ith joint at specified position and δxi(x), δyi (x) and δzi (x), which are the errors in the desired displacements along the ith joint. x is the axis of the carriage (Figure 20).

$$
J_i = \begin{bmatrix}
1 & -\varepsilon_{zi}(x) & \varepsilon_{yi}(x) & X_i + \delta_{xi}(x) \\
\varepsilon_{zi}(x) & 1 & -\varepsilon_{xi}(x) & Y_i + \delta_{yi}(x) \\
-\varepsilon_{yi}(x) & \varepsilon_{xi}(x) & 1 & Z_i + \delta_{zi}(x) \\
0 & 0 & 0 & 1
\end{bmatrix}
\tag{3.14}
$$

The general HTM for an inaccurate positioning element (Link+Joint);
$$T_i = S_i \times J_i \tag{3.15}$$

The combination of all element HTMs can be used to build a mathematical model. For the CMM under inspection, this kinematic model is shown in Figure 21. For the error expression form, the final form of the model matrix is compared to the final form of the ideal kinematic model of the CMM with no errors included [28]. The relationship between actual and measured position of vectors of the probe of the CMM is expressed as:
$$E = T_{actual} - T_{ideal} \tag{3.16}$$
where E is the final error term matrix and every T can be expressed as;
$$T = T_1 \times T_2 \times T_3 \times ... \times T_n \tag{3.17}$$
The ideal kinematic model matrix for the CMM can be obtained from the model including the errors by making all the error terms (ε_{xi} (x,y,z), ε_{yi} (x,y,z), ε_{zi} (x,y,z), δxi(x,y,z), δyi (x,y,z) and δzi (x,y,z)) equal to zero. For a reference constant temperature, the total error matrices can be calculated by using the equations above. The temperature parameter can be also included to the model as below;
The link model with temperature error:

$$
S_i = \begin{bmatrix}
1 & -\varepsilon_{zi} & \varepsilon_{yi} & a_i + \delta_{xi} + (a_i + \delta_{xi}) \times \alpha_{link} \times \Delta T \\
\varepsilon_{zi} & 1 & -\varepsilon_{xi} & b_i + \delta_{yi} + (b_i + \delta_{yi}) \times \alpha_{link} \times \Delta T \\
-\varepsilon_{yi} & \varepsilon_{xi} & 1 & c_i + \delta_{zi} + (c_i + \delta_{zi}) \times \alpha_{link} \times \Delta T \\
0 & 0 & 0 & 1
\end{bmatrix}
\tag{3.18}
$$

α_{link} is the thermal expansion coefficient of the link. The link material is stainless steel.

The joint model with temperature error:

$$J_i = \begin{bmatrix} 1 & -\varepsilon_{zi}(x) & \varepsilon_{yi}(x) & X_i + \delta_{xi}(x) + (X_i + \delta_{xi}(x)) \times \alpha_{scale} \times \Delta T \\ \varepsilon_{zi}(x) & 1 & -\varepsilon_{xi}(x) & Y_i + \delta_{yi}(x) + (Y_i + \delta_{yi}(x)) \times \alpha_{scale} \times \Delta T \\ -\varepsilon_{yi}(x) & \varepsilon_{xi}(x) & 1 & Z_i + \delta_{zi}(x) + (Z_i + \delta_{zi}(x)) \times \alpha_{scale} \times \Delta T \\ 0 & 0 & 0 & 1 \end{bmatrix} \quad (3.19)$$

α_{scale} is the thermal expansion coefficient of the scale. The scale material is glass scale with DIADUR grating.

4.4. Model Application on CMM under investigation

The model of bridge type coordinate measuring machine under inspection consists of three axes (X,Y,Z) so that it should have minimum 3 joint and 3 axis link, in other words i is equal to 3. If the input parameters of error model are known, the error mapping of machine can be constructed. With using this map, the software error compensation is applied on the real measurements. The model of machine under inspection is generated at Matlab and error parameters (translational and angular errors) are assumed as very small deviations. The values of translational and angular error of each axis (joints) are obtained from laser error correction files and used in kinematic model.

The joints, links and coordinate reference system of CMM under inspection could be seen in Figure 21. Coordinate reference system is chosen different from actual Machine Coordinate System to obtain required mathematical model of structure.
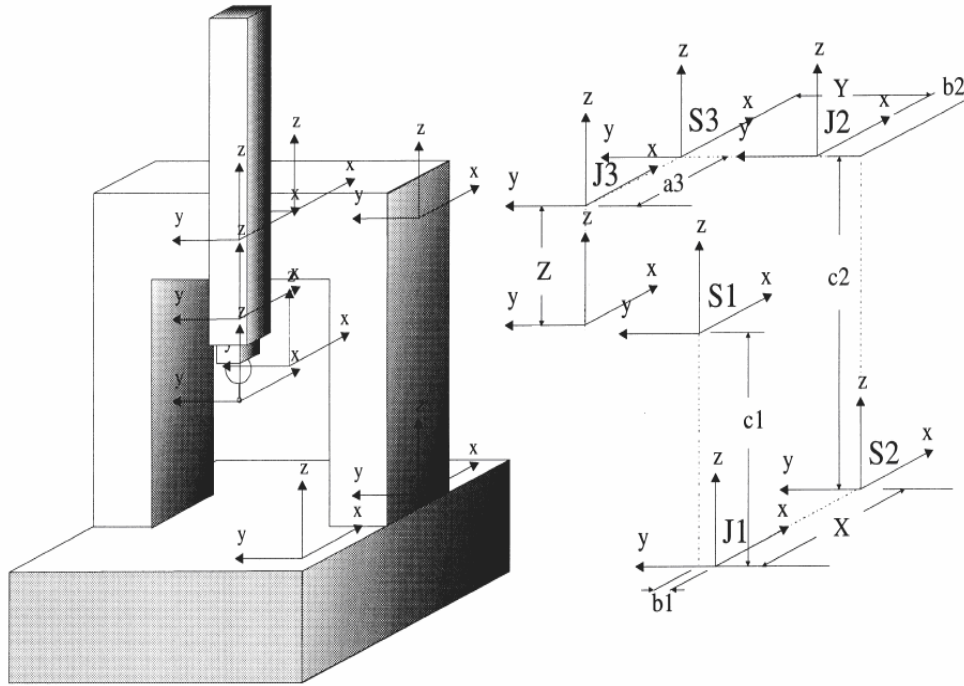
Figure 21: Structure of Machine and Model Elements. [28]

As considered before CMM under inspection has X, Y, Z, S axis scales. The linear transducers of X, Y, Z axis are made of glass and their thermal expansion coefficients (TEC) are 10×10^{-6} micron/ metre/ degree Celsius. This value is close to the TEC of steel, therefore for the modelling of whole structure, TEC of steel can be used.

If the values below are used as inputs to Matlab function, the error maps at Figure 22 are obtained with 50 mm increment at Z axis. It is a cumbersome procedure to obtain the link errors, because some assumptions are required. In thesis study, for all links, translational errors are taken as maximum %10 percent of the link dimensions, and angular errors of links are taken randomly between ±0.05 arcsec. It must be known that for all map figures below, the reference point (X=0, Y= 0) is kinematic model coordinate system, not the actual machine coordinate system.

The assumed link deviations for input of Matlab function are shown in Table 1.

39

Table 1: Assumed Link Deviations (See Appendices)

Temp	ε_{x1}	ε_{y1}	ε_{z1}	a1	b1	c1	TEC1	del_a1	del_b1	del_c1
20	-0,01	0,01	0,02	100	100	100	1,00E-05	8	8	8
	ε_{x2}	ε_{y2}	ε_{z2}	a2	b2	c2	TEC2	del_a2	del_b2	del_c2
	0,02	0,005	-0,01	100	100	500	1,00E-05	1	2	20
	ε_{x3}	ε_{y3}	ε_{z3}	a3	b3	c3	TEC3	del_a3	del_b3	del_c3
	0,005	-0,05	0,003	100	100	100	1,00E-05	9	9	9

Figure 22 and 23 are the surface and contour plots of volumetric errors obtained from kinematic model constructed with using the joint and link deviations.

$$Error\_X = X_{Actual} - X_{Ideal} \tag{3.20a}$$

$$Volumetric\_Error = \sqrt{(Error\_X)^2 + (Error\_Y)^2 + (Error\_Z)^2} \tag{3.20b}$$

where $Error\_X$, $Error\_Y$ and $Error\_Z$ are scalar axis errors.
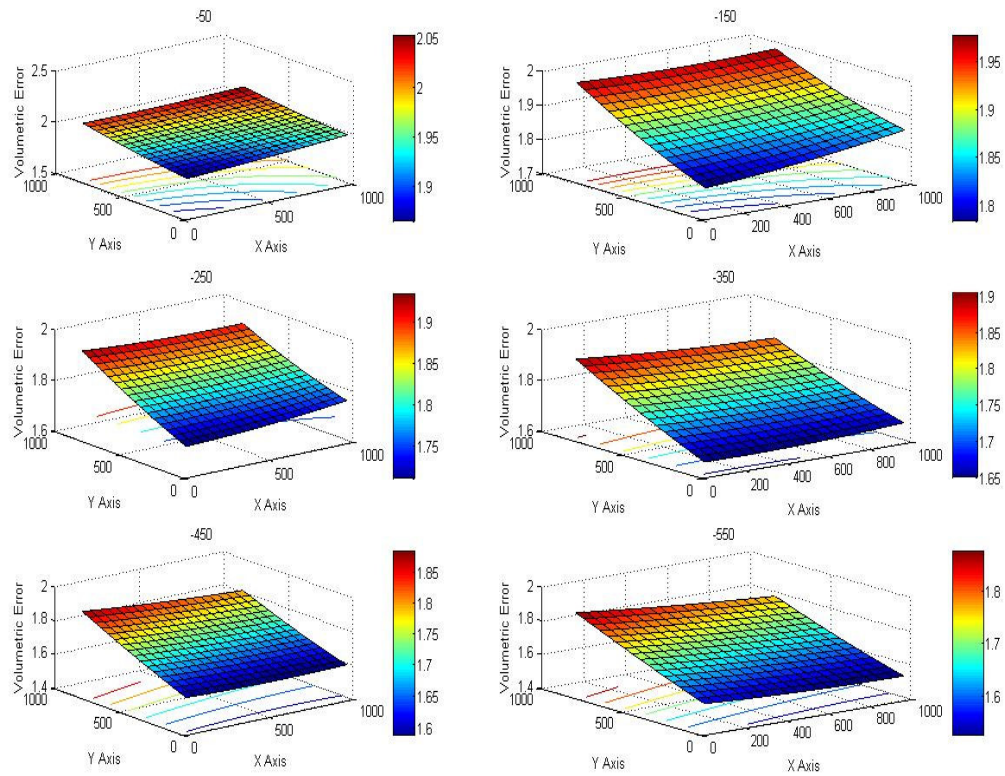
Figure 22: Volumetric Error Charts of Kinematic Model for Z= -50 mm to Z= -550 mm.
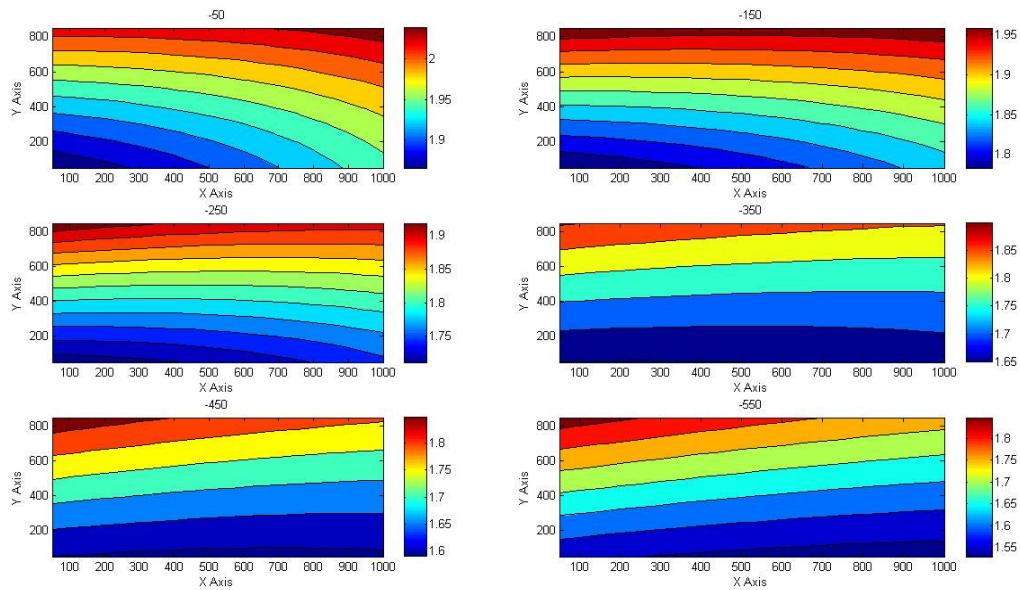
Figure 23: Volumetric Error Contour Plot of Kinematic Model for Z= -50 mm to Z= -550 mm.

41

4.5. Evaluation of Error Model's Results

Figure 22 denotes that while moving away from X axis along the far side of the Y axis, the volumetric error increases systematically. Although, the machine has S-Axis transducer (scale) parallel to X-Axis, the main reason of this increase is the yaw (walking) error of X axis. In other words, the effect of this error increases with the distance between measured point and main driver of X axis (linear scale).

In addition, the volumetric error along X Axis from front (X= 0 mm) to the back (X= 1000mm) increases between Z= -50 mm and Z= -300 mm positions. While moving from Z=-300 mm to the bottom of the Z axis, the error from front to the back along X-Axis starts decreasing. It means that the volumetric error at the back of machine is smaller than at front side at this volume of machine and this results denotes that Z position has a significant effect on the error profile. On the other hand, volumetric error decreases systematically, when probe comes close to the machine granite table (Z= -550 mm) because of the low effect of pitch motion of X Axis. Effects of all angular errors depend on the structure type of machine under inspection.

The axes error maps can be seen in Figure 24 and 25. These figures may help to clarify the contribution of axes individually to the volumetric error. Indeed, a general evaluation can be done as the effect of angular errors of all carriages is amplified by the distance to probe position. Also, the transitional (straightness) and linear (positional) errors may have dominant effect depending on the error magnitude.

Error Map of X Axis (Figure 24) represents that position error of X Axis increases while moving along the Y Axis and this result proves the yaw (walking) effect on the X Axis. Front side of machine, close to the model coordinate system, has higher X axis error than back side of the machine according to constructed model. Also, Figure 25 indicates Y axis error maps of constructed kinematic model with using laser error data.
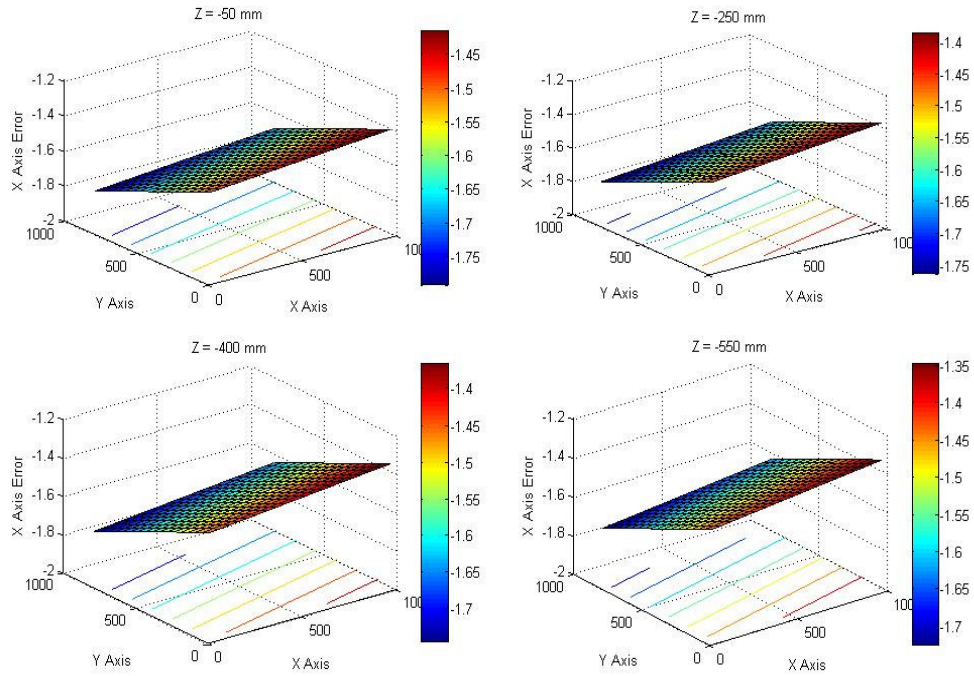
Figure 24: X Axis Error Map
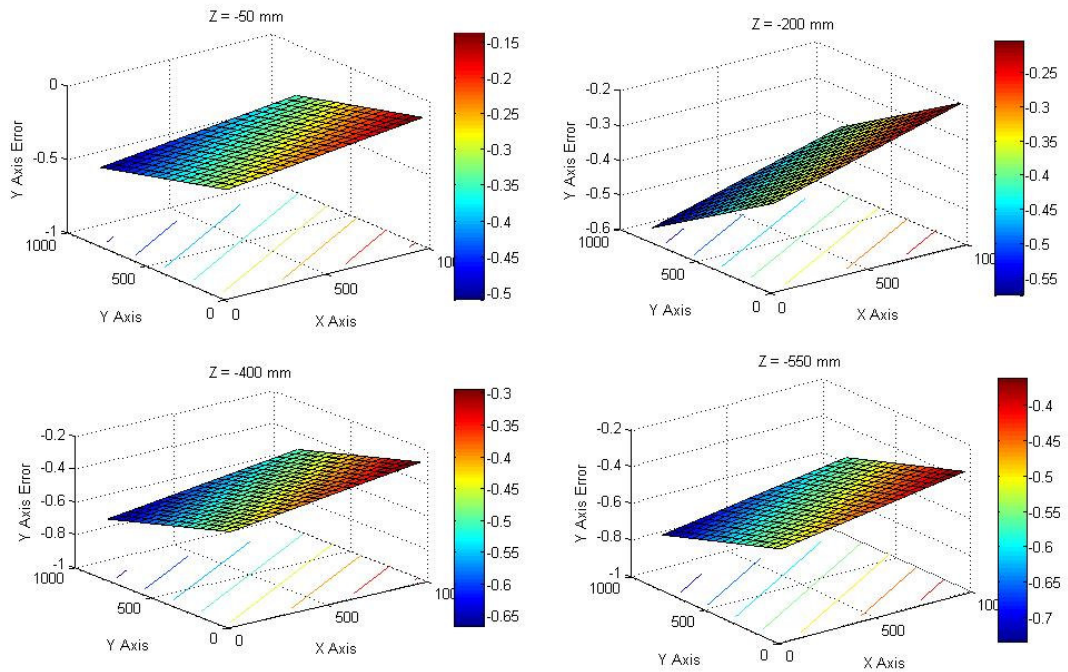
Figure 25: Y Axis Error Map

The other advantage of the model is simulating temperature change and its effect on the error map of machine. The thermal effects have been added to model linearly and the temperature distribution is assumed as uniform. If the temperature change is known in the environment, its uniform effect can be included in the error map of machine. When the input temperature is changed by 1 degree increments, deviations of X, Y, Z shown in Table 2 occurs.

Table 2: Temperature Effects on Errors

First Temp.	Second Temp.	ΔX (mm)	ΔY (mm)	ΔZ (mm)	ΔVolumetric(mm)
20.00	21.00	0.0007	0.0006	0.0003	0.00097
21.00	22.00	0.0007	0.0007	0.0002	0.00101
22.00	23.00	0.0007	0.0006	0.0003	0.00097
23.00	24.00	0.0006	0.0006	0.0002	0.00087

This compensation method requires high experience, difficult measurements and some approximations to define input parameters in order to plot the error model. To obtain this mapping, laser and optical technologies have been started to be used for defining errors precisely without evaluation links and joint geometric and kinematic deviations.

For example, in constructed model, the laser interferometer data is utilized for angular and translational error of joints. If this data can not be obtained, procedure becomes very cumbersome.

4.6. Kinematic Modelling with Laser Interferometer Data

As mentioned before, the machine has 3 orthogonal axis to measure the parts and, therefore in every condition 18 number error contributors are required to model

error mapping. To obtain kinematic error contributors (no need to obtain each link and joint errors), a laser interferometer and optical elements (Mirrors and prisms) are used.

For many years, the industry standard method of measuring machine tool or CMM performance has utilised a free-standing laser on a tripod, in combination with remote (i.e. separate) interferometer and reflector optics. This reflector optics are mounted directly to the machine table and probe. Each linear, angular (pitch,roll and yaw) or straightness measurements can be made interferometrically with the appropriate choice of interferometer optics.
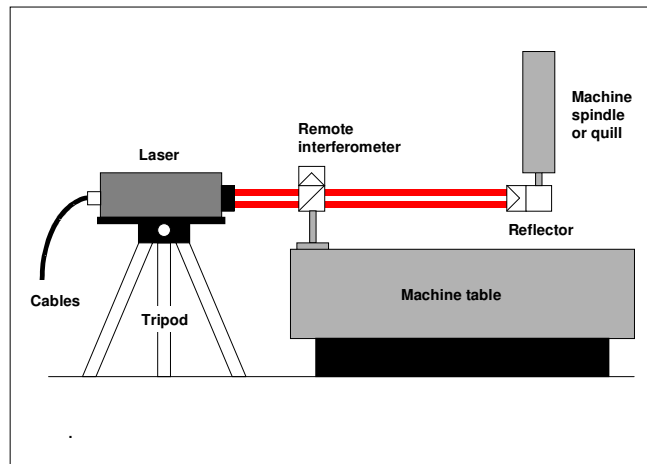
Figure 26: Tripod Mounted Laser Interferometer Measurement [10].

4.6.1. *Linear Error Measurement*

This is the most common form of measurement performed on machines. The system measures linear positioning accuracy and repeatability by comparing the position displayed on a machine's readout with the true position measured by the laser. These values can then be viewed and statistically analysed by the system's software. It is also possible to take this process one step further and automatically download the measured data to a compensation table in the machine's controller. In

this way, a machine's positioning accuracy can be verified and significantly improved, quickly and easily.
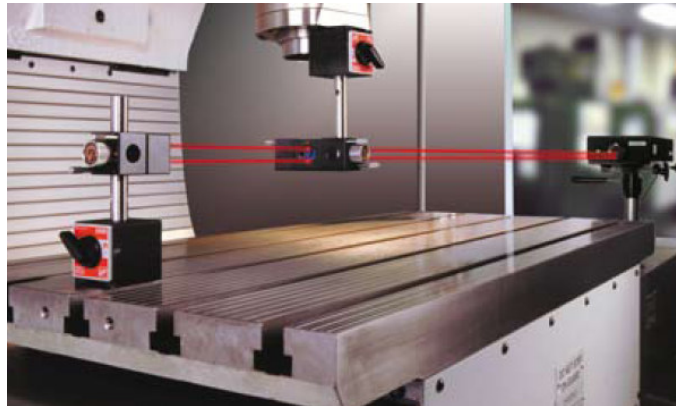
Figure 27: A View of Linear Error Measurement with Laser Interferometry [10]

4.6.2. Angular Error Measurement

Laser Interferometer System uses angular interferometry to measure angle, pitch, roll or yaw. The laser system measures relative changes in the lengths L_1 and L_2, and from this computes the angle. This is shown schematically in Figure 28.

$$Angle = \text{Arcsine}((L_1 - L_2)/S) \tag{3.21}$$
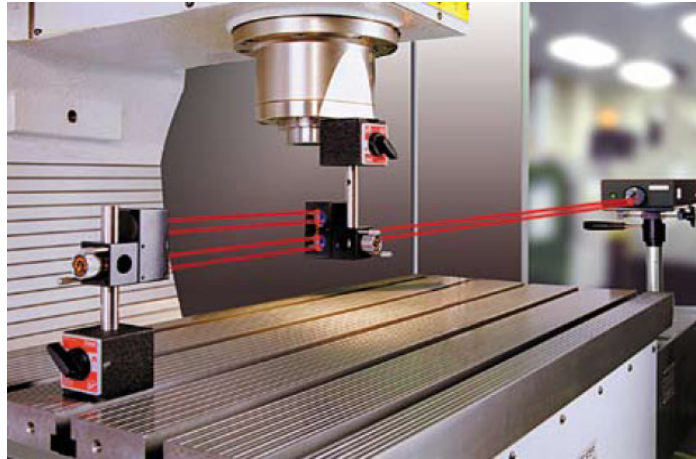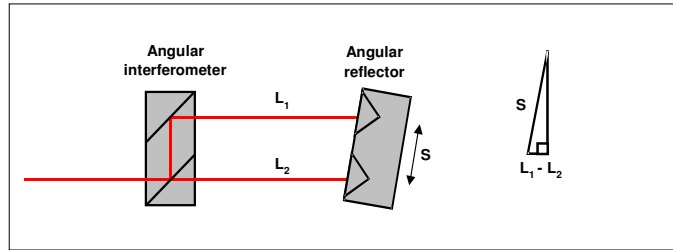
Figure 28: A View of Angular Measurement with an Interferometer [10].

4.6.3. Straightness Error Measurement

Laser System uses a straightness interferometer to measure horizontal or vertical straightness. The laser system measures relative changes in the lengths L_1 and L_2 as shown in Figure 29, and from this computes the straightness error according to the equation 3.22.

$$\text{Straightness Error} = 0.5 \times (L_1 - L_2)/Sin\theta \tag{3.22}$$
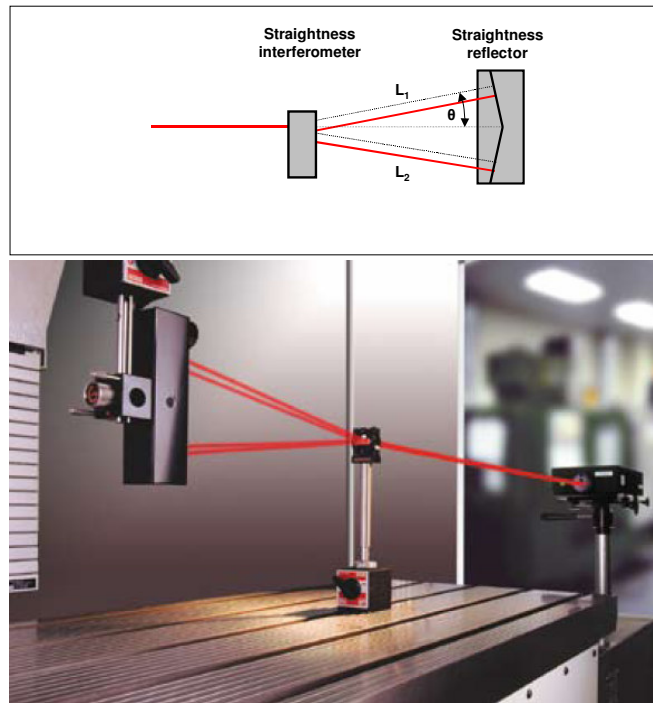
Figure 29: A View of Straightness Measurement with an Interferometer [10].

Linear, Angular and Straightness errors are inserted to the laser error model to obtain error map of machine and compensate this error by using the software. As mentioned before laser model just evaluates the probe position, does not include the links and joint errors. The errors;

$\varepsilon_x(x, y, z)$ Rotational errors about X-axis

$\varepsilon_y(x, y, z)$ Rotational errors about Y-axis

$\varepsilon_z(x, y, z)$ Rotational errors about Z-axis

$\delta_x(x, y, z)$ Translational (scale) errors along X axis

$\delta_y(x, y, z)$ Translational (horizontal straightness) errors along Y axis

$\delta_z(x, y, z)$ Translational (vertical straightness) errors along Z axis

Table 3 describes the mathematical model for any machine having an axis configuration of X, Y, Z for its kinematic chain. So, CMMs with different sequences

48

for their kinematic chains can be represented by similar modified table. The last
three columns show by which factor the quantities of column 2 are to be multiplied
in order to determine the overall errors in the correct coordinate system X_R, Y_R, Z_R.
x_T, y_T and z_T are the stylus length [1].

Table 3: Error Matrices [1]

Axis	Error	Correction Factor		
		Xr	Yr	Zr
Y	$\delta_x(y)$	1		
	$\delta_y(y)$		1	
	$\delta_z(y)$			1
	$\varepsilon_x(y)$		-z-z_T	y_T
	$\varepsilon_y(y)$	z+z_T		-x-x_T
	$\varepsilon_z(y)$	-y_T	x+x_T	
X	$\delta_x(x)$	1		
	$\delta_y(x)$		1	
	$\delta_z(x)$			1
	$\varepsilon_x(x)$		-z-z_T	y_T
	$\varepsilon_y(x)$	z+z_T		-x_T
	$\varepsilon_z(x)$	-y_T	x_T	
Z	$\delta_x(z)$	1		
	$\delta_y(z)$		1	
	$\delta_z(z)$			1
	$\varepsilon_x(z)$		-z_T	y_T
	$\varepsilon_y(z)$	z_T		-x_T
	$\varepsilon_z(z)$	-y_T	x_T	
	ywz		-z	
	xwz	-z		
	xwy	-y		

49
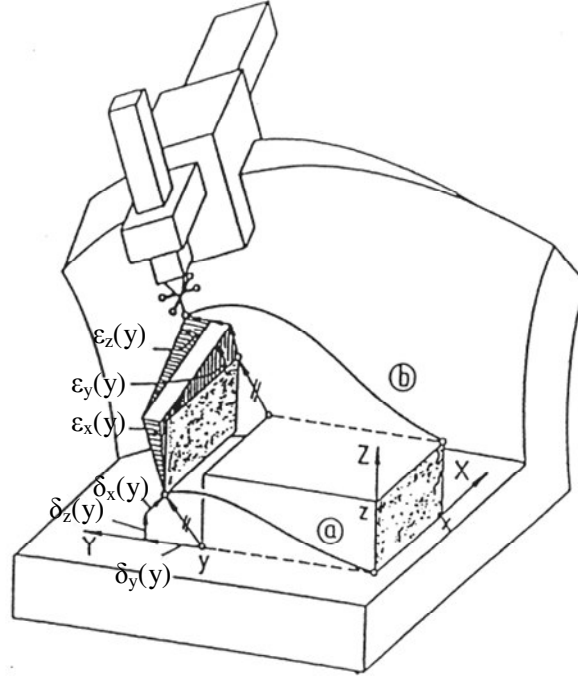
Figure 30: Error Contributors along Y Axis [1]

Total error for each location can be obtained from the equations below.

$$ErrorX = -z \times xwz - y \times xwy + \delta_x(y) + \varepsilon_y(y) \times (z + z_t) + \varepsilon_z(y) \times (-y_t) + \delta_x(x)$$

$$+\varepsilon_y(x) \times (z + z_T) + \varepsilon_z(x) \times (-y_T) + \delta_x(z) + \varepsilon_y(z) \times z_T + \varepsilon_z(z) \times -y_T \tag{3.23}$$

$$ErrorY = ywz \times (-z) + \delta_y(y) + \varepsilon_y(x) \times (-z - z_T) + \varepsilon_z(y) \times (x + x_T) + \delta_y(x) +$$

$$\varepsilon_x(x) \times (-z - z_T) + \varepsilon_z(x) \times x_T + \delta_y(z) + \varepsilon_x(z) \times (-z_T) + \varepsilon_z(z) \times x_T \tag{3.24}$$

$$ErrorZ = \delta_z(y) + \varepsilon_x(y) \times (y_T) + \varepsilon_y(y) \times (-x - x_T) + \delta_z(x) + \varepsilon_x(x) \times (y_T)$$

$$+\varepsilon_y(x) \times (-x_T) + \delta_z(z) + \varepsilon_x(z) \times (y_T) + \varepsilon_y(z) \times (-x_T) \tag{3.25}$$

Laser error correction files include the straightness, angular (roll, yaw, pitch), linear errors of each axis. So that, the laser error correction files of CMM under inspection shown in Figure 30 is utilized to find volumetric error map with using the kinematic model shown in Table 3.
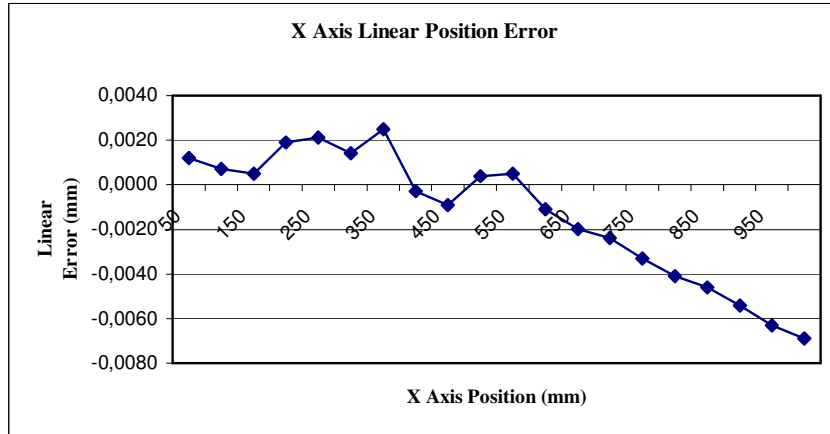
Figure 31. (a) : Laser Interferometry Error Correction Data
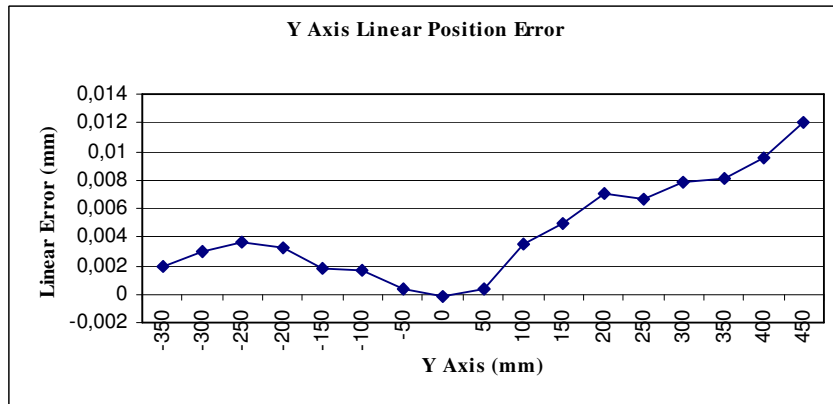
Figure 31. (b) : Laser Interferometry Error Correction Data
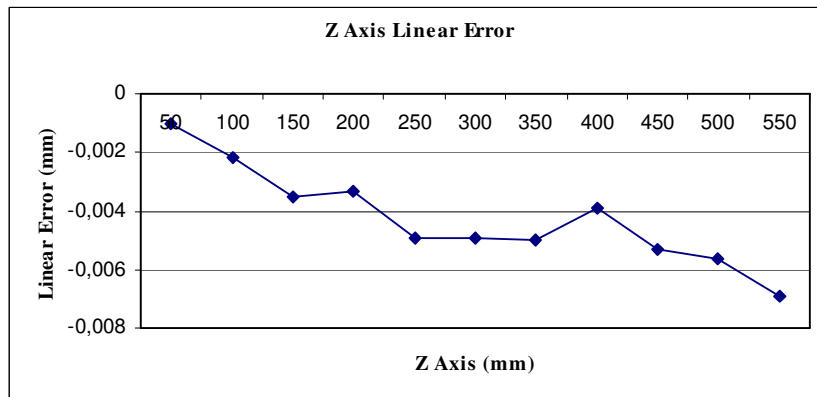
Figure 31. (c) : Laser Interferometry Error Correction Data

51
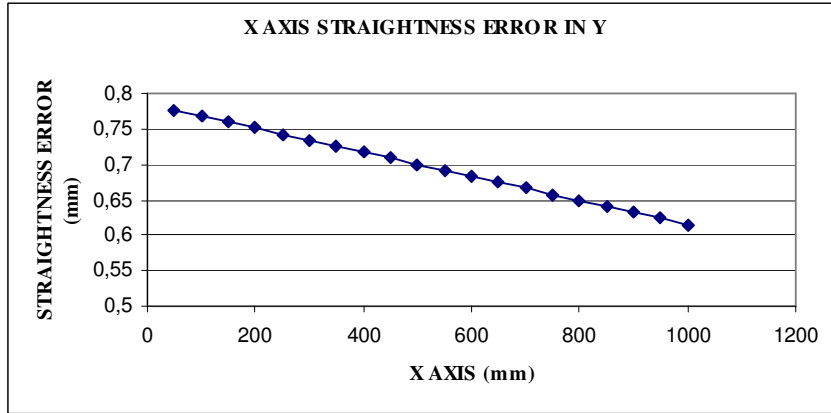
Figure 31. (d) : Laser Interferometry Error Correction Data
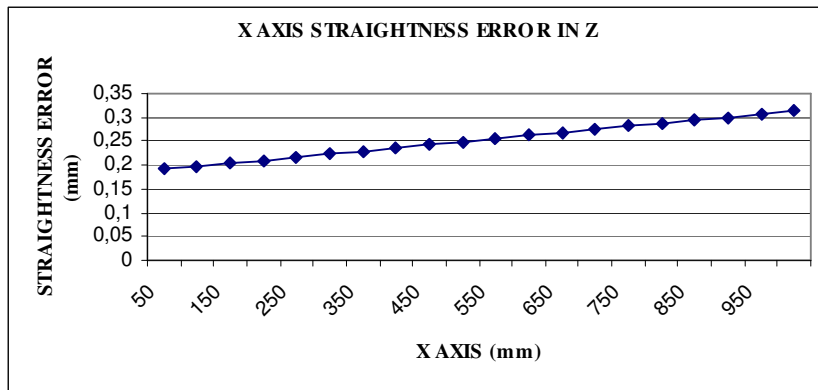
Figure 31. (e) : Laser Interferometry Error Correction Data
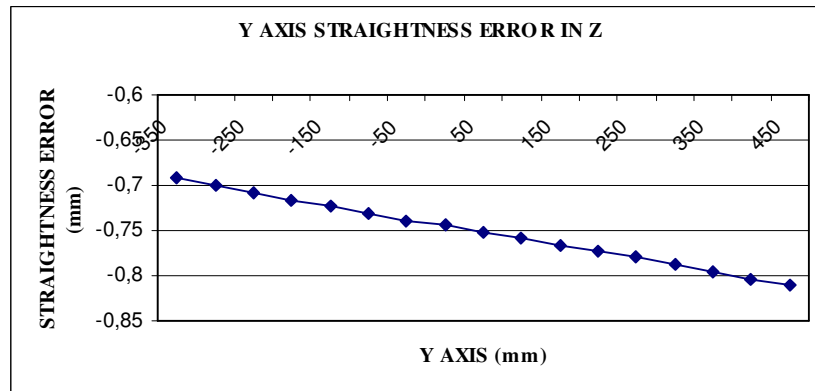
Figure 31. (f) : Laser Interferometry Error Correction Data
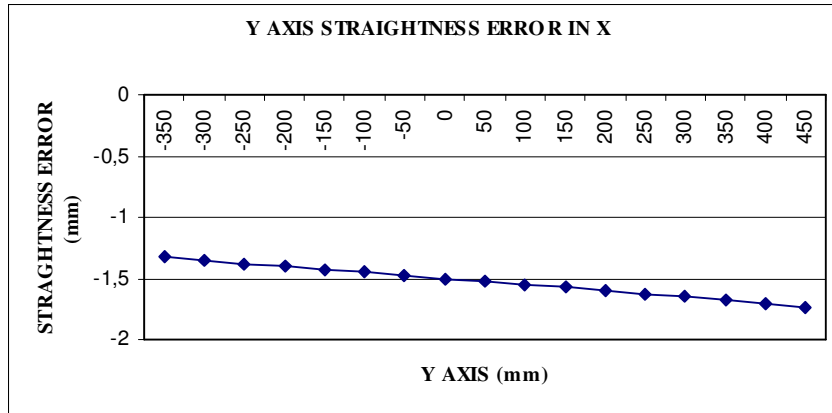
Figure 31. (g) : Laser Interferometry Error Correction Data
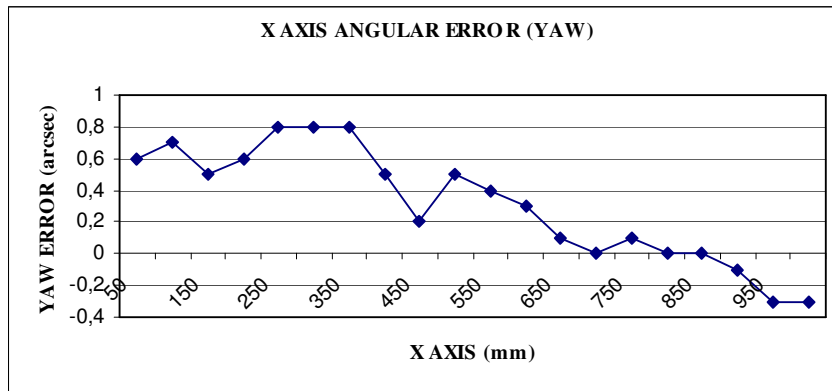
Figure 31. (h) : Laser Interferometry Error Correction Data
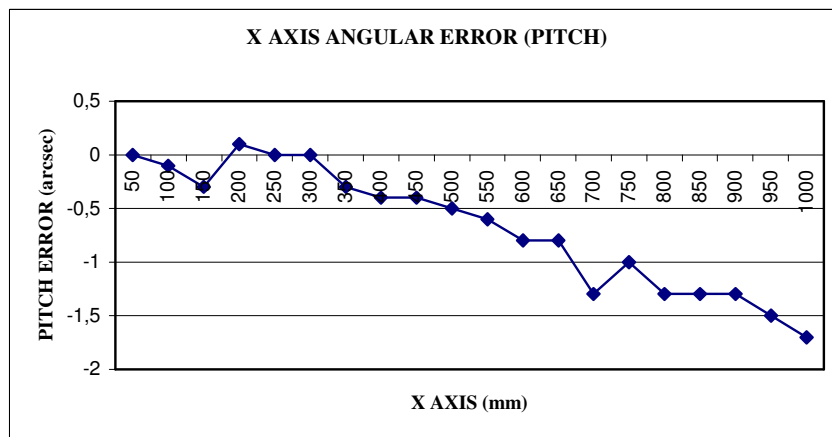
Figure 31. (i): Laser Interferometry Error Correction Data

53
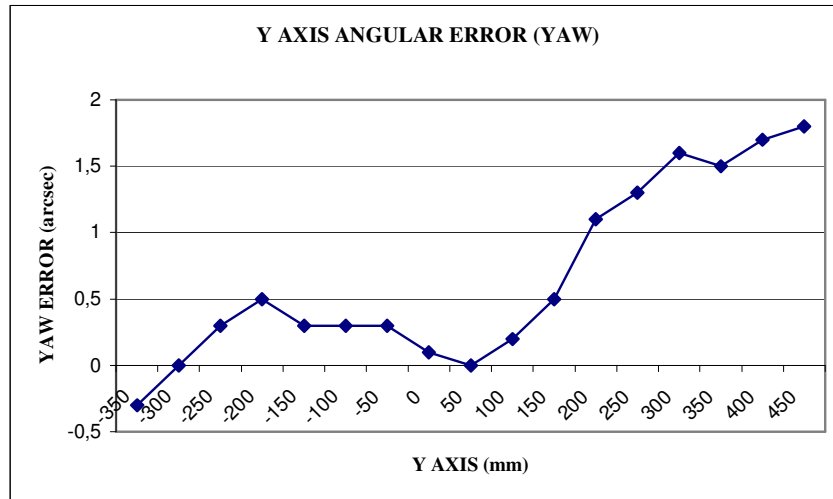
Figure 31. (j): Laser Interferometry Error Correction Data
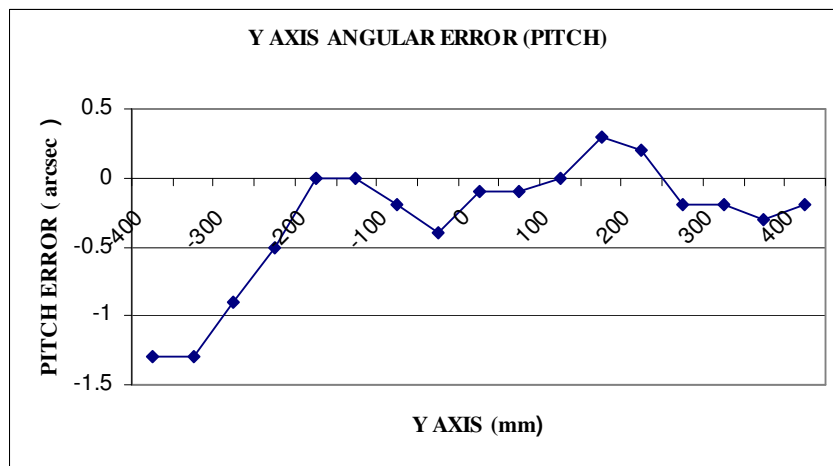
Figure 31.(k): Laser Interferometry Error Correction Data

4.7. *Evaluation of Kinematic Model Used Laser Error Data*

Numerical results and graphs of kinematic model with using laser interferometer error data are represented in Figure 32, 33, respectively.
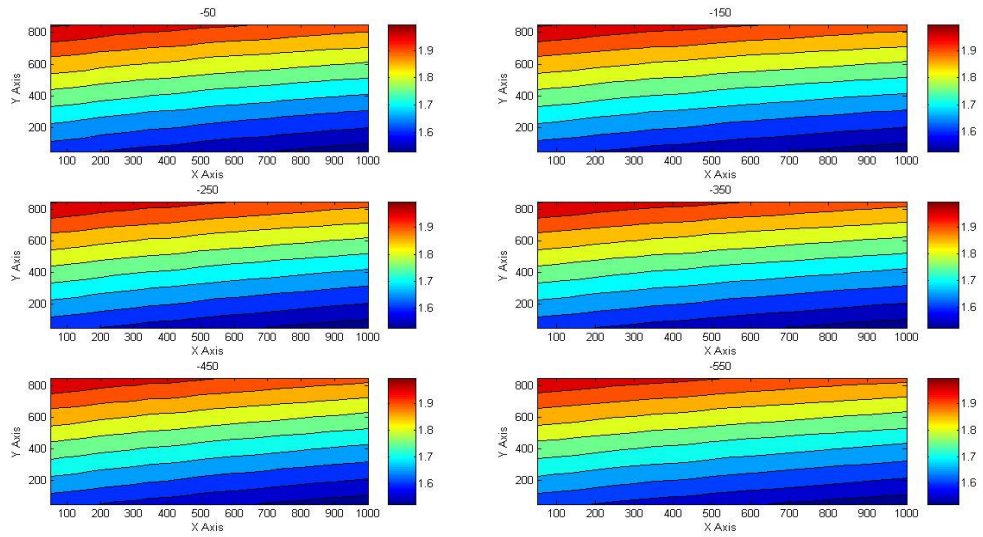
Figure 32: Volumetric Error Contour Plots of Kinematic Model with Laser Data
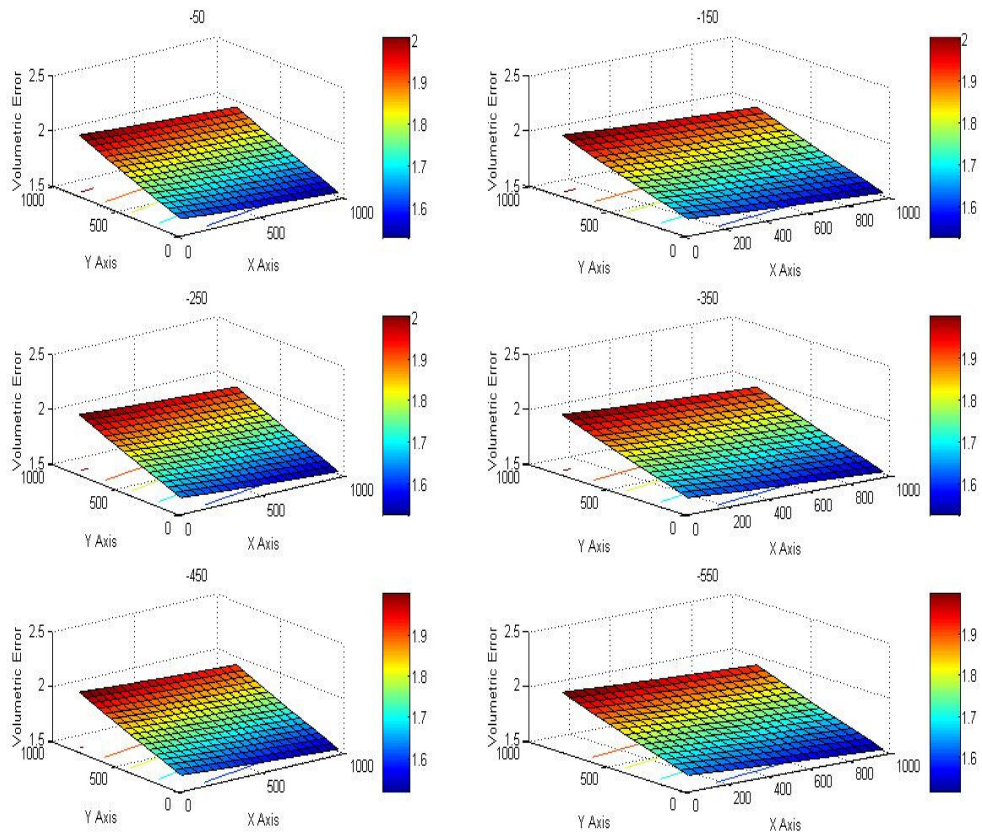
Figure 33: Volumetric Error Map of Kinematic Model with Laser Data

The surface plots at Figure 33 indicates the volumetric error map formed by using laser error data of machine in different Z positions. All graphs resemble a plane but actually the reason of that is the lower change of Z with respect to the change in X and Y Axis. If the Z scale of the graph is changed to logarithmic, it can be easily seen that the plot will not be a plane. At the back side, the machine has smaller error than at the front side. Volumetric error increases through the end of the Y axis and the reason is again "walking" error that occurs while going away from the driver and linear scale of x axis. Also, remember that the similar result is obtained from constructed kinematic model. As mentioned before, if the machine under inspection doesn't have S axis scale to reduce the leg difference error of the X axis, errors will become higher than laser model results. The other conclusion is that volumetric error is smaller at Z= -550 mm than error at Z= -50 mm. In other words, volumetric error decreases when closing to the granite table. The reason of this is the low effect of X Axis pitch error.

Figure 34, 35 and 36 indicate the surface plots of X, Y and Z axis errors obtained from the kinematic model by using laser error data.
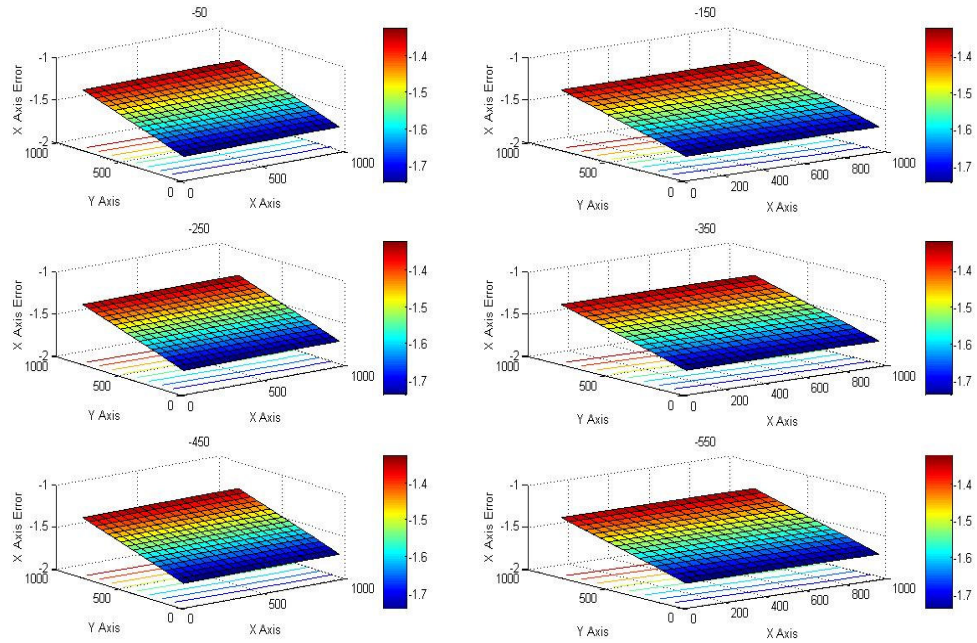
Figure 34: X Axis Error Map of Laser Model
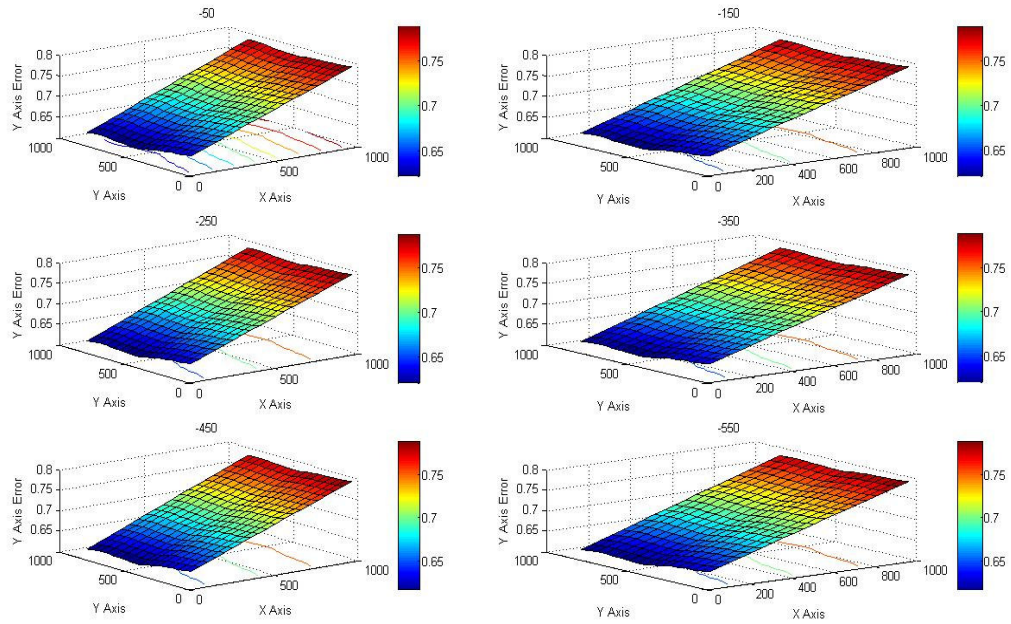
Figure 35: Y Axis Error Map of Kinematic Model with Laser Data

As seen at Figure 35, position error of Y axis increases through X axis path and does not change very much along the Y axis.
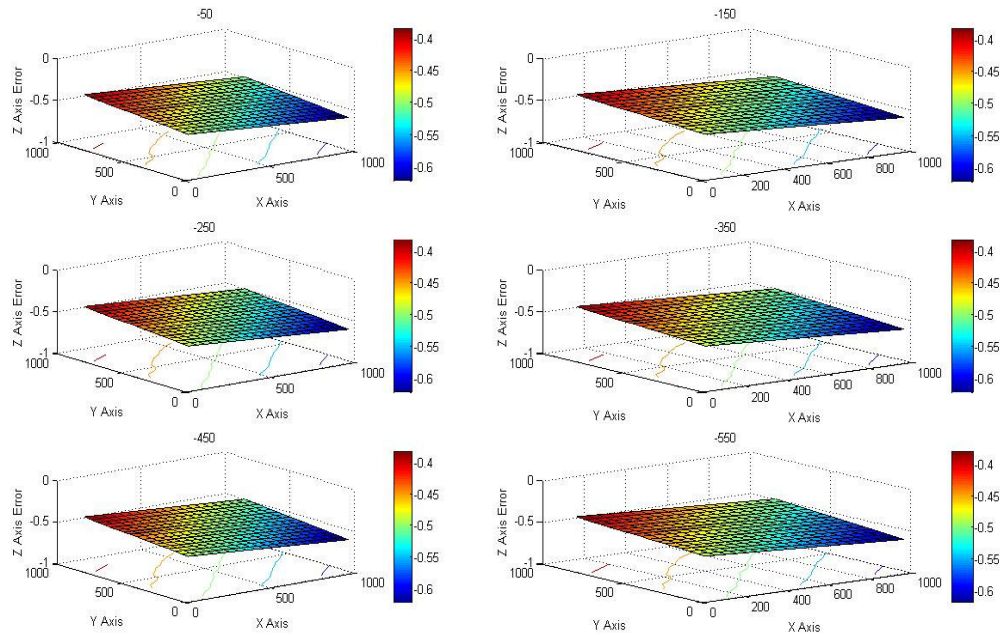
Figure 36: Z Axis Error Map of Kinematic Model with Laser Data

4.8. The Difference Between the Results of Constructed Kinematic model which uses Joint & Link Deviations and Laser Error Data

The models actually use same principles of kinematical analysis (Transformation Matrices). When results of constructed kinematic models by using joint & link deviations and laser interferometer error data are compared with respect to the each other, the differences could be evaluated to see the effects of assumptions for joint and link deviations. The main effect is assumptions about the deflections of the links, because for the errors of joints, same laser error measurement results have been used.

On the other hand, kinematic model according to the link and joint deviations depends on the structure of machine, therefore inspection of machine elements is a must to construct such a kinematic model.

At the Matlab, subtracting and dividing the results of kinematic models at the same location help to visualize the differences and ratios of models. Figure 37 implies that the maximum difference between two models is approximately 0,4 mm at the same location. On the other hand, Figure 38 implies that maximum ratio of the models is approximately 1,25 at the same location. Although, there are many approximations for first model, these are rather good observation for analysing the CMM under inspections.
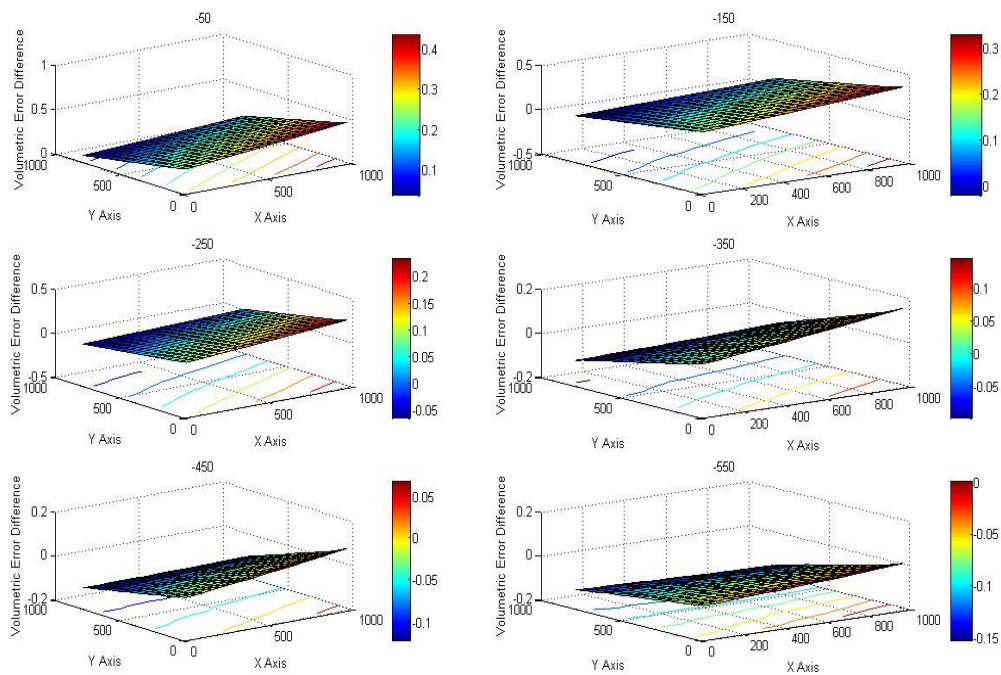
Figure 37: Differences Between the Models from Z=-50 mm to Z=-550 mm.
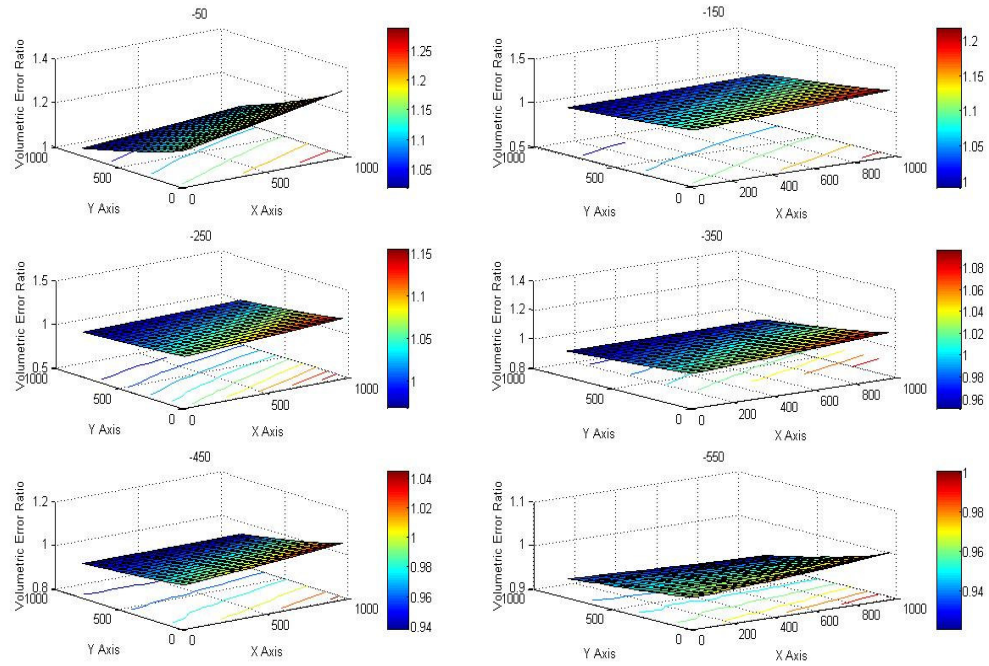
Figure 38: Ratio of Model's Results .

4.9. Summary

This chapter mentions the error sources of a CMM measurement and models the kinematic and geometric errors by utilizing common kinematic formulations and different error measurement techniques used in markets. Afterwards, the results are inspected in order to obtain relevance between structure and measurement errors. Finally, the results are compared with respect to the each other.

CHAPTER 5

THE UNCERTAINTY SOURCES IN CMM'S

Modern coordinate measurement systems, typically involving multi-axis CMMs, give rise to an extraordinary range of uncertainty sources. Thus, a complete assessment of the uncertainty sources and how they influence a specific measurement result can be a difficult task. Three general uncertainty categories are described, which encompass not only the CMM itself but the entire measurement process. In Chapter 4, kinematic and geometric error sources and modelling of CMM have been explained in detail. After, inspection and elimination of the error sources for CMMs, remaining errors are sources of the measurement uncertainty. Measurement uncertainties stem from factors explained below.

5.1. Hardware and Structure Factors

Uncertainty sources produce errors in the measurement point in space. This may be due to the uncompensated geometrical errors in the machine structure, errors in the probing system and errors in the temperature sensors if exists. These factors, many of which may be out of the control of the CMM manufacturer and user, affect the measurement uncertainty. They include a number of factors relating to non-ideal parts, such as :

- surface roughness,
- geometrical form errors,
- finite stiffness,
- environmental effects (vibration)
- thermal errors (both in the uncertainty of the expansion and the distortion of the part, both of which might be changing in time),
- part mounting problems, and variation among operators.

As previously described, measurements of CMM geometry errors are needed, whether or not a CMM is error corrected. This measurement process also has some uncertainty associated with it. For example, some uncertainties arise from the uncertainty in the measurements of the rigid body error parameters. Note the distinction between measuring a mechanical error, *e.g.* the pitch of the X axis and the uncertainty due to the measurement of this value.

Thermally induced distortions play a major role in the uncertainty of CMM measurements. Although, significant progress has been made in designing CMMs to minimize these effects, the user must know that the same distortions are presented in the part under inspection. Ideally, the part temperature is both constant and uniform during the dimensional measurement. However, in many applications, this is not possible because production processes may significantly heat up the part and insufficient time prevents to reach thermal equilibrium. Consequently, the part has a non uniform, temporarily changing temperature distribution. In particular, the surface temperature may not accurately reflect the internal temperature distribution due to conduction, convection, and radiation coupling to the environment. In addition, stresses and deformations may occur because of a non uniform temperature distribution throughout the part. Hence, a thermally insensitive CMM must contend with the thermally induced uncertainty in the part [1, 26].

Another significant source of structural deformation can arise from part loading effects if heavy parts are inspected. The nature of the deformation depends on the type of CMM structure, the load, the location of the load, and the details of the part mounting, *e.g.* the number of loading points in contact with the table and the load at each point. Hence loading effects are difficult to predict and as it is mentioned before, many different structure types are designed to overcome this problem. Since most performance evaluations are conducted by using very light loading, these deformations are often an overlooked, unquantified source of measurement uncertainty [16].

Consequently, an investigation of non-compensated structural distortions which introduce errors into the CMM coordinate system is needed to develop an effective uncertainty analysis.

Machine dynamics create another class of CMM geometry errors. These errors may depend on such factors as probing speed, probing direction, probe approach distance, acceleration settings, and the amount of extension of the CMM axes [23,20]. The size of the stylus ball is often required in order to carry out CMM measurements. The effective size of the stylus ball includes any calibration factors (especially stylus bending) that are specific to the probe in use. For example, many common touch trigger probes require a small displacement of the stylus before the probe triggers and records the point coordinates. This displacement, known as the **probe pretravel**, results in an effective stylus ball size which is smaller than its physical size. The CMM geometrical structure can accurately measure displacements of the stylus. Because of this while calibrating a probe by measuring a reference artifact (sphere) of known size, the difference between the size determined by the CMM and the known size of the artifact determines the effective stylus ball size. Any uncertainty in the size of the reference artifact (usually a sphere of calibrated diameter supplied by the CMM manufacturer) transfers directly to an uncertainty in the effective size of the stylus ball. Therefore, this uncertainty is seen directly in the part size measurements [1].

5.2. Measurement Strategy Factors

These factors include the effects of how the CMM user decides to execute the measurement. All these factors such as where the part is located and how it is orientated, which probes and styli are used in the measurement, the particular sampling strategy (number and location, i.e. distribution, of the measurement points), and which algorithm is selected to analyze the data affect the measurement uncertainty.

The choice of sampling plan can have a significant effect on the computed feature. If an inadequate plan in terms of number or distribution of measurement points is used, it will cause to an uncertainty in the values of the computed features. This uncertainty source can be a major contributor to the uncertainties in measurement. It is necessary to select a suitable measurement plan. This plan should

    (a) have very dense set of points,

    (b) be reliable estimates of the measurement,

(c) be economical.
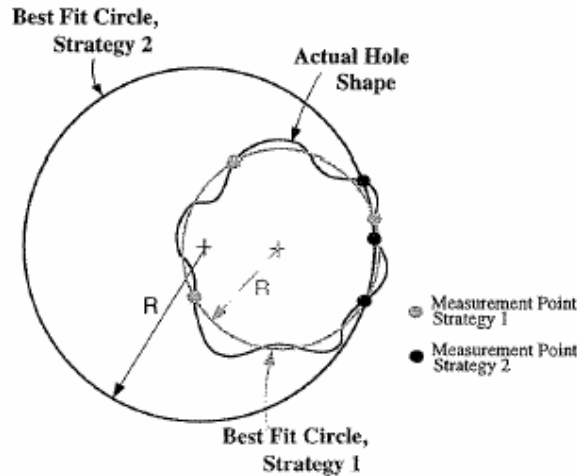
Figure 39: Two Different Sampling Strategy and Their Results When Measuring a Circle [1]

5.3. Software Factor

Measurement points are analyzed by the CMM software to produce a geometric result. In general, many software packages give different results for same measurement points. This represents that this difference is not due to the inaccuracies of the CMM hardware, but it is due to the mathematical algorithm of software and computer system. Manufacturers try to decrease the computer time to reach desired result. However, this is a cumbersome aim that minimising the computer time forces to simplify the problem. Simplification requires some approximations and they may work well for some measurements, but the same approximations may create errors for different sampling strategy. In addition, the software may contain coding errors. All these software related uncompensated errors are the source of uncertainty.
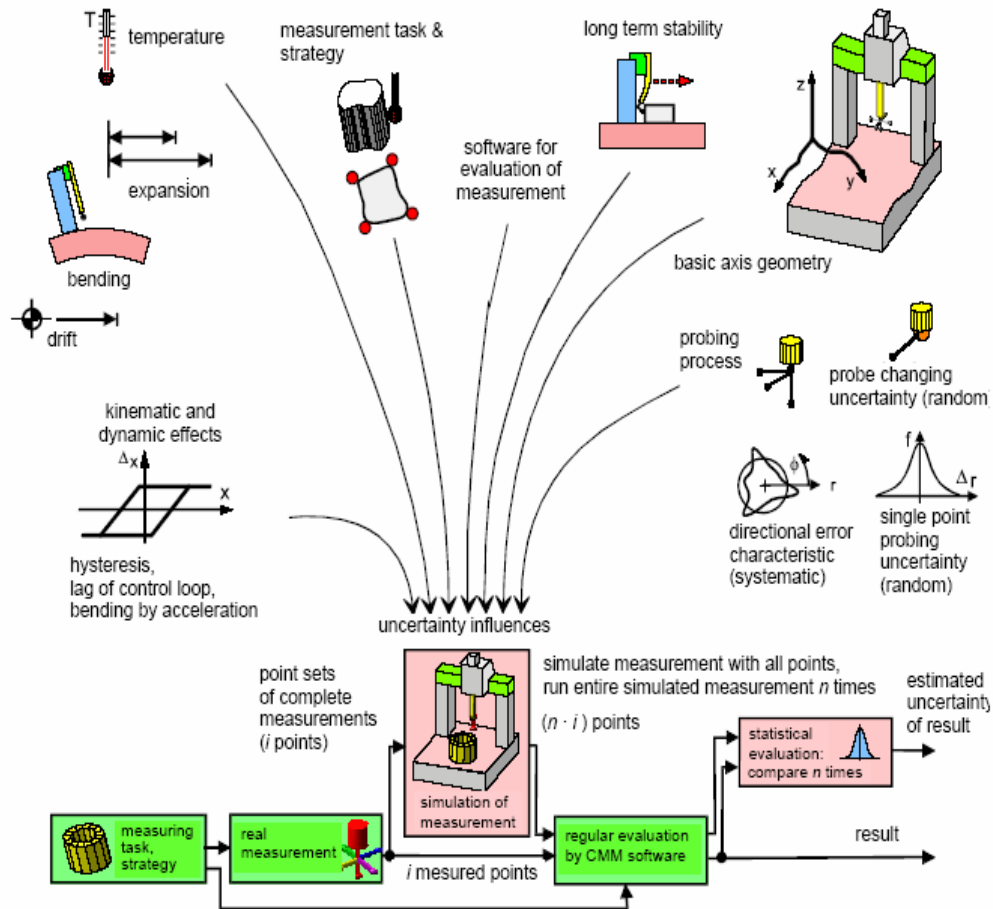
Figure 40: Uncertainty Source Chart [34]

5.4. Summary

In this chapter, the uncertainty sources in CMM measurements are classified into three main factors. These factors are hardware and structure, measurement strategy and software which contain many sub factors. Figure 40 indicates the uncertainty sources in a CMM measurement.

CHAPTER 6

BRIEF EXPLANATION OF METHODS TO DETERMINE THE MEASUREMENT UNCERTAINTY OF CMM'S

Precision engineering is a discipline to evaluate and quantify the measurement uncertainty. Different methods are developed for the quantification the measurement uncertainty and these methods standardize to distribute without violation. On the other hand, these methods have properties different from the others and differences cause many advantages and disadvantages. In this chapter, different methods to determine the measurement uncertainty of CMMs are explained, briefly.

6.1. Method 1: Uncertainty Budgeting

A general method is outlined in the GUM to determine an uncertainty statement. This uncertainty statement is associated with a quantity derived from measurements and or other information. Briefly, the procedure begins with listing each error source, and then quantifying the magnitude for each error source by a variance (square of the standard uncertainty) to check if any errors are correlated, if necessary. If they are correlated, their covariance is quantified; otherwise this covariance is set to zero. Next the sensitivity coefficient for each error source should be determined. Various formulas are given in the GUM to provide the standard uncertainty of the derived quantity. (Look at the Chapter 2.)

The various uncertainty sources may be quantified by a number of different techniques including:

- the results from performance verification standards,
- educated estimates of individual,
- historical records,
- results of experiments, and
- other uncertainty statements.

Due to the complexity of CMM measurements, it may be necessary to refer to suitable literature in order to complete this task.

6.2. Method 2: Comparison method

This method uses a calibrated gauge (artifact) to quantify instrumentation and measurement plan uncertainty sources. Additionally, by using repeated measurements on parts the method can be used to help in quantifying the uncertainty factors. This method has the advantage that traceability is relatively easy to demonstrate, but the disadvantage that several master gauges may be needed to cover the full range of measurements made and to do these measurements a lot of time is required.

6.3. Method 3: Statistical Evaluation of Measurement Uncertainty by Designing Fractional Factorial Experiment

This method is carried out using a calibrated gauge (artifact) and utilizes the statistical methods by designing an experiment. A performance test experiment is planned using the statistical technique to investigate the CMM uncertainty sources. An appropriate experiment can be selected among several designs of experiments with the purpose of reducing the amount of experimental runs. The use of analysis of variance (ANOVA) allows the determination of the most significant variables influencing the CMM measurement uncertainty and their quantities.

6.4. Method 4: Hybrid Methods

Many uncertainty budgets will be a combination of the methods previously described. In general, this approach is likely to provide the most effective solution to estimate measurement uncertainties. This method can include geometric, repeatability, thermal effects in the uncertainty analysis by using statistics.

6.5. Method 5: Simulation

The method of simulation, like uncertainty budgeting, quantifies each uncertainty source with a distribution of values (which can be characterized by a variance). However, instead of combining variances as in the case of uncertainty budgeting, simulation determines the measurement uncertainty by examining the variance of the measurement result. This is done by computing the result of a large number of virtual measurement scenarios, where each virtual measurement scenario is realized by selecting one possible error for each of the quantities affecting the measurement result and computing the measurement and using these values. The process is repeated many times, each time differing in the errors selected; the variance of the calculated measurement results represent its uncertainty. This procedure has the advantage on not requiring vast numbers of real measurements to be made so that not wasting time.

CHAPTER 7

UNCERTAINTY BUDGETING IN CMM MEASUREMENT

Uncertainty budgeting is common method for all machines to evaluate the performance of them. In this chapter, the detail examination and application of uncertainty budgeting method will be mentioned.

7.1. Theory of Uncertainty Budgeting

This method requires obtaining the information about the uncertainty contributions. This data is obtained from the certificates or measurements of contributors, generally. The contributors can be classified as Artifact and CMM based.

The main contributors for budgeting are below;

1) **Artifact Calibration Uncertainty (1):** This is a fixed contribution extracted from the calibration certificate of artifact.

2) **Artifact Calibration Uncertainty (2):** This is a length dependent contribution extracted from the calibration certificate of artifact.

3) **Artifact Geometry:** Flatness and parallelism of measurement faces, which is a fixed contribution. Value to be taken from the calibration certificate of artifact.

4) **Artifact Alignment:** This value will need to be determined by the laboratory, which is normally a fixed contribution. Although the contribution may be very small, this may interact with the geometry. So, it may be negligible.

5) **Artifact thermal expansion coefficient uncertainty:** Generally for steel artifacts this could be estimated at 1 micron per metre per degree C away from 20 degrees C. This is length dependent and calculated from the temperature difference. While calculating the temperature difference value,

the thermometer uncorrected error and thermometer resolution values are included as taking root sum of square.

6) **CMM Resolution:** CMM resolution is used during verification, which is a fixed contribution. This value is extracted from the technical specifications of CMM manufacturer.

7) **Artifact Calibration Resolution:** If the laboratory chooses to round the calibration results for the artifact, then this needs to be considered as a fixed contribution. This could be calculated as the difference between the reported calibrated length of the artifact and the length used for in calculations by the laboratory.

8) **Thermometer Resolution:** This value shall be taken from the calibration certificate of thermometer that is used to measure temperature, which will be a length dependent contribution.

9) **Thermometer Uncorrected Errors:** This value shall be taken from the calibration certificate of thermometer, and it is a length dependent contribution.

10) **CMM Repeatability:** This is the CMM's repeatability, which is a fixed contribution. This value could be obtained from repeated measurements artifacts.

11) **CMM scale Temperature Resolution:** This is a length dependent contribution. This depends also the material of scale.

12) **Probe Uncertainty:** Uncertainty causes from probing which is taken from the certificate of probe manufacturer.

7.2. Application of Uncertainty Budgeting to CMM under Inspection

Table 4 is an uncertainty budget for a CMM measurement. At this budget, the uncertainty of the contributors could be calculated by multiplying the value column with the *sensitivity coefficient* column and dividing with *divisor* column. *Divisors* are extracted from the type of probability distribution (Normal or Rectangular) of uncertainty sources (Look at Figure 2 and 3). For rectangular distribution, the divisor is square root of three.

Table 4: Uncertainty Budgeting For CMM Measurements

Source of Uncertainty	Value (+/-)		Probable Distribution	Divisor	Sensitivity Coeff.	Uncertainty at unit length (microns)	Uncertainty	
	Value	Units				Length Element (per metre)	Fixed	Length Element
Artifact Calibration Uncertainty (Fixed)	0,1	µm	Normal	2,00	1		0,050	
Artifact Calibration Uncertainty (Len Dep.)	1	µm	Normal	2,00	1	0,500		0,200
Artifact Geometry	0,5	µm	Rectangular	1,73	1		0,289	
Artifact Alignment	0,1	µm	Rectangular	1,73	1		0,058	
Artifact thermal expansion coefficient Uncertainty	2,005	Degrees C	Rectangular	1,73	1	1,158		0,463
Thermometer Calibration Uncertainty	0,15	Degrees C	Normal	2,00	11,6	0,870		0,348
CMM Resolution	0,1	µm	Rectangular	1,73	1		0,058	
Artifact Calibration Resolution	0,1	µm	Rectangular	1,73	1		0,058	
Thermometer Resolution	0,1	Degrees C	Rectangular	2,00	11,6	0,580		0,232
Thermometer Uncorrected Errors	0,1	Degrees C	Rectangular	1,73	11,6	0,670		0,268
Probe Uncertainty	0,44	µm	Rectangular	1,73	1		0,254	
CMM scale Temperature Resolution	0,1	Degrees C	Rectangular	2,00	11,6	0,580		0,232
CMM Repeatability	0,5	µm	Rectangular	1,73	1		0,289	
SUM of Uncertainties							0,766	1,511
Enter Longest Bar Length (metres)	0,4							
Enter Indicated Temperature Of Artifact	22							

	Fixed	Length Element	
Combined Uncertainty At K=1	0,494	0,745	Microns
Expanded Uncertainty at K=2	0,987	1,490	Microns

Total Uncertainty=	2,477 Microns

The distributions of all contributors are defined in Probable Distribution column and calculated with respect to the Type A and Type B methods of GUM. As seen in the table, the coefficient of the thermometer based contributors is 11.6, that is the thermal expansion coefficient of the steel and effects of these contributors depend on length. The scale material is also assumed as steel in this budget.

Uncertainty of fixed and length dependent contributors are added individually by using root sum square to calculate the combined uncertainty. After that, expanded uncertainty is acquired by multiplying with k factor 2. And, total uncertainty is obtained by adding the length dependent and fixed part of expanded uncertainty. Total uncertainty for measurement of 400 mm length at the CMM under inspection is approximately 2.5 microns. In reality, this value may not be such a high.

7.3. Evaluation of Uncertainty Budgeting Method

In conclusion, this method can give general idea about uncertainty of CMM and also helps to see the uncertainty contributors in a list manner. However, many contributors of uncertainty such as sampling method, stylus length and working volume effects can not be included and they require specific calculation and experimentations.

CHAPTER 8

EVALUATION OF MEASUREMENT UNCERTAINTY USING COMPARISON METHOD

Comparison method is a direct procedure to obtain the measurement uncertainty of a specific feature. This methodology includes the appropriate combinations of CMM error sources involved in a specific measurement. In this chapter, the theory of comparison method will be explained in detail and then this method will be applied on a CMM.

8.1. Theory of Comparison Method

The comparison method is conducted by inspecting a calibrated artifact which is essentially identical in all respects to the part feature under consideration. Numerous repeated measurements are carried out on the calibrated artifact. These measurements are conducted in exactly the same manner as the actual part measurement [1].
This includes:

- The same location within the work volume
- The same probe and stylus configuration
- The same sampling strategy
- The same fixturing

After the repeated measurements, the standard deviation of the resulting substitute geometry, *e.g.,* the diameter is calculated. The inspected ring gauge diameter has a combined standard uncertainty. This uncertainty is the RSS sum of the standard deviation found from the repeated measurements and the combined standard uncertainty in the diameter calibration certificate of the known ring gauge.

There may be additional uncertainties such as the thermal expansion of both the calibrated artifact and the part. If the same sensor is used to measure artifact and part temperature, then these two sources of uncertainty are highly correlated.

The effect of the part form error upon the measurement is a significant factor while using the comparison method. Most calibrated artifacts have very small form deviations from the ideal geometry. Hence, this factor is not assessed by repeated measurements of the calibrated artifact. If the actual part has significant form error relative to the errors in the CMM, then the actual part measurement will be influenced by the use of a finite sampling strategy in the presence of this form error.

"The effect of form error can be included in either of two ways. A distribution for the form error may be assumed yielding a standard deviation which is then multiplied by the sensitivity coefficient of the sampling strategy used in the measurement" (Bosch, 1995). Totally, the uncertainties below are added in Root Sum of Square (RSS) manner and yielded a combined standard uncertainty for the part measurement.

- Standard deviation which is then multiplied by the sensitivity coefficient of the sampling strategy is used in the measurement.
- Standard deviation of the repeated measurements.
- The combined standard uncertainty in the calibration of the artifact.

More accurately, the standard deviation of the measurement process can include the effect of form error by performing repeated measurements of the actual part with a reorientation of the part (or the sampling strategy) between each measurement; this forces the form error to be included in the measurement variation [1].

8.2. Application of Comparison Method to CMM under Inspection

In thesis study, this process is applied on a CMM as seen below.

For comparison, two ring gauges are used, one of them is manufactured by Federal and has calibration certificate as artifact. The other one is manufactured by Mitutoyo used as measured part and doesn't have calibration certificate . In this case a calibrated 69,6722 mm nominal diameter ring gauge (Federal) is selected as the comparison artifact. The calibrated diameter of the Federal's ring gauge is

D_{artifact_calibrated}= **69,6717 mm**, with a combined standard calibration uncertainty u_c = **0,0012 μm**.

The gauge is measured a total of n_a =**5** times on CMM under inspection, giving a mean measured diameter of **D**_{artifact_mean} = **69,6756 mm**, with a standard deviation of u_a = **0,259 μm**. Hence, estimated uncertainty for this CMM measurement is 0,116 μm, with an uncertainty of u_a /√n_a μrn.

The Mitutoyo's ring gauge as actual part is measured n_p = **5** times. The results are below;

Mean measured diameter ; **D**_{part_mean} = **40,0075 mm**

Standart deviation of repeated measurement; u_p = **0,497 μm**.

This values include form error but a ring gauge with a small form error is measured as a part measurement so nearly the same standard deviation value is obtained with artifact. If part that has a high form error is measured, high standard deviation will be expected with respect to sampling strategy. The total uncertainty is calculated by using the equation (8.10).

Both the artifact (Federal Ring Gage) and the part (Mitutoyo) were corrected for thermal expansion effects using the same temperature sensor which means the uncertainty of the two thermal corrections will be highly correlated. Finally, the task specific uncertainty of part measurement can be formulated as below.

$$L_p = L_o \times (1 + \alpha_p \times (T_p - T_o)) \tag{8.1}$$

$$u_{temp\_p} = \sqrt{(\frac{\partial L_o}{\partial \alpha_p})^2 \times u^2(\alpha_p) + (\frac{\partial L_o}{\partial T})^2 \times u^2(T)} \tag{8.2}$$

$$L_o = \frac{L_p}{(1 + \alpha_p \times (T_p - T_o))} \tag{8.3}$$

$$\frac{\partial L_o}{\partial \alpha_p} = \frac{L_p \times (T_p - T_o)}{(1 + \alpha_p \times (T_p - T_o)^2)} \tag{8.4}$$

$$\frac{\partial L_o}{\partial T_p} = \frac{L_p \times \alpha_p}{(1 + \alpha_p \times (T_p - T_o)^2)} \tag{8.5}$$

Substituting (8.3), (8.4), (8.5) into (8.2) yields (8.6).

$$u_{temp\_p} = \frac{L_p}{(1+\alpha_p \times (T_p - T_0))^2} \times \sqrt{(T_p - T_0)^2 \times u^2(\alpha_p) + \alpha^2{}_p \times u^2(T)} \tag{8.6}$$

Since α_p ($11{,}5 \times 10^{-6}$ m/m $\times$ ^{0}C) is too small with respect to 1.

$$\alpha_p \times (T_p - T_0) \approx 0 \tag{8.7}$$

Recall that,

$$u_{temp\_p} = L_p \times \sqrt{(T_p - T_0)^2 \times u^2(\alpha_p) + \alpha^2{}_p \times u^2(T)} \tag{8.9}$$

$$u_c{}^2 = u_{c\_cal}{}^2 + \frac{u_a{}^2}{n_a} + \frac{u_p{}^2}{n_p} + u_{temp}{}^2 \tag{8.10}$$

$$u_c{}^2 = u_{c\_cal}{}^2 + \frac{u_a{}^2}{n_a} + \frac{u_p{}^2}{n_p} + L_a{}^2 \times (T_a - T_o)^2 \times u^2(\alpha_a) + L_p{}^2 \times (T_p - T_o)^2 \times u^2(\alpha_p) \tag{8.11}$$

$$+(L_a{}^2 \times \alpha_a{}^2 + L_p{}^2 \times \alpha_p{}^2 - 2 \times L_a \times L_p \times \alpha_a \times \alpha_p) \times u^2(T)$$

where

- L_a and L_p are the sizes of artifact and part, *e.g.,* length or diameters,
- α_a and α_p are the thermal expansion coefficients of artifact and part respectively,

  For steel; $\alpha_a = \alpha_p = 11{,}5 \pm 1\ \mu m/m \times°C$

- $u(\alpha_a)$ and $u(\alpha_p)$ are uncertainties of thermal expansion coefficients,

  For steel; $u(\alpha_a) = u(\alpha_p) = 2/\sqrt{3} = 0{,}58\ \mu m/m \times°C$ (Type B Rectangular Uncertainty)

- T_a and T_p are temperature of the artifact and part respectively,
- T_o is the standard temperature, *i.e.,* 20 °C.
- $u(T)$ is the uncertainty of the temperature sensor (thermometer); $u(T) = 0.1$ °C
- u_{c_cal} is the (combined standard) uncertainty in the diameter of the ring gauge.

Finally, u_c is calculated by using equations above.

$u_c = 0{,}309\ \mu m$

8.3. Evaluation of Comparison Method

The disadvantage of the comparison method is the necessity of a similar and calibrated artifact to carry out the procedure. The similarity between the artifact and

part causes high the relevance in the comparison. Measurement of CMM consists of different features, e.g. circle, sphere, cylinder, plane etc, therefore finding a suitable artifact for required measurement is difficult process. Another disadvantage is the numerous measurements required on the artifact in addition to those on the part. Because of these disadvantages, in a production plant, time is a significant parameter of efficiency so that comparison is not appropriate for applying all task specific uncertainty analysis.

Nevertheless, the comparison method is a powerful technique to obtain measurement uncertainty, if an identical but calibrated part is available.

CHAPTER 9

STATISTICAL EVALUATION OF MEASUREMENT UNCERTAINTY BY DESIGNING FRACTIONAL FACTORIAL EXPERIMENT

In this chapter, the measurement uncertainty of CMM will be determined by using experimentation for different measurement combination of contributors and results of experiments will be evaluated statistically. Experiment shall be comprehensive for determination all contributors. With the design of efficient experimentation, the measurement uncertainty of CMM and effects of contributors can be obtained.

9.1. Design of Experiments

This method uses the fractional factorial experimentation approach to investigate the relationship between measurement uncertainty and parameters with a CMM [35, 36]. Experiments are designed according to the type of inspection strategies and uncertainty contributors. These contributors include travel speeds, probe angles, probe sizes and length, sampling strategies and feature sizes. The number of factors may be increased, but if the unimportant factors in affecting the measurement of uncertainty are used, the experiment becomes time consuming, expensive and inefficient.

Table 5: Design Factors for Experimentation.

FACTORS	**LOW**	**HIGH**
PROBE SIZE (Diameter, mm)	2	8
STYLUS LENGTH (mm)	50	100
MEASUREMENT ANGLE	180	360
MEASUREMENT POINT	6	24
SPEED (%)	25	90

To investigate the effect of the five contributors on the measurement uncertainty, a fractional factorial design 2^{5-1} is employed with minimum 3 replicates in the experiment [35]. This resolution V design with a generator I=ABCDE ensures that all the five factors and the six two-factor interaction terms will not be alised with each of themselves. When the factors shown at table above investigated at three probe angle, the experimentation is completed. Fractional factorial design of experiment was ordered by using Matlab related tool (Statistical Toolbox).

Table 6: Experiment Order Table According To the Fractional Factorial Design

	Factors				
Order	Probe Size (Diameter, mm)	Stylus Length (mm)	Meas. Point Number	Speed (%)	Measurement Angle
	A	B	C	D	E
1	2	100	6	25	180
2	2	100	6	90	360
3	2	100	24	25	360
4	2	100	24	90	180
5	2	50	6	25	360
6	2	50	6	90	180
7	2	50	24	25	180
8	2	50	24	90	360
9	8	100	6	25	180
10	8	100	6	90	360
11	8	100	24	25	360
12	8	100	24	90	180
13	8	50	6	25	360
14	8	50	6	90	180
15	8	50	24	25	180
16	8	50	24	90	360

Table 6 represents the order of experiment done for **each** probe angle. There are three probe angles which are defined as Y-Z, X-Z, X-Y Planes, so that 48 experiments shall be done with 3 replications for each one. Finally, the required number of ring gage measurements is 144. The ring gauges were in pristine condition, as they had never been used in production. When investigating the results obtained from the screening experiment, the standard deviation of diameter measurements is used for evaluation. As mentioned before, this method utilizes statistical tools to calculate the affect of each factor on uncertainty. Regression Model and Analysis of Variances (ANOVA) are the procedures to fit and calculate the related effect on results. The theory of ANOVA is below;

Sum of Square (SS) is defined as the amount of variability in the data due to different sources. A and B are the variables that affects the result.

$$SS\_A = b \times n \sum (\overline{x}_i - \overline{x})^2 \tag{9.1}$$

where
  b = Variable number of factor B.
  n = Number of replicates.
  $\overline{x}_i$ = Mean for each A.
  $\overline{x}$ = Grand Mean

$$SS\_B = a \times n \sum (\overline{x}_j - \overline{x})^2 \tag{9.2}$$

where
  a = Variable number of factor A.
  n = Number of replicates.
  $\overline{x}_j$ = Mean for each B.

$$SS\_Total = \sum \sum (\overline{x}_{ij} - \overline{x})^2 \tag{9.3}$$

  $\overline{x}_{ij}$ = Each observation.

$$SS\_A*B = SS\_Total - (SS\_A + SS\_B) \tag{9.4}$$

Degrees of Freedom (DF) measures how much independent information is available to calculate each SS.

$$DF\_A = a\text{-}1 \; ; \; DF\_B = b\text{-}1 \; ; \; DF\_Total = n\text{-}1 \; ; \; DF\_A*B = (a\text{-}1)\times(b\text{-}1) \qquad (9.5)$$

Mean Square (MS) takes into account that different sources have different number of levels or possible levels.

$$MS\_A=\frac{SS\_A}{DF\_A}; \; MS\_B=\frac{SS\_B}{DF\_B} \; ; \; MS\_A*B=\frac{SS\_A*B}{DF\_A*B} \qquad (9.6)$$

P-values are often used in hypothesis tests where you either accept or reject a null hypothesis. The p-value represents the probability of making a Type 1 error, or rejecting the null hypothesis when it is true. The smaller the p-value, the smaller is the probability that you would be making a mistake by rejecting the null hypothesis. A cutoff value often used is 0,05, that is, reject the null hypothesis when the p-value is less than 0,05. The p-value is calculated as "1 - The cumulative distribution function (cdf)."

Regression model constructs an equation that includes all variables with their coefficients. The influence quantities of variables are represented by this fitting procedure.

9.2. Experiments on Ring Gauge

Ordered experimentation in Table 6 is applied on three different measurement planes at CMM under inspection. These planes are Y-Z, X-Z, X-Y planes of machine coordinate system and requires the use different probe angles for ordered measurements. CMM uses a Renishaw TP7M probe and its specifications can be seen in the appendices. In addition, in this chapters all the undefined units are millimetres.

9.2.1. Ring Diameter Measurement in Y-Z Plane

Figure 41 indicates the first application which is the measurement of ring gauge in Y-Z plane of machine coordinate system and Table 7 gives the results of the repeated measurements for this experiment.

Figure 41: A View of Ring Measurement in Y-Z Plane

Table 7: Experimental Results for Y-Z Plane

Order	Probe Size (Diameter, mm) A	Stylus Length (mm) B	Meas. Point Number C	Speed (%) D	Measurement Angle E	MEASUREMENT RESULTS (ACTUAL, 4 REPLICATION) 1	2	3	4	Standard Deviation	Uncertainty (mm)
1	2	100	6	25	180	40,005	40,006	40,004	40,006	0,000957	0,0004787
2	2	100	6	90	360	40,005	40,005	40,005	40,005	0	0
3	2	100	24	25	360	40,007	40,007	40,007	40,007	0	0
4	2	100	24	90	180	40,001	40,008	40,005	40,008	0,003317	0,0016583
5	2	50	6	25	360	40,007	40,007	40,007	40,007	0	0
6	2	50	6	90	180	40,005	40,009	40,007	40,009	0,001915	0,0009574
7	2	50	24	25	180	40,002	40,01	40,007	40,009	0,003559	0,0017795
8	2	50	24	90	360	40,009	40,009	40,009	40,009	0	0
9	8	100	6	25	180	40,009	40,007	40,008	40,008	0,000816	0,0004082
10	8	100	6	90	360	40,008	40,009	40,009	40,009	0,0005	0,00025
11	8	100	24	25	360	40,009	40,009	40,009	40,009	0	0
12	8	100	24	90	180	40,011	40,008	40,011	40,008	0,001732	0,000866
13	8	50	6	25	360	40,007	40,008	40,008	40,008	0,0005	0,00025
14	8	50	6	90	180	40,006	40,007	40,006	40,007	0,000577	0,0002887
15	8	50	24	25	180	40,003	40,009	40,007	40,009	0,002828	0,0014142
16	8	50	24	90	360	40,007	40,008	40,008	40,008	0,0005	0,00025

Table 8: Analysis of Variance for the Screening Experiment.

```
----------------------------------------------------------------------------------------------------------------------------------------
General Linear Model: Uncertainty versus Probe Diamet; Stylus Lengt; ...

Factor              Type    Levels  Values
Probe Diameter      random    2     2; 8
Stylus Length       random    2     50; 100
Point Number        random    2     6; 24
Measurement Speed   random    2     25; 90
Measurement Angle   random    2     180; 360
Analysis of Variance for Uncertainty, using Adjusted SS for Tests
Source                          DF    Seq SS     Adj SS     Adj MS      F
Probe Diameter                   1  0,0000001  0,0000001  0,0000001    **
Stylus Length                    1  0,0000001  0,0000001  0,0000001    **
Point Number                     1  0,0000007  0,0000007  0,0000007    **
Measurement Speed                1  0,0000000  0,0000000  0,0000000    **
Measurement Angle                1  0,0000032  0,0000032  0,0000032   2,33
Probe Diameter*Point Number      1  0,0000000  0,0000000  0,0000000    **
Probe Diameter*Measurement Angle 1  0,0000004  0,0000004  0,0000004    **
Point Number*Measurement Angle   1  0,0000009  0,0000009  0,0000009    **
Probe Diameter*Point Number*     1  0,0000000  0,0000000  0,0000000    **
  Measurement Angle
Probe Diameter*Stylus Length     1  0,0000000  0,0000000  0,0000000    **
Stylus Length*Point Number       1  0,0000000  0,0000000  0,0000000    **
Error                            4  0,0000002  0,0000002  0,0000000
Total                           15  0,0000056

S = 0,000216902   R-Sq = 96,66%   R-Sq(adj) = 87,46%
Term                                     Coef   SE Coef      T      P
Constant                              0,000538  0,000054   9,91  0,001
Probe Diameter
2                                     0,000072  0,000054   1,32  0,257
Stylus Length
 50                                   0,000080  0,000054   1,47  0,215
Point Number
 6                                   -0,000208  0,000054  -3,84  0,018
Measurement Speed
25                                    0,000004  0,000054   0,07  0,948
Measurement Angle
180                                   0,000444  0,000054   8,18  0,001
Probe Diameter*Point Number
2         6                          -0,000042  0,000054  -0,77  0,484
Probe Diameter*Measurement Angle
2         180                         0,000165  0,000054   3,05  0,038
Point Number*Measurement Angle
 6        180                        -0,000240  0,000054  -4,42  0,012
Probe Diameter*Point Number*Measurement
Angle
2         6          180             -0,000011  0,000054  -0,19  0,856
Probe Diamet*Stylus Lengt
2         50                         -0,000005  0,000054  -0,09  0,932
Stylus Length*Point Number
 50       6                          -0,000035  0,000054  -0,65  0,554
```

Minitab ANOVA results of experiment are presented in Table 8. This experiment has been done on the Y-Z plane of machine by measuring a ring gauge. Based on the P values in the last column of regression model, the impacts of the main factor can be evaluated according to the commonly used alpha level of 0.05 (Null Hypothesis). If the P value of factor is higher than 0.05 and it is concluded that factor

does not have significant impact on the uncertainty. In contrast, for P values lower than 0.05, that factor has significant impact on the uncertainty.

When Table 8 is evaluated, the factors can be classified from the most significant to the least one. Variable Analysis of the experiment presents that point number and measurement angle have significant effect on the uncertainty. After that, the probe diameter and stylus length take the second importance level. Finally, the probe speed has the least significance impact on the uncertainty. Also, the interactions of factors can be evaluated such as, with no surprise, interaction of point number and measurement angle has the most significant effect on the results. The least important interaction is the probe diameter and stylus length.

After the evaluations of factor effects level with respect to each other, it is time to define how the internal change of factors effect the uncertainty. Figure 42 indicates the main effect plot of factors at Y-Z Plane.
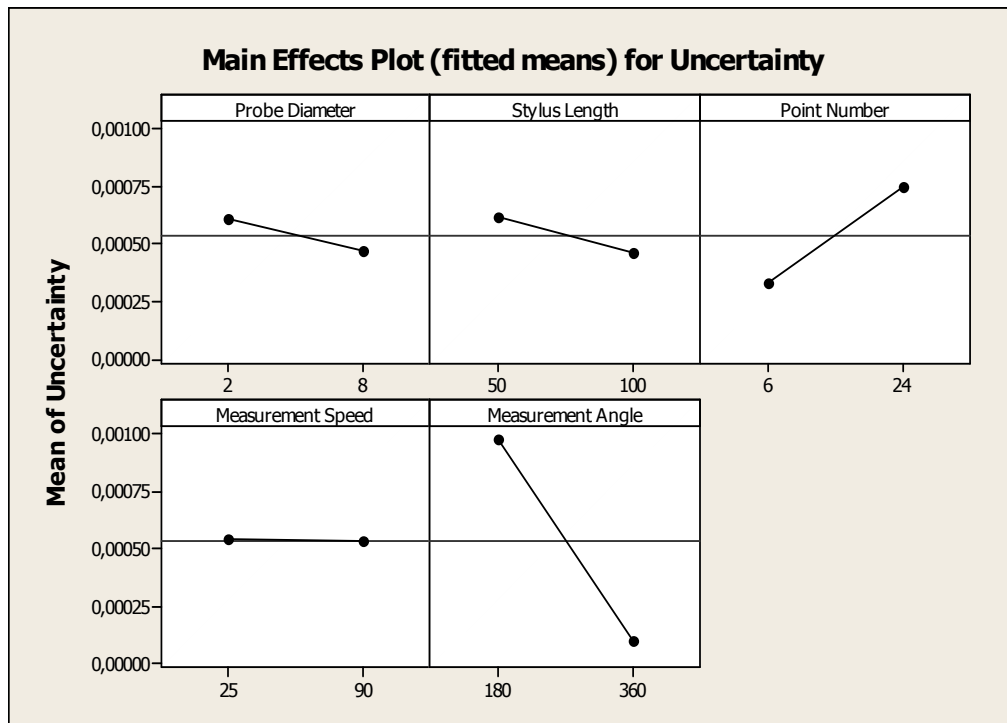
Figure 42: Main Effect Plot of Factors in Y-Z Plane

84

For experiment on X plane, low probe diameter (D=2 mm) causes to increase the uncertainty and high probe diameter (D=8 mm) decreases the measurement uncertainty. It is because of low probe diameter is vulnerable to surface defects and this vulnerability causes to obtain the different point coordinate and low repeatability. Stylus length results are very surprising that 50 mm stylus gives high uncertainty and opposite results are obtained for long stylus (100 mm). Third factor is point number and it has direct effect on results. When the point number is high (24 point), the uncertainty value is high especially for the partial coverage of circle. As seen in the chart, measurement speed is almost same and has low effect on the uncertainty. Finally, 180 degree measurements cause very high uncertainty. On the other hand, full coverage of ring (360 degree) decreases the measurement uncertainty.

At this evaluation, measurement bias, which is the difference between the mean value of the measurements and the calibrated value, is not inspected because another experimentation will be done for different angle measurements and the bias error can be seen easily.
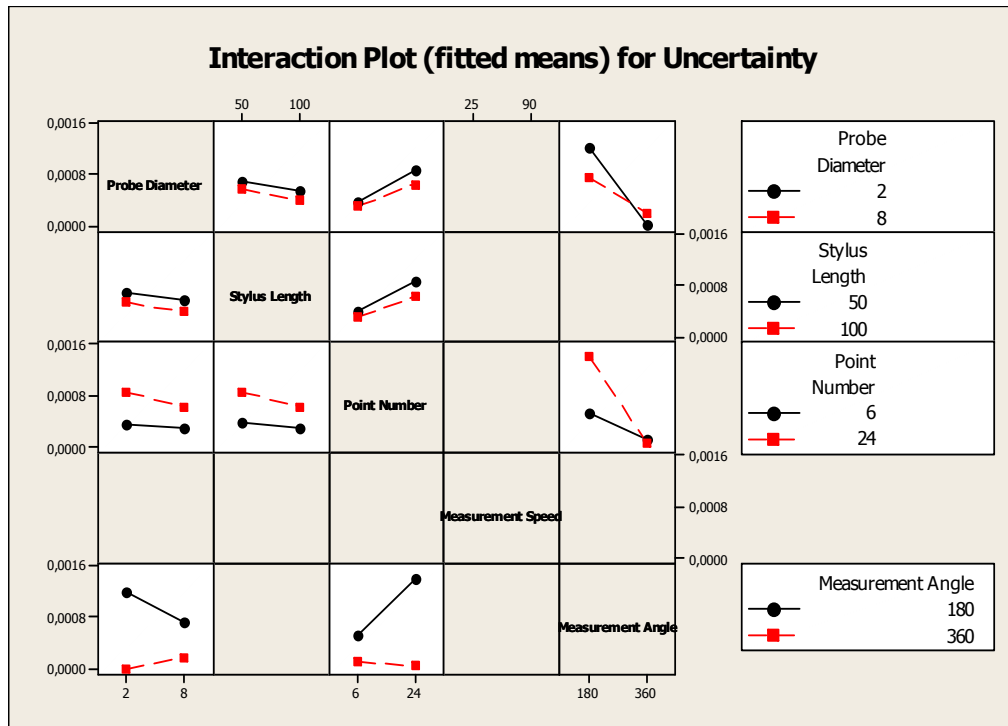
Figure 43: Interaction Plot of Ring Measurement Uncertainty in Y-Z Plane

Interaction plot guides about the correlated effects of the factors to the uncertainty. For example, looking at first column, in general low diameter of probe causes higher uncertainty than high diameter one. The only exception is the interaction with 360 degree coverage that results in higher uncertainty with using high diameter probes. In other words, for 180 degree coverage, small probe diameter gives high uncertainty and big diameter causes low uncertainty; for full coverage, measurement with small probe diameter is concluded low uncertainty and big diameter causes high uncertainty.

The other important observation is that the point number has inverse effect with respect to the measurement angle. Looking at the third column, in general measurement with low point number results in low uncertainty and high point number causes high uncertainty. The only exception is the interaction with 360 degree coverage that results high uncertainty with using low point number.

9.2.2. Ring Diameter Measurement in X-Z Plane

Figure 44 indicates the measurement of ring gauge on X-Z plane of machine coordinate system and Table 9 gives the results of the repeated measurements for this experiment.
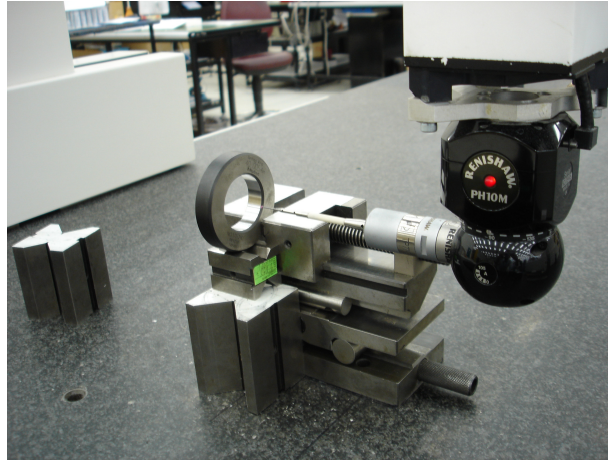
Figure 44: A View of Ring Measurement in X-Z Plane

Table 9: Experimental Results for X-Z Plane.

Order	Probe Size (Diameter, mm)	Stylus Length (mm)	Meas. Point Number	Speed (%)	Measurement Angle	MEASUREMENT RESULTS (ACTUAL, 4 REPLICATION)				Uncertainty (mm)
	A	B	C	D	E	1	2	3	4	
1	2	100	6	25	360	40,007	40,008	40,007	40,008	0,0002887
2	2	100	6	90	180	40,007	40,005	40,006	40,005	0,0004787
3	2	100	24	25	180	40,006	40,004	40,006	40,005	0,0004787
4	2	100	24	90	360	40,008	40,008	40,008	40,008	0
5	2	50	6	25	180	40,006	40,007	40,006	40,007	0,0002887
6	2	50	6	90	360	40,006	40,006	40,006	40,007	0,00025
7	2	50	24	25	360	40,008	40,008	40,009	40,008	0,00025
8	2	50	24	90	180	40,001	40,006	40,002	40,007	0,001472

Table 9 (Continued)

9	8	100	6	25	360	40,003	40,003	40,004	40,004	0,0002887
10	8	100	6	90	180	40,006	40,006	40,008	40,006	0,0005
11	8	100	24	25	180	40,007	40,005	40,008	40,005	0,00075
12	8	100	24	90	360	40,004	40,004	40,004	40,005	0,00025
13	8	50	6	90	360	40,007	40,008	40,007	40,007	0,00025
14	8	50	6	25	180	40,005	40,004	40,004	40,005	0,0002887
15	8	50	24	25	360	40,007	40,008	40,008	40,008	0,00025
16	8	50	24	90	180	40,003	40,005	40,002	40,006	0,0009129

Table 10: Output of ANOVA for X-Z Plane

```
-----------------------------------------------------------------------------------------------------------------------------
 General Linear Model: Uncertainty versus Probe Diamet; Stylus Lengt; ...

Factor              Type    Levels  Values
Probe Diameter      random     2    2; 8
Stylus Length       random     2    50; 100
Point Number        random     2    6; 24
Measurement Speed   random     2    25; 90
Measurement Angle   random     2    180; 360

Analysis of Variance for Uncertainty, using Adjusted SS for Tests
Source                           DF    Seq SS     Adj SS     Adj MS   F  P
Probe Diameter                    1  0,0000000  0,0000000  0,0000000  **
Stylus Length                     1  0,0000001  0,0000001  0,0000001  **
Point Number                      1  0,0000002  0,0000002  0,0000002  **
Measurement Speed                 1  0,0000001  0,0000001  0,0000001  **
Measurement Angle                 1  0,0000007  0,0000007  0,0000007  **
Probe Diameter*Point Number       1  0,0000000  0,0000000  0,0000000  **
Probe Diameter*Measurement Angle  1  0,0000000  0,0000000  0,0000000  **
Point Number*Measurement Angle    1  0,0000004  0,0000004  0,0000004  **
Probe Diameter*Stylus Length      1  0,0000001  0,0000001  0,0000001  **
Stylus Length*Point Number        1  0,0000002  0,0000002  0,0000002  **
Error                             4  0,0000001  0,0000001  0,0000000
Total                            15  0,0000019


S = 0,000182649   R-Sq = 92,81%   R-Sq(adj) = 73,05%
Term                                         Coef   SE Coef      T      P
Constant                                  0,000437  0,000046   9,58  0,001
Probe Diamet
2                                         0,000001  0,000046   0,02  0,983
Stylus Length
 50                                       0,000058  0,000046   1,27  0,273
Point Number
 6                                       -0,000108  0,000046  -2,37  0,077
Measurement Speed
25                                       -0,000077  0,000046  -1,68  0,168
Measurement Angle
180                                       0,000209  0,000046   4,57  0,010
Probe Diamet*Point Number
2          6                             -0,000004  0,000046  -0,08  0,939
Probe Diamet*Measurement Angle
2        180                              0,000032  0,000046   0,71  0,519
Point Number*Measurement Angle
 6        180                            -0,000149  0,000046  -3,26  0,031
Probe Diamet*Point Number*Measurement Angle
2          6        180                  -0,000035  0,000046  -0,77  0,487
Probe Diamet*Stylus Length
2         50                              0,000069  0,000046   1,51  0,206
Stylus Lengt*Point Number
 50         6                            -0,000118  0,000046  -2,58  0,061

-----------------------------------------------------------------------------------------------------------------------------
```
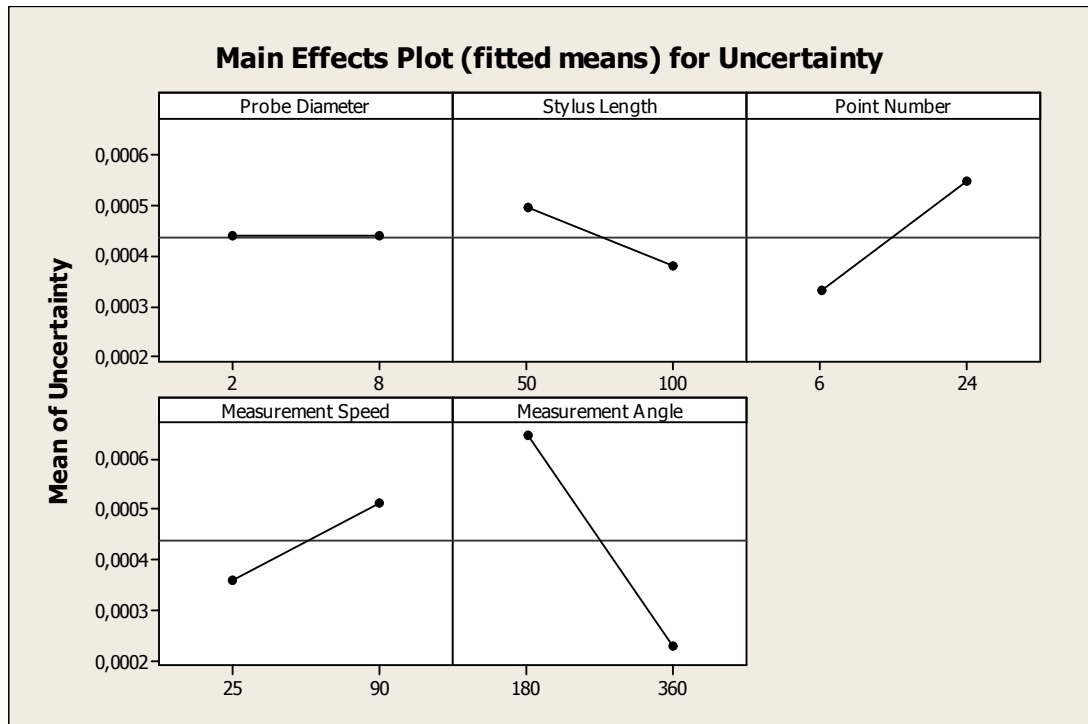
Figure 45: Main Effect Plot of Factors in X-Z plane

Figure 45 represents the main effect plots of measurements at X-Z Plane which are nearly same with the plots of measurements at Y-Z plane in terms of measurement angle and point number. The first difference that takes attention is the low effect of probe diameter change. Also measurement speed at X-Z plane has more significant impact than the measurement at Y-Z plane. The reason of this is the pretravel effect of probe. High measurement speed causes high uncertainty. At this experiment, change of the probe diameter has no effect on the measurement uncertainty. The other surprising effect, same with the first experiment, is that long stylus causes lower measurement uncertainty than short stylus.
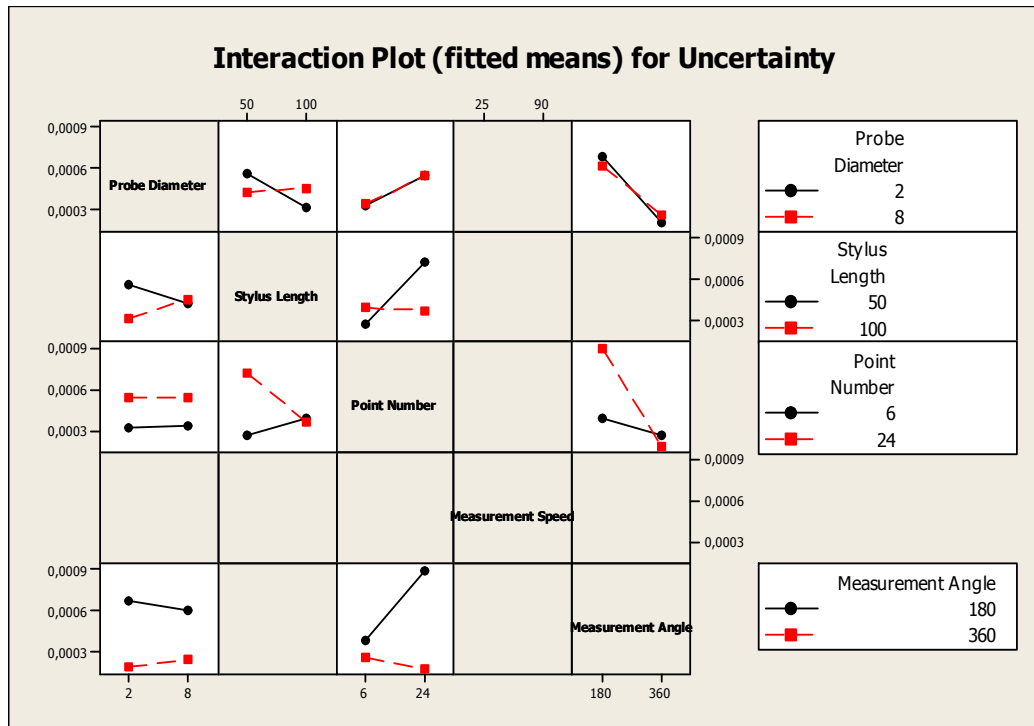
Figure 46: Interaction Plot of Uncertainty in X-Z Plane

Figure 46 indicates the interaction plots of measurements at X-Z plane which are almost the same with the plots of measurements at Y-Z Plane. Looking at the second column of the matrix, it can be easily seen that the high stylus length prone to increase the uncertainty with interaction of low point number. Also, interaction of high probe diameter and long stylus gives high uncertainty which is an unexpected results. On the other hand, Figure 46 represents that high point number increases the uncertainty with interaction of short stylus.

9.2.3. Ring Diameter Measurement in X-Y Plane

Figure 47 indicates the measurement of ring gauge on X-Y plane of machine coordinate system and Table 11 gives the results of the repeated measurements for this experiment.
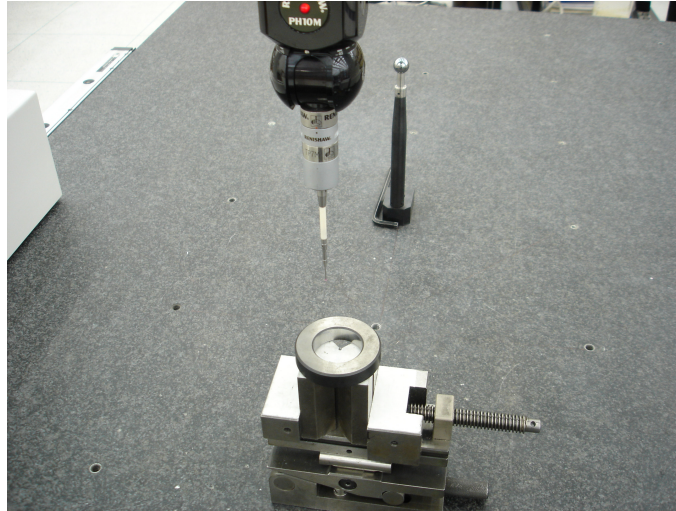
Figure 47: A View of Ring Measurement in X-Y Plane

Table 11: Experimental Results for X-Y Plane

Order	Probe Size (Diameter, mm)	Stylus Length (mm)	Meas. Point Number	Speed (%)	Measurement Angle	MEASUREMENT RESULTS (ACTUAL, 4 REPLICATION)				Uncertainty
	A	B	C	D	E	1	2	3	4	(mm)
1	2	100	6	25	360	40,004	40,003	40,004	40,003	0,0002887
2	2	100	6	90	180	39,996	39,999	39,999	40,000	0,0008660
3	2	100	24	25	180	40,002	40,003	40,003	40,003	0,0002500
4	2	100	24	90	360	40,002	40,003	40,003	40,003	0,0002500
5	2	50	6	25	180	40,005	40,005	40,005	40,004	0,0002500
6	2	50	6	90	360	40,005	40,004	40,005	40,004	0,0002887
7	2	50	24	25	360	40,006	40,006	40,006	40,006	0,0000000
8	2	50	24	90	180	40,005	40,006	40,004	40,005	0,0004082
9	8	100	6	25	360	40,008	40,007	40,007	40,008	0,0002887
10	8	100	6	90	180	40,005	40,006	40,005	40,006	0,0002887
11	8	100	24	25	180	40,005	40,006	40,005	40,005	0,0002500
12	8	100	24	90	360	40,005	40,005	40,006	40,006	0,0002887
13	8	50	6	90	360	40,005	40,005	40,005	40,005	0,0000000
14	8	50	6	25	180	40,006	40,006	40,007	40,006	0,0002500
15	8	50	24	25	360	40,006	40,006	40,006	40,006	0,0000000
16	8	50	24	90	180	40,008	40,008	40,008	40,007	0,0002500

91

Table 12: Output of ANOVA for X-Y Plane.

```
---------------------------------------------------------------------------------------------------------------------------------
General Linear Model: Uncertainty versus Probe Diamet; Stylus Lengt; ...
Factor              Type    Levels  Values
Probe Diameter      random     2    2; 8
Stylus Length       random     2    50; 100
Point Number        random     2    6; 24
Measurement Speed   random     2    25; 90
Measurement Angle   random     2    180; 360
Analysis of Variance for Uncertainty, using Adjusted SS for Tests
Source                            DF     Seq SS      Adj SS      Adj MS    F  P
Probe Diameter                     1   0,0000001   0,0000001   0,0000001   **
Stylus Length                      1   0,0000001   0,0000001   0,0000001   **
Point Number                       1   0,0000000   0,0000000   0,0000000   **
Measurement Speed                  1   0,0000001   0,0000001   0,0000001   **
Measurement Angle                  1   0,0000001   0,0000001   0,0000001   **
Probe Diameter*Point Number        1   0,0000000   0,0000000   0,0000000   **
Probe Diameter*Measurement Angle   1   0,0000000   0,0000000   0,0000000   **
Point Number*Measurement Angle     1   0,0000000   0,0000000   0,0000000   **
Probe Diameter*Point Number*       1   0,0000000   0,0000000   0,0000000   **
  Measurement Angle
Probe Diameter*Stylus Length       1   0,0000000   0,0000000   0,0000000   **
Stylus Length*Point Number         1   0,0000000   0,0000000   0,0000000   **
Error                              4   0,0000001   0,0000001   0,0000000
Total                             15   0,0000006
S = 0,000171113   R-Sq = 80,37%   R-Sq(adj) = 26,38%
Term                                         Coef   SE Coef       T      P
Constant                                  0,000264  0,000043   6,16  0,004
Probe Diameter
2                                         0,000062  0,000043   1,44  0,223
Stylus Length
 50                                      -0,000083  0,000043  -1,93  0,125
Point Number
 6                                        0,000051  0,000043   1,20  0,295
Measurement Speed
25                                       -0,000066  0,000043  -1,55  0,195
Measurement Angle
180                                       0,000088  0,000043   2,06  0,109
Probe Diameter*Point Number
2          6                              0,000047  0,000043   1,09  0,337
Probe Diameter*Measurement Angle
2          180                            0,000030  0,000043   0,71  0,517
Point Number*Measurement Angle
 6         180                            0,000011  0,000043   0,25  0,817
Probe Diameter*Point Number*Measurement Angle
2          6          180                 0,000006  0,000043   0,13  0,900
Probe Diameter*Stylus Length
2          50                            -0,000006  0,000043  -0,13  0,900
Stylus Length*Point Number
 50        6                             -0,000035  0,000043  -0,82  0,457
```

The important result is that the highest bias error is obtained from the configuration of experiment number 2 at Table 11. This configuration consists of the small probe size, long stylus, low measurement number, high measurement speed and low coverage (measurement angle).
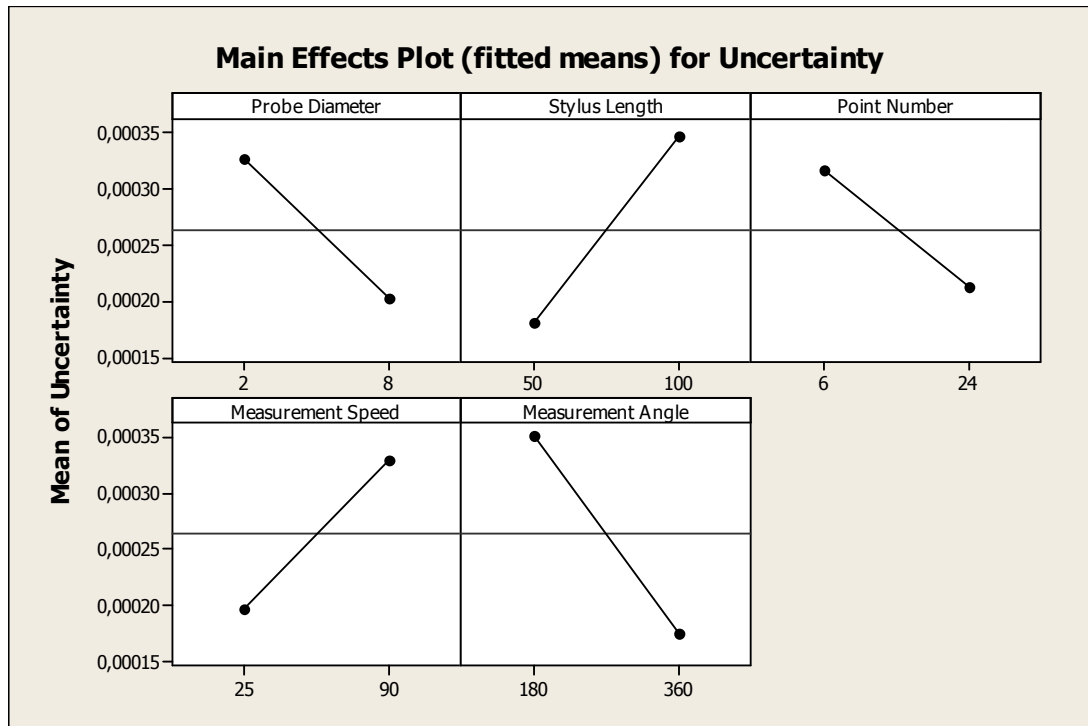
Figure 48: Main Effects Plot of Factors in X-Y Plane

Main effects plot of measurements at X-Y Plane shown in Figure 48 represents two different results from the plots obtained before. One of them is the point number effect on the uncertainty. Measurements with using 24 points are concluded lower uncertainty than measurement with using 6 points. Actually, this effect of point number on result can be envisioned before the experiment, but after the experimentation, it is seen that the probe angle changes the effect of point number and expectations.

The other difference is the effect of stylus length on the uncertainty. At the Y-Z and X-Z plane experimentation, in general long stylus causes less uncertainty than short stylus and actually this is not a foresighted result. However, at the X-Y plane experimentation, long stylus causes more uncertainty than short stylus which is an expected result. The interaction plot of contributors on X-Y plane can be seen in Figure 49.
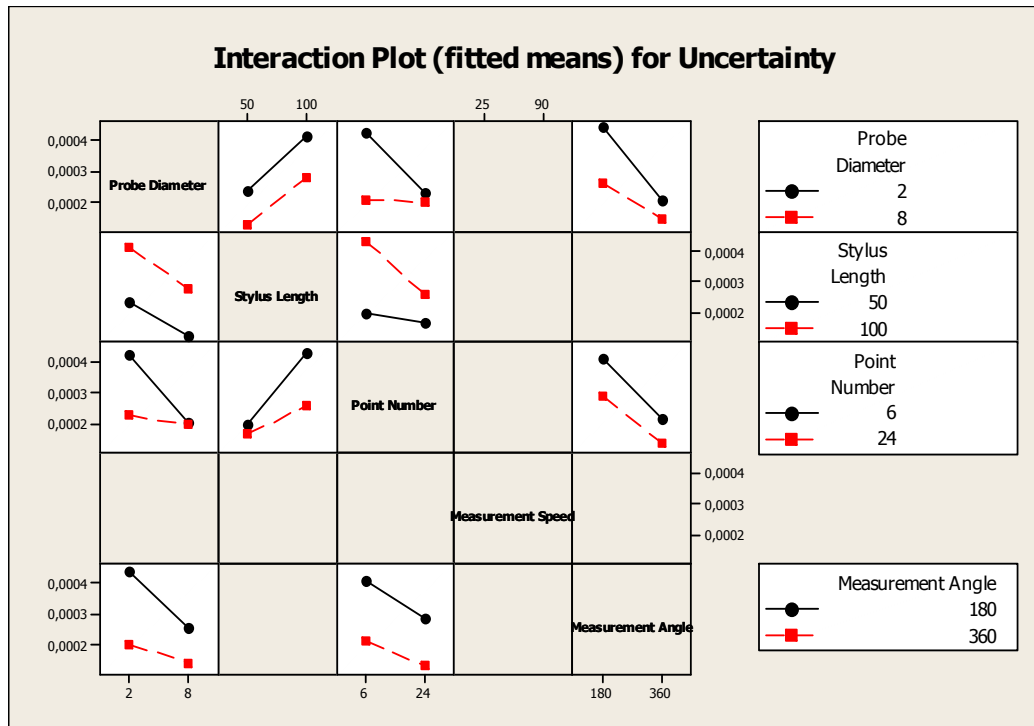
Figure 49: Interaction Plot of Uncertainty in X-Y Plane

9.3. Evaluation of Design of Experiment

In this experimentation, the effect of each uncertainty contributor can be evaluated and the difference between expectations and real effects could be clarified. Interaction plot of measurements at X-Y plane implies that this probe angle is the most predictable and stable one. This means that for example, long stylus gives high uncertainty with all interactions and it is opposite for short stylus. In addition, big probe diameter causes low measurement uncertainty. Also, low uncertainty is obtained from measuring full coverage of ring surface with interactions of all other contributors.

To see the whole picture of the measurement process, it is necessary to look at Table 13.

Table 13: Complete Experimentation Table

Standart Order	Probe Size (Diameter, mm)	Stylus Lenght (mm)	Probe Angle (Y-Z,X-Z, X-Y Plane)	Meas. Point Number	Speed (%)	Measurement Angle	STANDARD DEV.	UNCERTAINTY
	A	B	C	D	E	F		
1	2	100	1	6	25	180	0,000957427	0,000478714
2	2	100	1	6	90	360	0	0
3	2	100	1	24	25	360	0	0
4	2	100	1	24	90	180	0,003316625	0,001658312
5	2	100	2	6	25	360	0,00057735	0,000288675
6	2	100	2	6	90	180	0,000957427	0,000478714
7	2	100	2	24	25	180	0,000957427	0,000478714
8	2	100	2	24	90	360	0	0
9	2	100	3	6	25	360	0,00057735	0,000288675
10	2	100	3	6	90	180	0,001732051	0,000866025
11	2	100	3	24	25	180	0,0005	0,00025
12	2	100	3	24	90	360	0,0005	0,00025
13	2	50	1	6	25	360	0	0
14	2	50	1	6	90	180	0,001914854	0,000957427
15	2	50	1	24	25	180	0,003559026	0,001779513
16	2	50	1	24	90	360	0	0
17	2	50	2	6	25	180	0,00057735	0,000288675
18	2	50	2	6	90	360	0,0005	0,00025
19	2	50	2	24	25	360	0,0005	0,00025
20	2	50	2	24	90	180	0,00294392	0,00147196
21	2	50	3	6	25	180	0,0005	0,00025
22	2	50	3	6	90	360	0,00057735	0,000288675
23	2	50	3	24	25	360	0	0
24	2	50	3	24	90	180	0,000816497	0,000408248
25	8	100	1	6	25	180	0,000816497	0,000408248
26	8	100	1	6	90	360	0,0005	0,00025
27	8	100	1	24	25	360	0	0
28	8	100	1	24	90	180	0,001732051	0,000866025
29	8	100	2	6	25	360	0,00057735	0,000288675
30	8	100	2	6	90	180	0,001	0,0005
31	8	100	2	24	25	180	0,0015	0,00075

Table 13: (Continued)

32	8	100	2	24	90	360	0,0005	0,00025
33	8	100	3	6	25	360	0,00057735	0,000288675
34	8	100	3	6	90	180	0,00057735	0,000288675
35	8	100	3	24	25	180	0,0005	0,00025
36	8	100	3	24	90	360	0,00057735	0,000288675
37	8	50	1	6	25	360	0,0005	0,00025
38	8	50	1	6	90	180	0,00057735	0,000288675
39	8	50	1	24	25	180	0,002828427	0,001414214
40	8	50	1	24	90	360	0,0005	0,00025
41	8	50	2	6	90	360	0,0005	0,00025
42	8	50	2	6	25	180	0,00057735	0,000288675
43	8	50	2	24	25	360	0,0005	0,00025
44	8	50	2	24	90	180	0,001825742	0,000912871
45	8	50	3	6	90	360	0	0
46	8	50	3	6	25	180	0,0005	0,00025
47	8	50	3	24	25	360	0	0
48	8	50	3	24	90	180	0,0005	0,00025

According to the results of experiments, in conclusion;

1) The highest uncertainty value is obtained from the measurement taken from the semi circle with using low probe diameter and 24 points. (Look at Experiment 15)

2) In general, measurements taken from semi circle result in high uncertainty values. In other words, the lowest uncertainties are obtained from the full coverage of ring surface.

3) Rows marked have the highest uncertainties. Looking at these rows, three of four measurements are done with the 2 mm probe.

4) This experimentation shows that the highest uncertainty of diameter measurement of CMM under inspection is 0,00178 mm for ring gauge measurement.

5) When looking at the average of uncertainty values at different probe angles, it can be seen that the lowest average, nearly half of the other angle's, is obtained at X-Y plane. (Look at the table 14) The main reason of this is pretravel effect at probes because at Y-Z and X-Z plane measurements, probe

is horizontal and effected by g force and length of stylus. These effects cause changes in the pretravel length and increase the uncertainty value.

Table 14: Average Uncertainty of Different Angles

Probe Angle	Average Uncertainty
Y-Z Plane	0,00054
X-Z Plane	0,00044
X-Y Plane	0,00026

To confirm the results of the experiments, factor of measurement angle is evaluated in detail. Table 15 and Figure 50 indicate the 4 different angle measurement of ring gage whose calibration diameter is 40,005 mm, with using 2mm diameter probe, 50 mm stylus and 24 points at X-Y plane. The results are useful to quantify uncertainty values and evaluate the measurement bias with respect to coverage angle. As predicted, low angle causes high uncertainty and also high bias error, and therefore to obtain measurement with low uncertainty and bias error, minimum 270 degree circular coverage is needed.

Table 15: Uncertainty Calculation of Four Different Angle Measurements (LK G80)

Angle =	90	180	270	360
1	40,008	40,005	40,004	40,005
2	40,019	40,004	40,004	40,004
3	40,004	40,006	40,004	40,004
4	40,016	40,004	40,004	40,004
Uncertainty=	0,003473	0,000479	0	0,00025

97
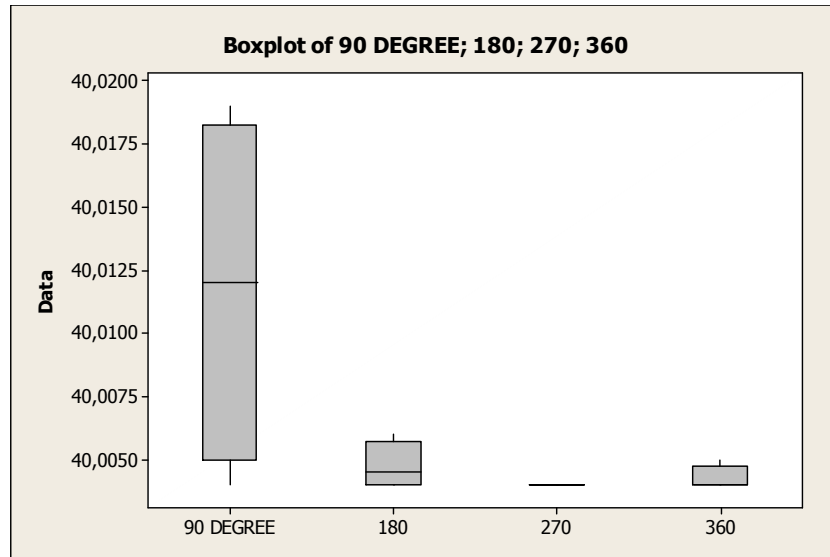
Figure 50: Box Plot of Table 15

Table 16 and Figure 51 represent another confirmation experiment with different machine that has lower accuracy.

Table 16: Uncertainty Calculation of Four Different Angle Measurements at another CMM (LK G90)

Angle (Degree) =	90	180	270	360
1	39,9869	40,0076	40,008	40,0085
2	39,9785	40,0075	40,0083	40,009
3	39,9918	40,009	40,0075	40,0093
4	39,98	40,0075	40,0076	40,0087
Uncertainty(mm)	0,003098	0,000367	0,000185	0,000175
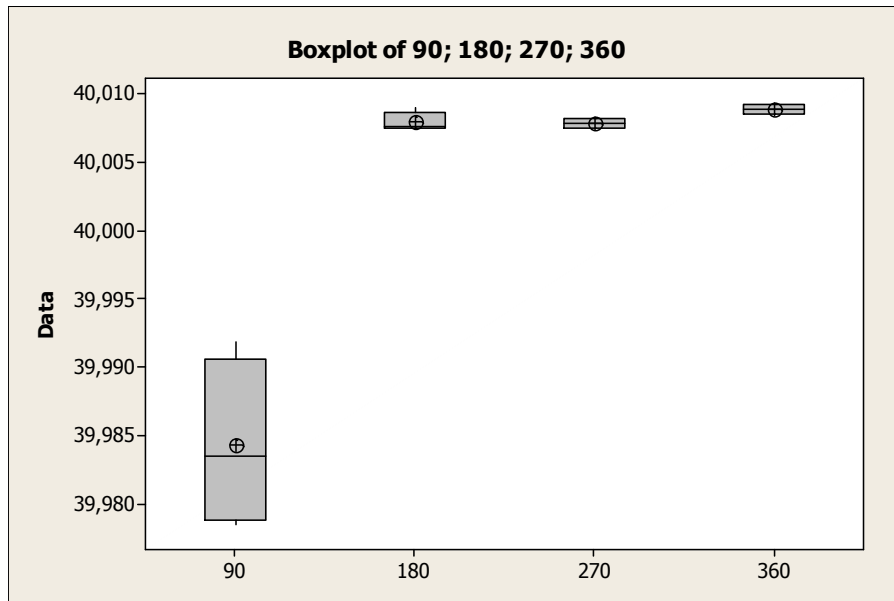
Figure 51: Box Plot of Table 16

9.4. Mapping of Uncertainty in Measurement for CMM under Inspection

Similar to the error mapping of machine, the uncertainty mapping can be obtained by using repeated gauge measurements at different place of machine working volume. Table 17 indicates the results of the ring gauge measurements at the different place of machine. Z axis column implies that the maps are formed at the same elevation (Z=- 560 mm) where are on the machine granite table. All the coordinates are taken in machine coordinate system (MCS).

Table 17: Uncertainty Map Table of CMM Studied

X Axis	Y Axis	Z Axis	Diameter Uncertainty	X Axis Uncertainty	Y Axis Uncertainty
54	40	-560	0,000131	0,0000871	0,0000812
43	593	-560	0,000115	0,0000632	0,00002
384	619	-560	0,000073	0,000115	0,000132
435	41	-560	0,000086	0,00006	0,0000748
850	21	-560	0,000086	0,000086	0,0000509
872	462	-560	0,00008	0,0000547	0,00016
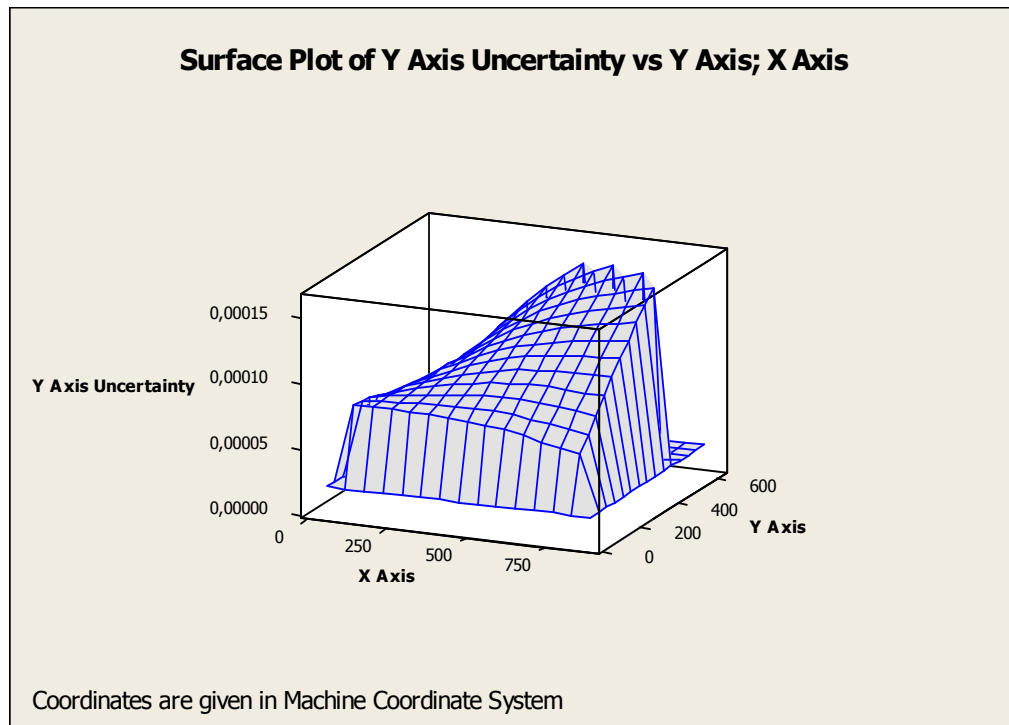
Figure 52: Y Axis Uncertainty Map of CMM under Inspection
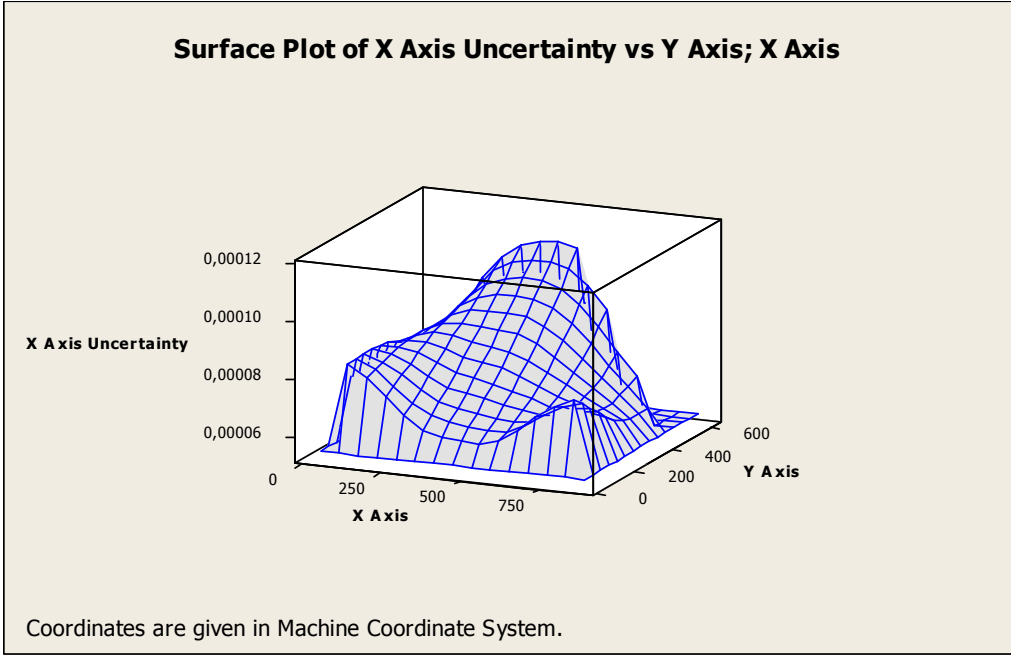
Figure 53: X Axis Uncertainty Map of CMM under Inspection
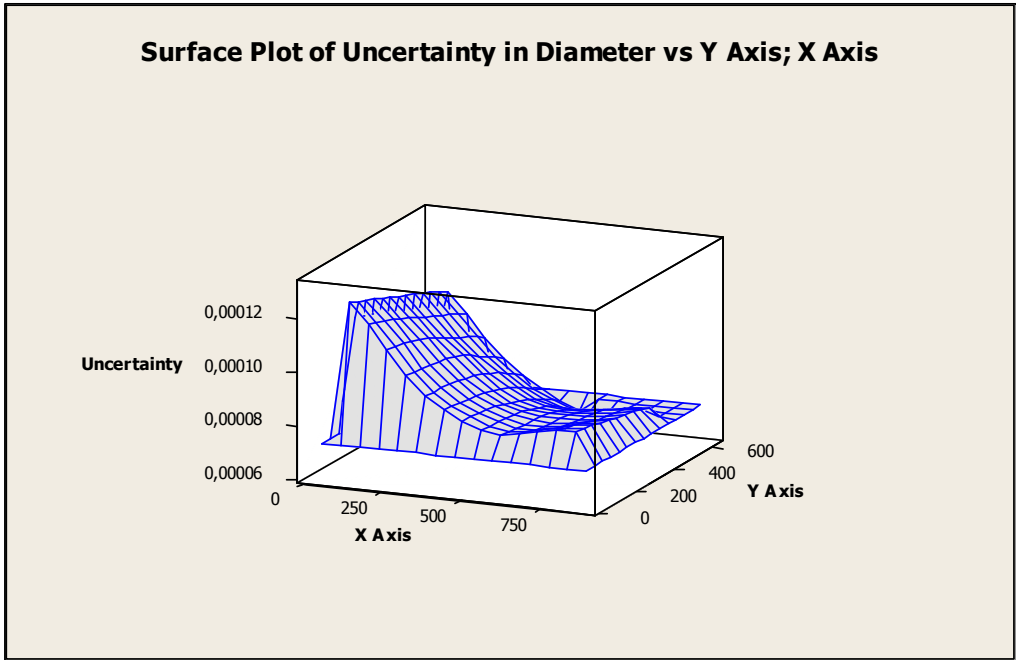
Figure 54: Map of Uncertainty in Diameter Measurement for CMM under Inspection

The surface plot of diameter uncertainty implies that back side of machine has higher uncertainty than front side. Also, diameter uncertainty decreases along Y axis from 0 mm to 650 mm. Uncertainties of X and Y Axis represent different profile at different position of machine volume.

The other important conclusion is that comparing the laser error map and ring gauge uncertainty map, there is a relation between the X axis error and uncertainty maps. At the right side of the machine, close to the X axis drive system, there are high error and uncertainty at X axis. In addition of this, there is another relation between the volumetric error and diameter uncertainty maps. Along the Y axis when closing to the outer leg, there are high volumetric error and diameter uncertainty.

CHAPTER 10

UNCERTAINTY EVALUATION OF CMM MEASUREMENT BY USE OF
MULTIPLE MEASUREMENT STRATEGIES OF ARTIFACTS: HYBRID
METHOD

In this chapter, multiple measurement strategies of artifacts (repeatability and reproducibility tests) will be explained. This method is a widely used indicator for the variability of CMM measurements and known as hybrid of the methods explained before. For example, the comparison method can be used to determine task-specific measurement uncertainty since it includes all error sources relevant to the measurement *under consideration*, whereas multiple measurement strategies of artifacts usually focus on measurement variation that depends on different contributors which is resemble the statistical evaluation method.

10.1.   Theory of Hybrid Method

From hybrid point of view, if the location and orientation of the part within the CMM work zone is not specified, then the multiple measurement strategies should vary both the location and orientation over all positions that might be practically realized during production measurements. Sampling strategy is another significant factor as mentioned before so that different sampling strategies will be evaluated to cover the real measurements. Even simple factors, such as the allowable probe and stylus configurations, must be stated since this can have a substantial impact on the measurement results. The standard deviation of the repeated measurements is described as the type A uncertainty.

The main principle of this method is to carry out the measurement on the artifact several times, varying the measurement conditions such as "distribution of measuring points" and "artifact orientation on the CMM". This requirements implies that some experimentation is needed to integrate the contributors and this is similar with method at Chapter 9. The main difference between two methods is the aim. Statistical evaluation with experimentation is used to see the effects of significant

contributors on uncertainty with design of experiment. However, this method is used to obtain the total measurement uncertainty value with integrating different contributors especially thermal uncertainties.

ISO/TS 15530-2 defines the procedure of multiple measurement strategies as below [29].

An analysis of variances is performed on the results, isolating two uncertainty contributions and this another similarity with statistical evaluation method at Chapter 9:

1) The effect of the **repeatability of the CMM** for the specific task includes **the effect of the measurement point distribution** in interaction with the form, waviness and the roughness of the artifact on the measurement uncertainty.

2) The effect of the **geometry errors** of the CMM together with the effect of the probe qualification process.

In those cases where the measurand is a distance, size or position, additionally three more uncertainty contributions are determined:

1) The *average error of distance measurement* is determined by measuring a standard of distance; those measurement results containing distance, size or position, are corrected (length-proportionally) for this average error of distance measurement.

The uncertainty contribution of this average distance error correction is calculated, taking into account the calibration uncertainty of the standard of distance and the repeatability of the measurements on the standard of distance.

2) The average *probe tip diameter errors* and the related standard deviations for internal and separately for external features are determined, measuring standards of internal and external diameters.

3) The *uncertainty of the temperature correction* of the CMM and artifact is estimated based on the knowledge of the CMM' s thermal behaviour , artifact and temperature situation during the measurements.

Finally, all uncertainty contributions are combined and expanded to yield the *task-related measurement uncertainty for a feature.*

The procedure is based on the assumption that for any type of geometrical features (distance, angle, etc.), there will be sufficient artifact orientations. The measurements

on the calibrated artifact shall be carried out with in normal case at least 4 times. (Repetition = 4)

Measurements are taken on two artifacts; Length bar (or ball bar) and ring gauge. Length bar is appropriate for distance measurements and ring gauge is appropriate for diameter measurements. Length bars are placed parallel to the linear axis of machine. The lines of measurement shall pass approximately through the centre of the used measuring volume. In each orientation, the measurement of the bar is carried out at least 3 times [7]. Diameter of ring gauge is measured in working volume with at least 3 different probe styli.

The formulas of this procedure are similar with methods before.

$$U = k \times \sqrt{u_{rep}^2 + u_{geo}^2 + u_D^2 + u_{temp}^2} \tag{10.1}$$

Table 18: Sample Measurement Table [29]

	orientation j=1	orientation j=2	orientation j=3
cycle i=1	y_{11}	y_{12}	y_{13}
cycle i=2	y_{21}	y_{22}	y_{23}
cycle i=3	y_{31}	y_{32}	y_{33}
cycle i=4	y_{41}	y_{42}	y_{43}
Standard Deviations	S_1	S_2	S_3
Average	Y_1	Y_2	Y_3

S_j : The standard deviation for the measurements of each feature orientation.

Y_j : The average value for the measurements of each feature orientation.

j : 1 to n_2 → Number of orientation. ($n_2 = 3$)

i : 1 to n_1 → Number of repetition. ($n_1 = 4$)

10.1.1. Calculation of Repeatability Component

u_{rep} is standard uncertainty contribution originating from;

- repeatability of the CMM,
- choice of point distribution,
- artifact's form and roughness,
- handling.

The standart uncertainty component u_{rep} is obtained as the quadratic average of the standart deviations for the individual tests on the artifact [29].

$$S_j = \sqrt{\frac{1}{(n_1-1)} \sum_{i=1}^{n_1} \left(y_{ij} - \frac{1}{n_1} \sum_{i=1}^{n_1} y_{ij}\right)^2} \qquad (10.2)$$

$$u_{rep} = \frac{1}{\sqrt{n_1}} \sqrt{\frac{1}{n_2} \sum_{j=1}^{n_2} (S_j)^2} \qquad (10.3)$$

10.1.2. Calculation of Geometry Component

u_{geo} is standart uncertainty contribution to the measurand from the errors of geometry of the CMM (for example from the errors of squareness, roll, yaw, pitch, straightness). The uncertainty contribution from the CMM geometry errors u_{geo} is calculated as the standard deviation of the averages from each orientation [29].

$$Y = \frac{1}{n_1 \times n_2} \sum_{j=1}^{n_2} \sum_{i=1}^{n_1} y_{ij} \qquad (10.4)$$

$$u_{geo} = \frac{1}{\sqrt{n_2}} \sqrt{\frac{1}{(n_2-1)} \sum_{j=1}^{n_2} (Y_j - Y)^2} = \frac{\text{Standart Deviation}}{\sqrt{n_2}} \qquad (10.5)$$

10.1.3. Calculation of Diameter Component

u_D is the standard uncertainty of the error of internal or external diameters. It is calculated as RSS (Root Sum Square) of expanded calibration uncertainty for internal or external diameter of artifact and standard deviation of the measurements of the internal or external diameter [29].

U_{calD} is the expanded calibration uncertainty for internal or external diameter of artifact according to its calibration certificates.

u_{measD} is the standard deviation of the measurement of the internal or external diameter.

$n_4 = 12 \rightarrow$ Total number of measurements.

$$u_{measD} = \frac{1}{\sqrt{n_4}} \sqrt{\frac{1}{(n_4 - 1)} \sum_{i=1}^{n_4} (D_i - \frac{1}{n_4} \sum_{i=1}^{n_4} D_i)^2} \qquad (10.6)$$

$$u_D = \sqrt{u^2_{measD} + U^2_{calD}} \qquad (10.7)$$

10.1.4. Calculation of the uncertainty of the temperature correction

As formulated former method, temperature correction uncertainty u_{temp} which is not covered by the experiments has to be estimated. There are some differences between comparison and multiple measurement (hybrid) method while calculating the temperature effect on uncertainty. At this method, u_{temp} is the uncertainty with which the effective temperature of the scales and the effective temperature of the artifact are corrected for during the measurements. This uncertainty is caused by uncertainty in the temperature correction due to uncertain temperature measurement (or from not applying a correction) and the average temperature offset from the temperature at which the average scale factor error was determined (typically 20°C); these are effects which are not covered by the experimental assessment.

The assessment of the uncertainty u_{temp} requires the knowledge of the temperatures of the machine scales, the artifact, during the measurements. Here calibrated thermometers must be used. This assessment furthermore requires the knowledge of the thermal expansion coefficients of the machine scales, and the artifact. These contributions are calculated as described in the following equation and they have to be included in the uncertainty of distance, size and position measurements [29].

$$u_{temp} = L \times \sqrt{\begin{array}{l}(u_{TMtrans}^2 + u_{TMcal}^2) \times \alpha_M^2 + (u_{TWtrans}^2 + u_{TWcal}^2) \times \alpha_N^2 \\ + (u_{\alpha M} \times (T_M - 20))^2 + (u_{\alpha W} \times (T_W - 20))^2\end{array}} \qquad (10.8)$$

10.2.   *Application of Hybrid Method to CMM under Inspection*

The procedure and formulas mentioned above were used on the CMM under inspection that has 1,2 micron + L/ 400 certified accuracy. The configuration table of internal diameter measurements of artifact is shown in Table 19. In addition, the results of measurements are tabulated in Table 20 that contains the Repetition, Geometric and Diameter Error Uncertainties.

Table 19: Measurement Configuration Table

CONFIGURATION (Ring Gauge Calibration Diameter =40,005 mm)				
Probe Angle (X,Y,Z Plane)	Probe Size (Diameter, mm)	Stylus Lenght (mm)	Meas. Point Number	Measurement Angle (Arc Angle)
1	2	100	24	360
2	2	100	24	360
3	2	100	24	360

Table 20: The Repetition, Geometric and Diameter Error Uncertainties

Orientation (X,Y,Z Plane)	4 REPLICATION RESULTS (ACTUAL,mm)				STANDART DEV. (S)	STD SQUARE (S^2)	AVERAGE (Y_j)
	i=1	i=2	i=3	i=4			
j=1	40,0073	40,0077	40,0074	40,0078	0,000238048	5,66667E-08	40,00755
j=2	40,0083	40,0085	40,0084	40,0088	0,000216025	4,66667E-08	40,0085
j=3	40,0019	40,0026	40,0029	40,003	0,000496655	2,46667E-07	40,0026

U_{calD} =±0,0015	

u_{rep} =	0,0002
u_{geo}=	0,0018
u_D =	0,0017

Parameters of temperature uncertainty is explained in Table 21 [29].

Table 21: Uncertainty Due to Temperature

		VALUE	UNITS
L	Distance, position or size of the feature to be measured	0,040005	Meters
$u_{TMtrans}$	standard uncertainty of transmitting the effective machine scale temperature to the respective thermometers (estimated from experience but if you don't have it may not be used)	0	Degree C
$u_{TWtrans}$	standard uncertainty of transmitting the effective artifact temperature temperature to the respective thermometers (estimated from experience but if you don't have it may not be used)	0	Degree C
u_{TMcal}	standard uncertainty of the thermometer to measure the machine scale temperature (this is 0.5 times the expanded uncertainty from the calibration certificate)	0,04	Degree C
u_{TWcal}	standard uncertainty of the thermometer to measure the artifact temperature (this is 0.5 times the expanded uncertainty from the calibration certificate)	0,04	Degree C
α_M	linear thermal expansion coefficient of the machine scales (DR.Johannes Heidenhain Linear Scale that's substrate is glass with DIADUR grating)	10	µm/(m × degree C)
α_W	linear thermal expansion coefficient of the artifact that's substrate is stainless steel.	11,5	µm/(m × degree C)
$u_{\alpha M}$	standard uncertainty of the linear thermal expansion coefficient of the machine scales	0,58	µm/m × degree C
$u_{\alpha W}$	standard uncertainty of the linear thermal expansion coefficient of the artifact	0,58	µm/m × degree C
T_M	average temperature of the machine scales during the respective measurements	22	Degree C
T_W	Average temperature of the artifact during the measurements	22	Degree C
	$u_{temp}=$	0,115350448	µm

10.3. *Evaluation of Hybrid Method Results*

From Equation 10.1 , total measurement uncertainty can be calculated. The coverage factor k obtained from GUM for a level of confidence of 95% is approximately equal to 2.

Total Uncertainty= $2 \times \sqrt{0,0002^2 + 0,0018^2 + 0,0017^2 + 0,00011^2}$

Total Uncertainty=$2 \times 0,00248 = 0,00497$ mm

The results of length bar measurements can be seen in Table 22 in detail. Finally, Table 23 summarizes the uncertainty components that can be evaluated by hybrid method with required number of measurement.

Table 22: Uncertainty of Length Bar Measurements in Detail

Orientation (X,Y,Z Plane) Length Bar= 300 mm	i=1	i=2	i=3	i=4	STANDARD DEVIATION (S)	S^2	AVERAGE (Y)		
j=1	300,0013	300,0013	300,0007	300,0011	0,00028284	8E-08	300,0011	u_{rep1} =	0,0001
j=2	299,9996	299,9996	299,9996	299,9997	5E-05	2,5E-09	299,999625		
j=3	300,0004	300,0004	300,0004	300,0003	5E-05	2,5E-09	300,000375	u_{geo1}=	0,0004
					STD OF AVERAGE=		0,000737535		
Length Bar= 400 mm									
j=1	400,0007	400,0012	400,0011	400,0009	0,00022174	4,91667E-08	400,000975	u_{rep2} =	0,0001
j=2	400,0001	400,0001	400,0001	400,0001	0	0	400,0001		
j=3	400,0005	400,0005	400,0005	400,0006	5E-05	2,5E-09	400,000525	u_{geo2}=	0,0003
					STD OF AVERAGE=		0,00043756		
Length Bar= 500 mm									
j=1	500,0023	500,0024	500,0017	500,0019	0,0003304	1,09167E-07	500,002075	u_{rep2} =	0,0002
j=2	500,0021	500,0021	500,0021	500,0021	0	0	500,0021		
j=3	500,0036	500,0036	500,0026	500,0027	0,00055	3,025E-07	500,003125	u_{geo2}=	0,0003
					STD OF AVERAGE=		0,000599131		
								U_{rep} =	0,000123
								U_{geo}=	0,000349
								U_{temp}=	0,00115
								U_{total}=	0,002416

Table 23: Uncertainty Contributors of Hybrid Method [29]

Uncertainty component	Taken into account by Hybrid Method			
	u_{rep}	u_{geo}	u_D	u_{temp}
	repeatability & sampling	CMM geometry	diameter	temperature influence
Point-to-point repeatability	√			
Resolution	√			
Dirt on surface and roughness	√			
Geometry errors of the CMM		√		
Relative probe tip location		√		
Probe tip directional characteristic		√		
Probe tip diameter uncertainty		√	√	
Under-sampling of surfaces	√			
Artifact alignment	√	√		
Average distance error				
Temperature variation, drift	√	√		
Temperature gradient variation	√	√		
Clamping, handling		√		
Temp. correction of CMM		√		√
Temp. correction of artifact		√		√
Dynamic errors when probing	√			

10.4. Summary

This method includes effects of temperature, probing and geometric errors which are the combination of budgeting, comparison and experimentation. This combination can provide many advantages to the method. However, repeated measurements of artifacts are requirements for the evaluation of uncertainty in CMM measurements.

CHAPTER 11

SIMULATION METHOD TO ANALYSE THE MEASUREMENT UNCERTAINTY

As mentioned before, a CMM does not directly measure geometric features such as distances, angles or diameters. Instead it measures the coordinates of a set of points on the surface of an artifact and then fits them to evaluate the desired geometric feature. Therefore, a CMM measurement requires some processing of the combination of measured values to produce an estimate of feature. Clearly, the outputs from a CMM will depend on the algorithm and the properties of points chosen to sample the surface of artifact.

Estimating the uncertainty for a CMM measurement is a difficult task because there are many specific situations in which uncertainty sources arise. For comparison method, corrections and uncertainty for a test parts are obtained from the measurement of a master gauge. Due to the this reason, these methods have many weaknesses such as requiring a calibrated master gauge suitable to measured part, repeated measurements and so on.

Simulation method is a new alternative that calculates uncertainties for any CMM measurements that does not depend on task. The main idea is modelling the entire measurement process theoretically to produce a computer simulation of the real CMM. For the same input data, this simulator will mimic the real CMM and deliver the similar outputs with uncertainties according to the process model. This method allows putting the thermal effect as uncertainty contributor. The technique is independent of the type of measurement, therefore it works for even the most complicated tasks.

The accuracy of the simulation depends on the accuracy of modelling of the measurement process. Some assumptions may be required for applicable simulation. However, high simplification means less accurate simulation so that optimization is a necessity.

Monte Carlo Simulation is used to simulate point cloud at the process model and allows the random number generation according to defined coordinate deviations. In this chapter, the theory and capabilities of designed software as thesis work will be explained and this software is titled as **V**irtual **C**MM **Tür**kiye (VCTR).

11.1.   Principles of Simulation Software VCTR

After the geometric, kinematic and thermal error modelling, compensation and uncertainty analysis with different methods of CMM (Moving Bridge) under inspection, the other section of thesis work is related to preparing software that simulates the CMM measurement and calculates the uncertainty for some tasks such as sphere, circle and plane measurements. Actually, this is a virtualization of real measurement process.

After the error compensation with laser error data, there are also uncompensated systematic and random errors which cause the measurement uncertainties. A CMM measurement occurs when a probing event triggers the CMM to take reading of its three orthogonal scales. All uncompensated errors lead to each measured coordinate departing from the true coordinate of the actual point. Therefore, the measurement of each coordinate is characterized by a region of uncertainty that has a particular likelihood centred on the measured point. When the deviations at each axis are expanded to three dimensions, an ellipsoid is produced centred on the measured point. This is shown graphically for the two dimensional case in Figure 55.
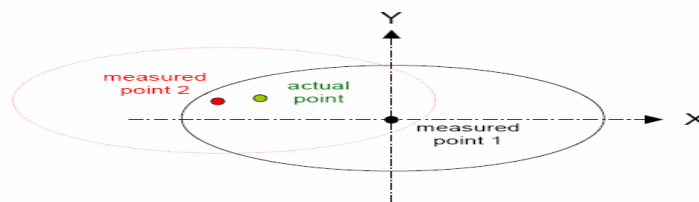
Figure 55: Two Measured Coordinate Data with Deviation Ellipse for an Actual Point. [17]

114

The figure also implies that if a second measurement of the same point is made with the CMM, a different estimation of the actual point's coordinates is obtained. Thus, repeating measurements provides additional information and combination of them gives better estimation of the actual point's coordinates. Also, every repetition results with different feature properties because of the uncertainty in the coordinates of the measured coordinates [17].

Most of the methods mentioned before utilize the repetition of information about the task specific measurement but there may not be such a chance for taking repeated measurement every time. Because of this, the best approach is obtaining approximate uncertainty ranges of each point at machine coordinate system, and then producing the geometric feature by fitting a number of simulated points.

For example, consider the simple two dimensional circles with its properties (diameter, centre position); if the measurement of the points is simulated, a different diameter and centre position will be obtained because of the uncertainty in the coordinates of the measured points.
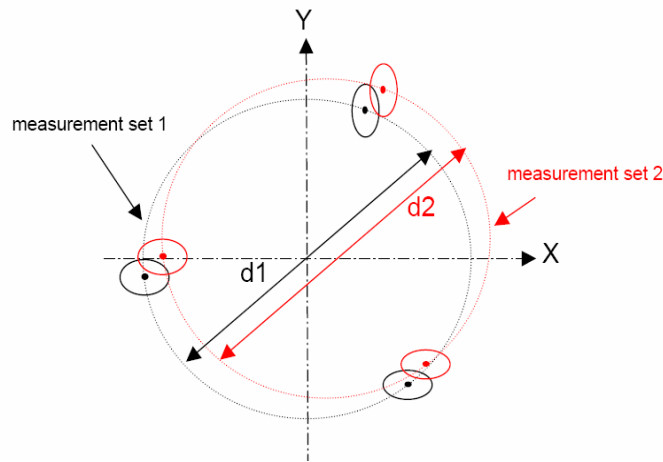
Figure 56: Finding The Diameter of a Circle By Fitting a Theoretical Circle to a Set of Measured Points on Its Surface. [17]

A distribution of diameter values would be produced. This distribution gives the probability and is characterized by a mean value and distribution width or variance.
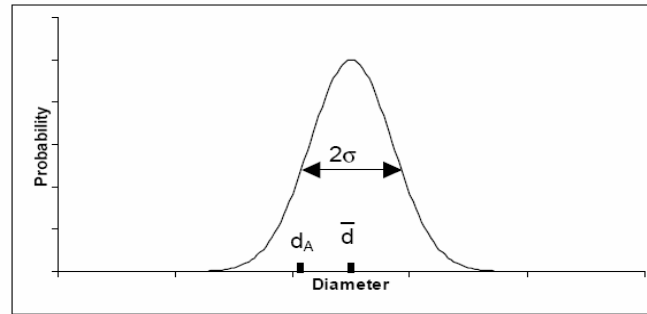
Figure 57: Probability Distribution Produced By Multiple Measurements of The Diameter. The Parameter D_a Is The Actual Diameter.

If this assumes that all systematic errors and their effects have been corrected, it can be said that the mean value of the probability distribution gives an estimation of the diameter and the width of the distribution provides a prediction of the uncertainty.

11.2.   Procedure of Simulation

The main problem with performing multiple repetitions is the time, so it is not a feasible procedure. Simulation of repeated measurements is the solution and this principle requires to be modelled on computer. The most significant point of this approach is accuracy of the simulation of the multiple repeated measurements. The artifact is measured once and the measured points and their uncertainties at machine volume are used as the input parameters to the model. Each simulated measurement run generates new coordinates randomly for each of the points by **randomly** (Monte Carlo Simulation Method) selecting values from the **probability** distributions

defined by the measured points and their uncertainties. These new point coordinates are then used to evaluate a simulated value for the geometric feature of interest.
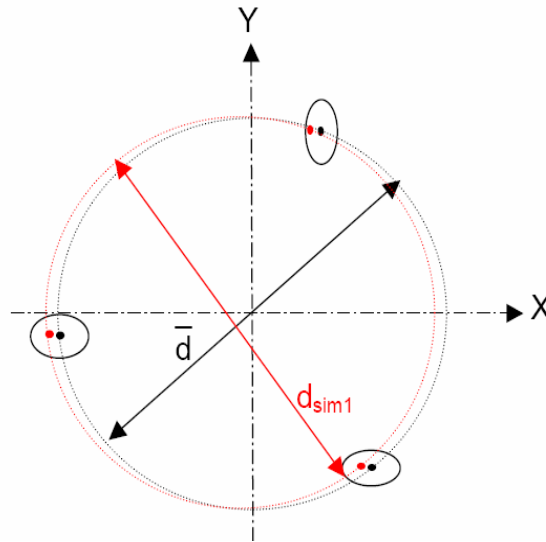
Figure 58: Multiple Measurements on Diameter of a Circle Simulated by Randomly Varying the Measured Point Values throughout Their Uncertainty Range. [17]

The simulation is repeated until the required number of iterations has been performed to sufficiently map out the probability distribution for the geometric feature. The **width** of this distribution gives an estimation of the uncertainty in the parameter.

11.2.1. Problems and Assumptions of Simulation

There is one **important difference** between the results generated by repeating the actual measurements and those by simulating them. When real repeated measurements are made, the *mean value for a geometric feature* is obtained from the

117

resulting distribution, whereas when the measurements are simulated, the mean value is fixed to be *equal to the given by the initial measurement*. This assumption to simulate the measurement requires an input for each measured point constructing the geometric feature. This input is simulated distribution of the point coordinate [17]. (Look at the difference between the figure 56 and 58)

For both figures, attention should be paid to a significant point that ellipsoid regions around the measured points and the initial measured points (Figure 58) seem %95 likelihood to find the true coordinates of the points. However, this is not true for the repeated measurement shown in Figure 56. Here the ellipsoid around each measured point has %95 chance of encompassing the true coordinate values but does not necessarily have a %95 chance of containing a repeat measurement of the point.

Similar case is viable with the simulation method. It can give information about the shape and width of the probability distribution of feature, but it cannot imply anything about the distribution's mean value. Information about the mean value can only be obtained from further actual measurements. Jaatinen stated that assuming that the mean of the simulated point distribution is equal to the initially measured value is the problem, and it leads to *an underestimate of the uncertainty*. The initial measurement is just one of the distribution of possible outcomes and could be poor estimation of the actual value. If the worst case scenario is evaluated, the solution to overcome this underestimation could be found. In a worse case, the measured point could deviate from the actual point by its uncertainty. Then, this would mean that the half of the simulated points would also be bad estimates of the actual points as they depart by more than uncertainty. Constructed simulation software avoids this problem by expanding the uncertainties of initial measured points' axis coordinate by a coverage factor of 3. This ensures that there is at least a 95% chance of any repetition of measured point within the distribution while using to generate the simulated points [17]. (Look at Figure 59)
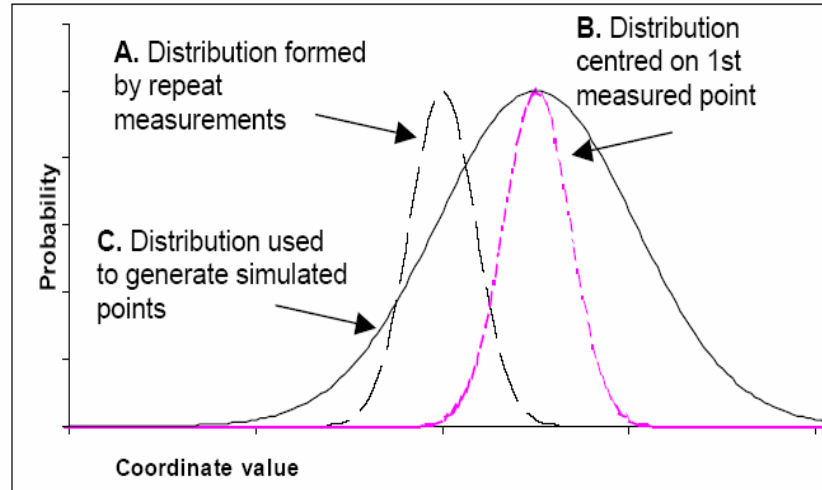
Figure 59: Distributions of Repeated Measurements, Simulated Points And 1st Measured Point. [17]

If the measurement is repeated many times, distribution A is obtained. B is the distribution centred on the first measurement value. C is the distribution of B expanded so that at least 95% of all distribution A lies within it.

11.2.2. Estimating the Uncertainty in the Coordinates of a Measured Point

The most significant parameter of a simulation method is the uncertainties of measured point's coordinates. These uncertainties result from the uncompensated systematic and random errors explained in detail before. These errors resulting in uncertainties are not constant and depend on the location within the working volume. Because of this, for high accuracy requirements, full characterization of all errors must be done at position to position within working volume. However, if ultra high levels of accuracies are not required then a significant time saving can be gained with some simplification. At this point, the solution of this problem to gain common use of VCTR is utilizing calibration data of machine. To calibrate and check the machines according to international standards every year is a must, therefore if a detail calibration is done, this supplies enough information for characterization of CMM. Another way is to assume a simple relationship for the coordinate uncertainty

119

and use certificate accuracy equation of producer. One common form of such a relationship is,

$$U = A + L / B \hspace{5cm} (11.1)$$

Where L is the distance from machine coordinate systems, A and B are constants.

11.2.3. Simulation of Measurement with VCTR

The measured point and their uncertainties are the input parameters to the simulation model that mimics the behaviour of the CMM. The model shall process the measured coordinates in exactly the same way as what the CMM does for producing reliable uncertainty. Therefore, the model must use similar fitting algorithm used by the CMM, *even if superior one exists*. Most CMM's use the Least Squares Fit as the fitting algorithm. This method minimizes the sum of square of the points' deviation from a best fitted theoretical surface.

Verification of the model is relatively straightforward. The outputs from the model should be exactly the same as which are obtained from the CMM, in case both use the same measured points as inputs. After explaining the principles of simulation, VCTR could be considered in detail.

11.3. Implementing VCTR

First of all, VCTR is designed in Visual Basic 6 powerful compiler for different applications. Communication skills of Visual Basic 6 with the Excel™ control supplies flexibility for mathematical requirements such as matrix multiplication, inverse matrix, standard deviation…etc. Therefore, this compiler has been chosen for this application. VCTR has a main menu graphical user interface (GUI) to guide the user about simulation procedure. Closing the main menu window or pushing the "EXIT" button end the software.
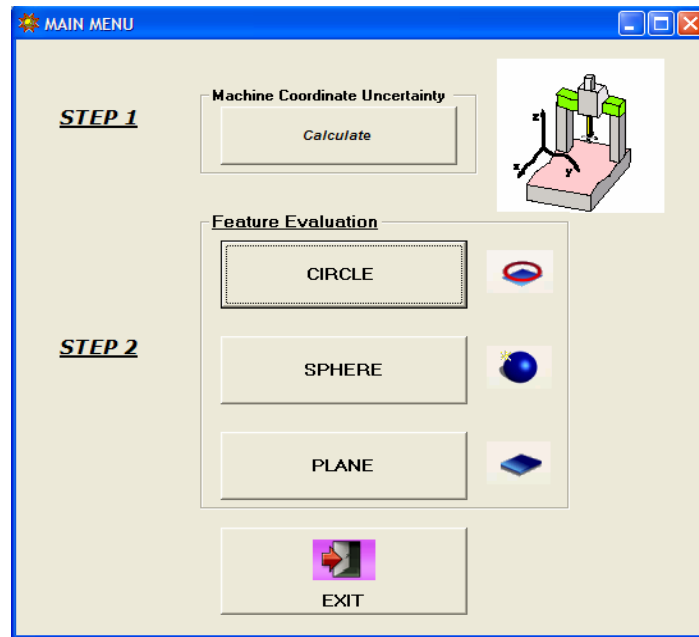
Figure 60: Main Menu GUI of VCTR

Simulation procedure can be understood easily by looking at steps of the main menu. First of all, user should calculate the uncertainties of the CMM coordinates at step 1. Afterwards, measurement uncertainty of features can be evaluated at "Step 2" frame that consists of three different features. Most common features of metrological applications are used in VCTR.

When clicking the "Calculate" Button, a new GUI appears to help the user for modelling the coordinate uncertainty of the CMM volume. GUI of Coordinate Uncertainty initializes with a warning message box for the user as *"Please put the calibration data to grid and select the type of calibration data; X,Y,Z respectively or Volumetric. Calibration data should consist of the length and standard deviation of repeated measurements. X,Y,Z axis and volumetric data can not be used at the same time"*. When user reads this message box, the requirements and rules of calculation could be clear.

Figure 61: GUI for Calculation of the Point Coordinates.

The upper zone of Figure 61 is the input part for the required information to calculate the uncertainty of the point within the machine volume. User should select the linear scale material of the machine and measured part material for estimating the thermal effect on the CMM. There are two types of material for the linear scale as Steel and Glass. For material of part, the choices are steel, aluminium and glass. The reason to select the material type is their different Thermal Expansion Coefficient

which affects the measurement uncertainty. The other information required for thermal effect is temperature of environment and measurement uncertainty of the thermometer used for measuring the environment. These four inputs are used to add uncertainty results from thermal deviation according to the equation seen below.

$$u_{tempW} = L \times \sqrt{\begin{array}{l} (u_{Termometer}{}^2) \times \alpha_{linear\_scale}{}^2 + u_{Termometer}{}^2 \times \alpha_{part}{}^2 \\ + (u_{\alpha\_linear\_scale} \times (T_{Machine} - 20))^2 + (u_{\alpha\_part} \times (T_{Part} - 20))^2 \end{array}} \qquad (11.2)$$

where

L= Distance from Machine Coordinate System(MCS)

After entering the contribution of thermal deviation on uncertainty of points, calibration data or detail evaluation of machine should be put in the calibration data grid. This data consists of the distance from machine coordinate system (MCS) and standard deviation of repeated measurement at this location. To derive the uncertainty value from the standard deviation, the number of measurement repetition shall be entered. When the mouse stays on the calibration data grid, an explanation text as "*Enter the repeated measurements of artifacts (Length or Ball Bar) on the axis of the machine with conforming to the rules of calibration standards (CMMA, VDI). The minimum number of measurement should be four.*" appears to guide the user about process. The reasons for the minimum number of the measurement are modelling the machine more accurately and satisfying the requirements for polynomial fitting. There are two options in modelling working volume of machine and they can be seen inside "Axis of Calibration Data" frame at the GUI. One of them is using axis X, Y, Z separately for data input and the other one is using volumetric data as input. The software doesn't allow using both of them. After entering the all required data, the "Calculate" button does the fourth order polynomial fitting of data by using the Excel worksheet object. The fitting method is least square of the equation which is shown below.

$$U = A1 + A2 \times \alpha + A3 \times \alpha^2 + A4 \times \alpha^3 + A5 \times \alpha^4 \qquad (11.3)$$

where U is uncertainty of coordinate.

$$F = \sum_{i=1}^{N} (u_i - (A1 + A2 \times \alpha_i + A3 \times \alpha_i^2 + A4 \times \alpha_i^3 + A5 \times \alpha_i^4))^2 \qquad (11.4)$$

Least Square Equation Partial Derivative of F equal to zero;

$$\frac{\delta F}{\delta A1} = -2 \sum_{i=1}^{N} (u_i - (A1 + A2 \times \alpha_i + A3 \times \alpha_i^2 + A4 \times \alpha_i^3 + A4 \times \alpha_i^4)) = 0 \qquad (11.5)$$

$$\frac{\delta F}{\delta A2} = -2 \sum_{i=1}^{N} (u_i - (A1 + A2 \times \alpha_i + A3 \times \alpha_i^2 + A4 \times \alpha_i^3 + A4 \times \alpha_i^4)) \times \alpha_i = 0 \qquad (11.6)$$

$$\frac{\delta F}{\delta A3} = -2 \sum_{i=1}^{N} (u_i - (A1 + A2 \times \alpha_i + A3 \times \alpha_i^2 + A4 \times \alpha_i^3 + A4 \times \alpha_i^4)) \times \alpha_i^2 = 0 \qquad (11.7)$$

$$\frac{\delta F}{\delta A4} = -2 \sum_{i=1}^{N} (u_i - (A1 + A2 \times \alpha_i + A3 \times \alpha_i^2 + A4 \times \alpha_i^3 + A4 \times \alpha_i^4)) \times \alpha_i^3 = 0 \qquad (11.8)$$

$$\frac{\delta F}{\delta A5} = -2 \sum_{i=1}^{N} (u_i - (A1 + A2 \times \alpha_i + A3 \times \alpha_i^2 + A4 \times \alpha_i^3 + A4 \times \alpha_i^4)) \times \alpha_i^4 = 0 \qquad (11.9)$$

Rearrange;

If the term in equation defined as below;

$$
\begin{bmatrix}
1 & s_i & s_i^2 & s_i^3 & s_i^4 \\
s_i & s_i^2 & s_i^3 & s_i^4 & s_i^5 \\
s_i^2 & s_i^3 & s_i^4 & s_i^5 & s_i^6 \\
s_i^3 & s_i^4 & s_i^5 & s_i^6 & s_i^7 \\
s_i^4 & s_i^5 & s_i^6 & s_i^7 & s_i^8
\end{bmatrix}
\times
\begin{bmatrix}
A1 \\ A2 \\ A3 \\ A4 \\ A5
\end{bmatrix}
=
\begin{bmatrix}
\sum_{i=1}^{N} u_i \\
\sum_{i=1}^{N} u_i \times \alpha_i \\
\sum_{i=1}^{N} u_i \times \alpha_i^2 \\
\sum_{i=1}^{N} u_i \times \alpha_i^3 \\
\sum_{i=1}^{N} u_i \times \alpha_i^4
\end{bmatrix}
\qquad (11.10a)
$$

where

$$s_i^n = \sum_{i=1}^{N} \alpha_i^n \qquad (11.10b)$$

α is the distance between the machine coordinate system and point on the X, Y, Z axis or Volumetric and this depends on the choice of the options.

$$
\begin{bmatrix} A1 \\ A2 \\ A3 \\ A4 \\ A5 \end{bmatrix} = \begin{bmatrix} 1 & s_i & s_i^2 & s_i^3 & s_i^4 \\ s_i & s_i^2 & s_i^3 & s_i^4 & s_i^5 \\ s_i^2 & s_i^3 & s_i^4 & s_i^5 & s_i^6 \\ s_i^3 & s_i^4 & s_i^5 & s_i^6 & s_i^7 \\ s_i^4 & s_i^5 & s_i^6 & s_i^7 & s_i^8 \end{bmatrix}^{-1} \times \begin{bmatrix} \sum_{i=1}^{N} u_i \\ \sum_{i=1}^{N} u_i \times \alpha_i \\ \sum_{i=1}^{N} u_i \times \alpha_i^2 \\ \sum_{i=1}^{N} u_i \times \alpha_i^3 \\ \sum_{i=1}^{N} u_i \times \alpha_i^4 \end{bmatrix} \tag{11.11}
$$

This interface gives the constants of fitted polynomial as result. Also, "Plot" button plots the polynomial for all axes within axis range of input data. This is required to see uncertainty behaviour of the axis and a sample can be seen in Figure 61. The last part shown in Figure 62 is the alternative method for calculating the point uncertainty of machine and uses the specification of machine producers. The disadvantage of using this equation is that it is not precise and it contains more approximation than detail investigation. The user of software shall click the "Use Certificate Constants" box to use certificate equation of machine producer and then the message box appears to warn the user for putting the A and B constants. For all dimensions, the units are millimetre.

Figure 62: Uncertainty Function of Producer's Certificate
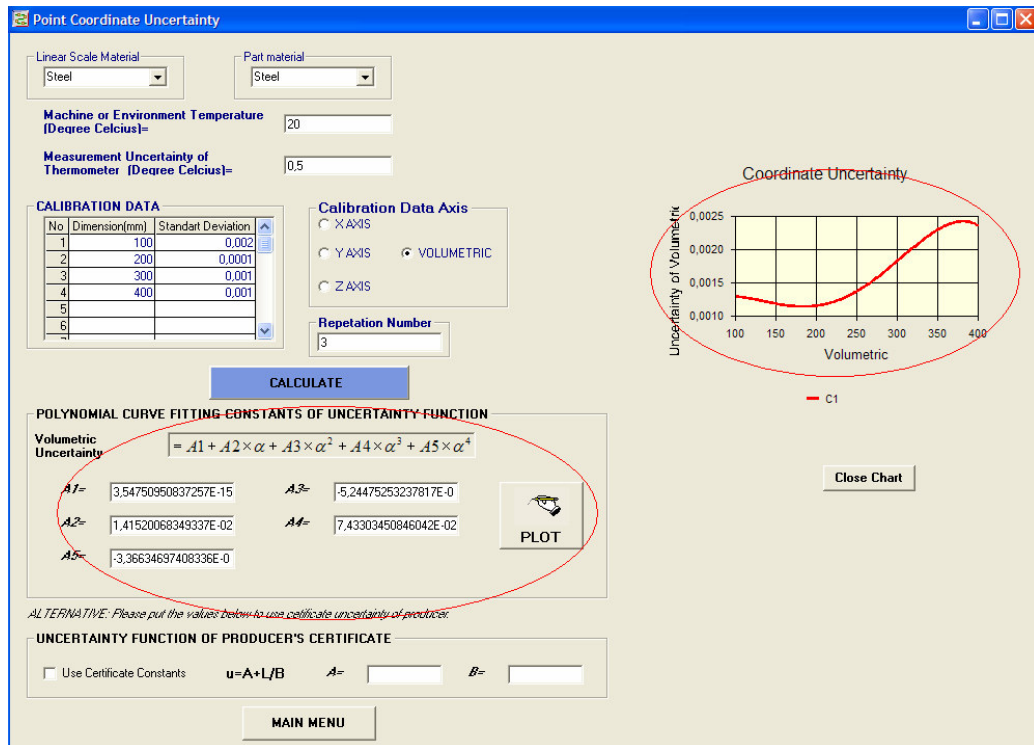
Figure 63: Fitting Results And Plotting

Uncertainties of each points supply the range of the deviation used to simulate the point deviation. This is achieved by utilizing the randomize function (according to the standard deviation) of Microsoft Excel that uses measured coordinate and its uncertainty at this location for each point.

After evaluation of point uncertainty, the "main menu" button may be clicked or this form may be minimized. The second step is the calculation of the properties of geometric features (circle, plane, sphere).

11.3.1. Measurement Uncertainty of Circle

When clicking the "Circle" button from the form of "Main Menu", the "Circle Uncertainty" form indicated in Figure 64 appears.
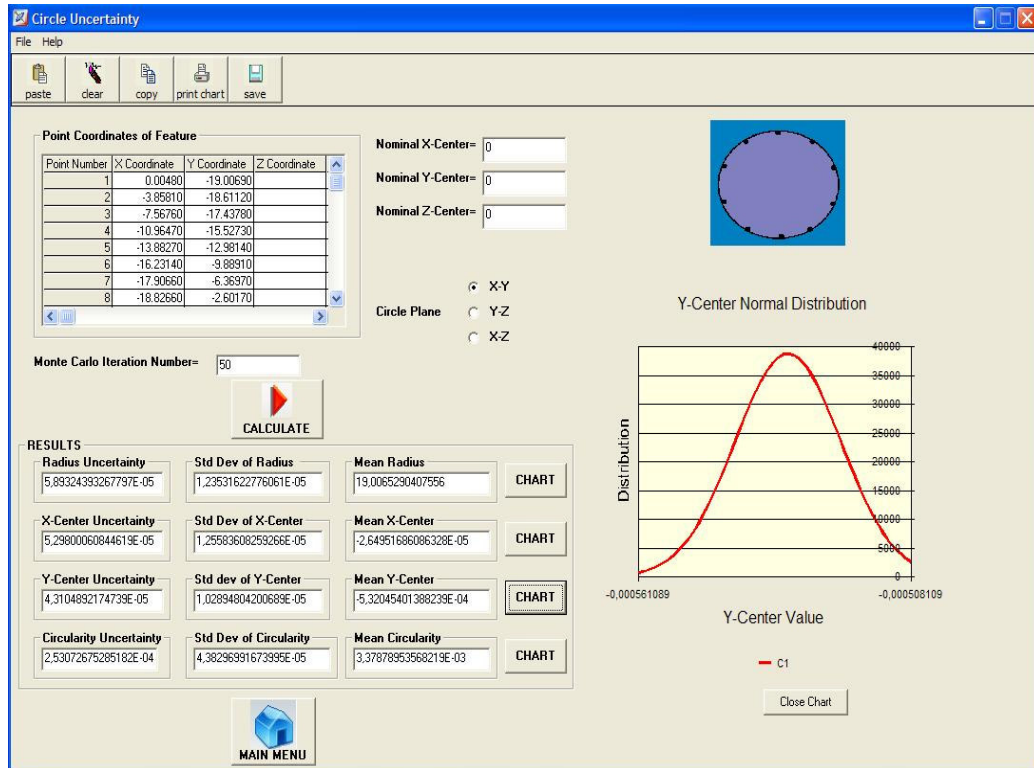
Figure 64: Circle Uncertainty Form.

When looking at the "Circle Uncertainty" form, three parts could be seen on the form. One of them is the data input part which is used to enter the coordinate of each point, nominal center and projection plane of the circle and also Monte Carlo Iteration Number. The reason is to utilize the nominal center of feature is obtaining the correct actual center of circle. After completing the input data for evaluation, "Calculate" button is clicked and then all the results appear in the "RESULTS" frame. Results consist of uncertainty, standard deviation, mean of the Radius, Center Coordinates and Circularity values. Calculation is done by Excel at background that user cannot see. Linear Least Square Method (LLSM) is utilized to calculate the feature properties of circle. The method of least squares is used to solve a set of linear equations having more equations than unknown variables. Since there are more equations than variables, the solution will not be exactly correct for each equation; rather, the process minimizes the sum of squares of the residual errors. The method is very powerful and can be applied to numerous applications.

127

For sets of linear equations, the least-squares process will produce a direct solution for the unknowns. The linear case is mathematically the same as the general case where an adjustment is performed by using zero as the initial guess of all parameters. Only a single iteration is required for convergence.

The equations must be of the form,

$$F_i(x_1, x_2, x_3, ...) = a_1 \times x_1 + a_2 \times x_2 + a_3 \times x_3 + ... = k_i \tag{11.12}$$

The Jacobian matrix, J, is therefore

$$J = \begin{bmatrix} a_{11} & a_{12} & a_{13} & ... \\ a_{21} & a_{22} & a_{23} & ... \\ a_{31} & a_{32} & a_{33} & ... \\ ... & ... & ... & ... \end{bmatrix} \tag{11.13}$$

where a_{ij} is the th i coefficient of the th j equation.

Since the initial guesses are all zero, the vector of residuals, **K** , is

$$K = \begin{bmatrix} k_1 & k_2 & k_3 & ... \end{bmatrix}^{\mathrm{T}} \tag{11.14}$$

If the weighting matrix is diagonal, then $\Delta \mathbf{X}$ can be solved by row reduction of the matrix

$$\begin{bmatrix} \sum_i (a_{1i}{}^2 w_i) & \sum_i (a_{1i} a_{2i} w_i) & \sum_i (a_{1i} a_{3i} w_i) & \cdots & \sum_i (a_{1i} k_i w_i) \\ \sum_i (a_{1i} a_{2i} w_i) & \sum_i (a_{2i}{}^2 w_i) & \sum_i (a_{2i} a_{3i} w_i) & \cdots & \sum_i (a_{2i} k_i w_i) \\ \sum_i (a_{1i} a_{3i} w_i) & \sum_i (a_{2i} a_{3i} w_i) & \sum_i (a_{3i}{}^2 w_i) & \cdots & \sum_i (a_{3i} k_i w_i) \\ \vdots & \vdots & \vdots & \ddots & \vdots \end{bmatrix} \tag{11.15}$$

The final solution will be the adjustment values. That is

X=ΔX or $x_i = \Delta x_i$

A circle can be defined by the equation below:

$$\sqrt{(x - x_0)^2 + (y - y_0)^2} = r \tag{11.16}$$

where (x_0, y_0) is the centre of the circle and r is the radius of the circle.

Ideally, it is desirable to minimize the square of the distance between the points defining the circle and the circle.

That is, minimize

$$\sum_i [(\sqrt{(x - x_0)^2 + (y - y_0)^2} - r)^2] \tag{11.17}$$

This is equivalent to performing the least-squares process using the equations

$$F_i(x_0, y_0, r) = \sqrt{(x_i - x_0)^2 + (y_i - y_0)^2} - r_i = 0 \qquad (11.18)$$

The equation of a circle is not linear in the unknown values x_0, y_0, and r. The equation of a circle can be written in the linear form;

$$A \times (x^2 + y^2) + B \times x + C \times y = 1 \qquad (11.19)$$

where

$$A = \frac{1}{r^2 - x_0^2 - y_0^2} \qquad (11.20)$$

$$B = \frac{-2 \times x_0}{r^2 - x_0^2 - y_0^2} \qquad (11.21)$$

$$C = \frac{-2 \times y_0}{r^2 - x_0^2 - y_0^2} \qquad (11.22)$$

This can be rewritten for the original unknowns as;

$$x_0 = \frac{-B}{2 \times A} \qquad (11.23)$$

$$y_0 = \frac{-C}{2 \times A} \qquad (11.24)$$

$$r = \frac{\sqrt{4 \times A + B^2 + C^2}}{2 \times A} \qquad (11.25)$$

Note that by using the linear form of the circle equation, the square of the distance from each point to the circle is not the value that is being minimized.

Using the equation $A \times (x^2 + y^2) + B \times x + C \times y = 1$ with the unknowns A, B, and C, the Jacobian matrix is

$$F = A \times (x^2 + y^2) + B \times x + C \times y \qquad (11.26)$$

$$\frac{\delta F}{\delta A} = (x^2 + y^2); \quad \frac{\delta F}{\delta B} = x \; ; \quad \frac{\delta F}{\delta A} = y \qquad (11.27)$$

$$J = \begin{bmatrix} \dfrac{\delta F_1}{\delta A} & \dfrac{\delta F_1}{\delta B} & \dfrac{\delta F_1}{\delta C} \\[2mm] \dfrac{\delta F_2}{\delta A} & \dfrac{\delta F_2}{\delta B} & \dfrac{\delta F_2}{\delta C} \\[2mm] \dfrac{\delta F_3}{\delta A} & \dfrac{\delta F_3}{\delta B} & \dfrac{\delta F_3}{\delta C} \\[2mm] \cdots & \cdots & \cdots \end{bmatrix} = \begin{bmatrix} x_1^2 + y_1^2 & x_1 & y_1 \\ x_2^2 + y_2^2 & x_2 & y_2 \\ x_3^2 + y_3^2 & x_3 & y_3 \\ \cdots & \cdots & \cdots \end{bmatrix} \qquad (11.28)$$

Since all initial guesses are zero, the residual vector is

$$K = \begin{bmatrix} k_1 \\ k_2 \\ k_3 \\ \vdots \end{bmatrix} = \begin{bmatrix} 1 \\ 1 \\ 1 \\ \cdots \end{bmatrix} \tag{11.29}$$

In the lack of other informations, the weighting matrix, **W**, is the identity matrix.

That is **W=I**

The unknowns; A, B, and C, can be solved for using the equation

$$X = (J^t W J)^{-1} J^t W K = (J^t J)^{-1} J^t K \tag{11.30}$$

This can be simplified to

$$\begin{bmatrix} A \\ B \\ C \end{bmatrix} = \begin{bmatrix} \sum_i ((x_i^2 + y_i^2)^2) & \sum_i ((x_i^2 + y_i^2)x_i) & \sum_i ((x_i^2 + y_i^2)y_i) \\ \sum_i ((x_i^2 + y_i^2)x_i) & \sum_i (x_i^2) & \sum_i (x_i y_i) \\ \sum_i ((x_i^2 + y_i^2)y_i) & \sum_i (x_i y_i) & \sum_i (y_i^2) \end{bmatrix}^{-1} \begin{bmatrix} \sum_i (x_i^2 + y_i^2) \\ \sum_i x_i \\ \sum_i y_i \end{bmatrix} \tag{11.31}$$

When the A, B and C are known, they could be obtained easily from equation 31 [30]. The circularity is another output of circle and many engineering drawings require these properties and therefore the uncertainty of circularity becomes significant for part inspection. The circularity is obtained from the equation below. This equation is integrated into the algorithm and uncertainty of each point is simulated.

For each point;

$$R_i = \sqrt{(x_i - x_0)^2 + (y_i - y_0)^2} \tag{11.32}$$

$$Circularity = Max(R_i) - Min(R_i) \tag{11.33}$$

x_0, y_0 are the calculated center coodinates of circle with Least Square Method.
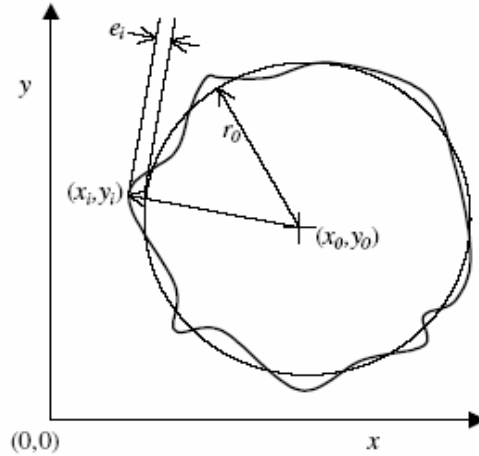
Figure 65: Circularity [30]

The contribution of Monte Carlo Iteration is to change each x_i and y_i according to the standard deviation of this location. The time of calculation is directly related with the number of Monte Carlo Iteration and points that form the circle.

"Chart" buttons show the frequency distribution of each property of circle and user could visualize the results, such as how results deviate, what maximum and minimum values are. For this visualization, the normal distribution function is used as seen below. The **normal distribution**, also called the **Gaussian distribution**, is an important family of continuous probability distributions, applicable in many fields.

Normal Distribution Function:

$$N(\sigma,\mu) = \frac{1}{\sigma \times \sqrt{2\pi}} \times \exp(-\frac{(x-\mu)^2}{2\sigma^2}) \qquad (11.34)$$

$\sigma =$ Standard Deviation

$\mu =$ Mean Value

Software plots the normal distribution charts of all feature properties.

11.3.2. Measurement Uncertainty of Sphere

When clicking the "Sphere" button at step 2 zone of the "Main Menu" form, the "Sphere Uncertainty" form appears. The input part of this form is similar with the

circle's form that inputs are the coordinates of the points and nominal center position and also the Monte Carlo Iteration number.
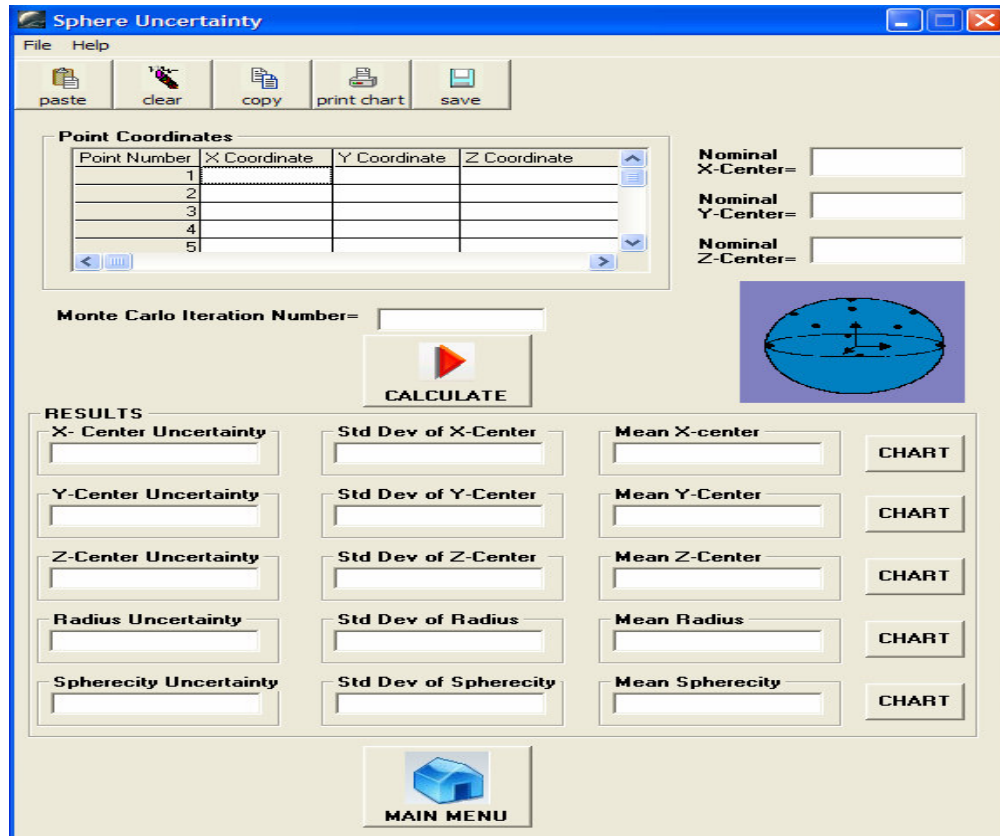
Figure 66: Graphical User Interface of Measurement Uncertainty of Sphere

Calculation method of sphere properties, e.g. actual center coordinate, radius and spherecity, is Linear Least Square Method (Linear LSM) that is common method for metrology application. There are also other methods such as Best Fit Chebyshev Method but they are not common as LSM.

The same procedure with circle gives the required properties of sphere as seen below [31].

Sphere equation;

$$R = \sqrt{(x - x_0)^2 + (y - y_0)^2 + (z - z_0)^2} \tag{11.35}$$

Convert;

$$x_0 = A, \qquad\qquad y_0 = B, \qquad\qquad z_0 = C$$

If (11.35) is denoted as below,

$$F_i = \sqrt{(x_i - A)^2 + (y_i - B)^2 + (z_i - C)^2} \tag{11.36}$$

The equation below should be minimized;

$$T(A, B, C, R) = \sum_{i=1}^{n}(F_i^2 - R^2)^2 \tag{11.37}$$

$$D = R^2 - A^2 - B^2 - C^2 \tag{11.38}$$

The necessary condition to minimize;

$$\frac{\delta T}{\delta A} = \frac{\delta T}{\delta B} = \frac{\delta T}{\delta C} = \frac{\delta T}{\delta R} = 0 \text{ (Jacobian)}$$

Then, above equation is written in matrix form;

$$\begin{bmatrix} 2\sum_{i=1}^{n}x_i^2 & 2\sum_{i=1}^{n}x_i y_i & 2\sum_{i=1}^{n}x_i z_i & \sum_{i=1}^{n}x_i \\ 2\sum_{i=1}^{n}x_i y_i & 2\sum_{i=1}^{n}y_i^2 & \sum_{i=1}^{n}y_i z_i & \sum_{i=1}^{n}y_i \\ 2\sum_{i=1}^{n}x_i z_i & \sum_{i=1}^{n}y_i z_i & 2\sum_{i=1}^{n}z_i^2 & \sum_{i=1}^{n}z_i \\ \sum_{i=1}^{n}x_i & \sum_{i=1}^{n}y_i & \sum_{i=1}^{n}z_i & n \end{bmatrix} \times \begin{bmatrix} A \\ B \\ C \\ D \end{bmatrix} = \begin{bmatrix} \sum_{i=1}^{n}x_i(x_i^2 + y_i^2 + z_i^2) \\ \sum_{i=1}^{n}y_i(x_i^2 + y_i^2 + z_i^2) \\ \sum_{i=1}^{n}z_i(x_i^2 + y_i^2 + z_i^2) \\ \sum_{i=1}^{n}(x_i^2 + y_i^2 + z_i^2) \end{bmatrix} \tag{11.39}$$

The unknowns; A, B, C and D can be solved for using the equation (11.30).

The radius;

$$R = \sqrt{D + A^2 + B^2 + C^2} \tag{11.40}$$

This linear solution satisfies the uncertainty simulation and gives good results. The other necessary output for engineering drawing and metrology application is sphericity.

For each point;

$$R_i = \sqrt{(x_i - x_0)^2 + (y_i - y_0)^2 + (z_i - z_0)^2} \tag{11.41}$$

$$Sphericity = Max(R_i) - Min(R_i) \tag{11.42}$$

x_0, y_0, z_0 are the calculated center coodinates of circle with Least Square Method.

"Chart" buttons have same function with the circle's one and they show the Normal Distribution plot of the properties of sphere by using equation 11.34 .

11.4.   Evaluation of Flatness Uncertainty on Plane Measurement

When clicking the "Plane" button at step 2 zone of the "Main Menu" form, the "Plane Uncertainty" form appears to calculate the uncertainty of plane measurements. Different from the circle and sphere input part, plane input part consists of the only point coordinates and Monte Carlo Iteration Number; there is no need for nominal center coordinates. Plane fitting is also done with Least Square method by minimizing the error between points and fitted plane.

For fitting, the assumption is that the z–component of the data is functionally dependent on the x– and y–components.

To determine A, B and C,   the plane $z = Ax + By + C$ fits the a set of samples (x_i, y_i, z_i) in the sense that the sum of the squared errors between the z_i and the plane values $z_i = Ax_i + By_i + C$ is minimized. Note that the error is measured only in the z–direction.

Define $F(A,B,C) = \sum_{i=1}^{n}[(Ax_i + By_i + C) - z_i]^2$. This function is non-negative and its graph is a hyper paraboloid whose vertex occurs when the gradient satisfies $\Delta F = (0, 0, 0)$. This leads to a system of three linear equations in A, B, and C which can be easily solved. Precisely,

$$\frac{\delta F}{\delta A} = 2\sum_{i=1}^{n}[(Ax_i + By_i + C) - z_i] \times x_i = 0 \tag{11.43}$$

$$\frac{\delta F}{\delta B} = 2\sum_{i=1}^{n}[(Ax_i + By_i + C) - z_i] \times y_i = 0 \tag{11.44}$$

$$\frac{\delta F}{\delta C} = 2\sum_{i=1}^{n}[(Ax_i + By_i + C) - z_i] = 0 \tag{11.45}$$

And so

$$
\begin{bmatrix}
\sum_{i=1}^{n} x_i^2 & \sum_{i=1}^{n} x_i y_i & \sum_{i=1}^{n} x_i \\
\sum_{i=1}^{n} x_i y_i & \sum_{i=1}^{n} y_i^2 & \sum_{i=1}^{n} y_i \\
\sum_{i=1}^{n} x_i & \sum_{i=1}^{n} y_i & n
\end{bmatrix}
\times
\begin{bmatrix}
A \\ B \\ C
\end{bmatrix}
=
\begin{bmatrix}
\sum_{i=1}^{n} x_i z_i \\
\sum_{i=1}^{n} y_i z_i \\
\sum_{i=1}^{n} z_i
\end{bmatrix}
\tag{11.46}
$$

The solution provides the least square of $z = Ax + By + C$.

The approach to flatness assessment is the use of a least squares method. In this method, a sampled data set is represented by a fitted feature. The distance between the nearest and furthest points from the reference plane is calculated for the data set. Flatness for the given data set is obtained by the difference between the nearest and furthest distances. When normal deviations, (deviations of the data set normal to the fitted feature (Fig. 67)), are used at the reference plane to a data set, the method is called the normal or orthogonal least squares method.

Flatness tolerance of the plane is calculated with respect to equation below.

$$
D_i = \frac{(Ax_i + By_i - z_i + C)}{\sqrt{(A^2 + B^2 + 1)}}
\tag{11.47}
$$

$$
Flatness = \max(D_i) - \min(D_i)
\tag{11.48}
$$
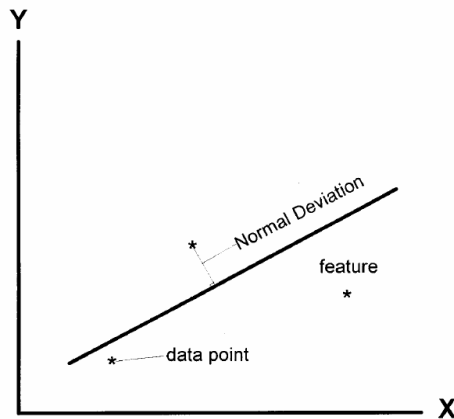
Figure 67: Flatness Theory [32]

135
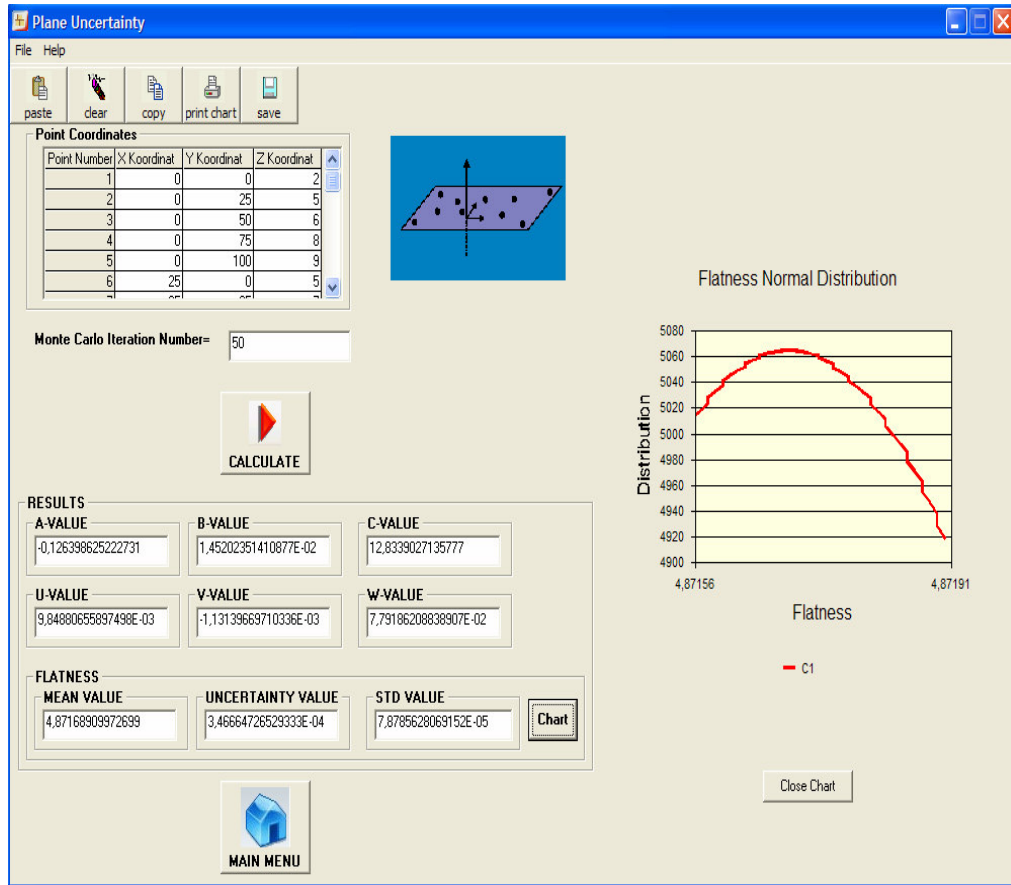
Figure 68: GUI for Measurement Uncertainty of Plane

11.5.   Comparison of the Experimental and VCTR Results

The test of software for the circle's measurement uncertainty is done on LK Coordinate Measuring Machine in house. At six uniformly distributed positions, a ring gauge is measured with five replication of each measurement. The necessity of replication is calculating the uncertainty of actual measurements. On the other hand, the calibration data of machine (Table 25) is used as input for calculation of point uncertainty at simulation.

Table 24: Comparison of Experimental and Simulation Results

Meas. No:1	1	2	3	4	5	Experimental Uncertainty	VCTR Uncertainty	Difference	Software / Actual Ratio
X-axis	54,9777	54,978	54,9775	54,9777	54,9779	8,7178E-05	0,00027	0,000183	3,1
Y-axis	40,8119	40,8122	40,8121	40,8118	40,8118	8,124E-05	0,00022	0,000139	2,7
Diameter	69,6775	69,6771	69,6774	69,6771	69,6778	0,00013191	0,000458	0,000326	3,0
Circularity	0,0047	0,0045	0,0045	0,0045	0,0049	8E-05	0,000246	0,000166	3,0

Meas. No:2	1	2	3	4	5	Experimental Uncertainty	VCTR Uncertainty	Difference	Software / Actual Ratio
X	850,117	850,1167	850,1169	850,1171	850,1172	8,60233E-05	0,0001169	3,08767E-05	1,36
Y	21,6159	21,6161	21,6159	21,616	21,6158	5,09902E-05	0,0001115	6,40098E-05	2,26
Diameter	69,6769	69,6774	69,677	69,6771	69,6772	8,60233E-05	0,0001869	9,99767E-05	2,16
Circularity	0,0035	0,0025	0,0027	0,0023	0,0025	0,000209762	0,000544	0,000334238	2,59

One of the difference between results of the experimental and simulated uncertainty is the experimental measurements that are replicated at finite number (5) so that the whole picture of uncertainty could not be obtained. The other one is the statistical assumption which is the coverage factor 3 of simulation. If smaller coverage factor is taken, the difference will be smaller. But in that case, this is not a good choice because as mentioned before (Look at "Problems and Assumptions of Simulations" section) finite number of reputation will be obtained every time for actual measurements. So that coverage factor is a safety factor for simulation software.

Table 25: Calibration Data of CMM

LENGTH (mm)		100	200	300	400	500	600
X AXIS							
	1	100,0012	200,0033	300,0072	400,0112	500,0123	600,0152
	2	100,0014	200,0034	300,0072	400,0112	500,0128	600,0158
	3	100,0012	200,0036	300,0077	400,0107	500,0128	600,0159
STDEV		0,000115	0,000153	0,000289	0,000289	0,000289	0,000379
Y AXIS							
	1	100,0009	200,0061	300,01	400,0116	500,015	600,0182
	2	100,0009	200,006	300,01	400,0116	500,0151	600,0181
	3	100,0009	200,0062	300,01	400,0116	500,0141	600,0169
STDEV		0	0,0001	0	0	0,000551	0,000723
Z AXIS							
	1	100,0015	200,0061	300,0117	400,0136	500,0145	600,011
	2	100,0014	200,006	300,0117	400,0136	500,0145	600,011
	3	100,0017	200,0062	300,0107	400,0136	500,0145	600,012
STDEV		0,000153	0,0001	0,000577	0	0	0,000577

With using equation 11.47 and 11.48, VCTR calculates the measurement uncertainty of a plane and flatness tolerance. The accuracy of plane fitting algorithm has been checked with using sample set of point coordinates at the paper " Straightness and Flatness Tolerance Evaluation: An Optimization Approach" [16].

Table 26: Accuracy Check Table for Plane Fitting Algorithm

X	-2	-1	0	1	2	-2	-1	0	1	2	-2	-1	0	1	2
Y	1	1	1	1	1	0	0	0	0	0	-1	-1	-1	-1	-1
Z	5	4	1	2	2	4	3	3	2	2	3	4	2	1	2

Example=	1	2	3
Flatness Value (mm) [32]=	2,3664	0,1856	0,04381
VCTR Result (mm)=	2,3664	0,1882	0,04497

Table 24 shows the verification of flatness algorithm by using coordinates in table and appendices. Results imply that VCTR calculates the flatness value correctly with using Least Square method. In addition, the normal distribution of the flatness values can be seen at the right side of GUI after pushing "Chart" button.

The success of simulation method depends on the validity of the uncertainty model of entire machine volume. Therefore, the most significant part of VCTR is "Machine Coordinate Uncertainty". The limit of axes should be covered while inspecting the machine volume and probing effect may be included this study. Actually, prepared software is applicable to a range of coordinate metrology systems, such as conventional CMM, multilateration and laser trackers. This software is general and effective for estimating task specific uncertainties arising from the CMM. On the other hand, this method contains some difficulties which is the unpredictable environmental effects and geometric errors along the axes.

CHAPTER 12

CONCLUSION

12.1.   *Discussion of Results and Conclusions*

The study about the measurement uncertainty of CMM is concluded with many useful information about the performance and traceability of this machine. Error maps of the CMM are constructed with using principals of kinematic modelling and two different error measurement techniques. Kinematic and geometric error model depends on the structure of the machine and needs the information about the deviations of links and joints. Obtaining this deviations is a difficult task and required many measurements with different type of sensors. On the other hand, kinematical model evaluated by using laser error utilize a pure 3 dimensional kinematical motion matrices and the required linear, angular and translational errors of probe motion can be measured with interferometer optics. This error measuring technique supplies high flexibility and accuracy. Subsequently, all the mathematical expressions of both kinematical methods and the algorithms were imposed in user-defined Matlab functions in m-files to visualize the error within the machine volume. Entire error map of the CMM designates that the errors are highly correlated with the machine hardware such as axes motor position and structure type.

After the compensation of major part of the systematic errors, the remainder is the source of measurement uncertainty. Evaluation of the measurement uncertainty requires the definition of all contributors. Although, the uncertainty estimation of measurement is tried to standardized by GUM, the results of methods differ with respect to the evaluation of contributors.

First inspected method "Uncertainty Budgeting" is the most common method for the analysis of uncertainty, because it is easy to implement. The process is adding the squares of the uncertainty values of each contributors and taking the root of sum. Nearly all the uncertainties of contributors extracted from the certificates and experiences. Consequently, the method is very rough. This conclusion is proven by

comparing the uncertainty value (u= 2.477 microns for 400 mm length bar measurement), which is obtained from budgeting for the CMM under inspection, with other methods and actual measurements.

Next method is comparison which involves the inspection of a calibrated artifact identical to the piece under measurement. If such an artifact can be obtained, this approach is most efficient uncertainty evaluation for the specific measurements and the results is very close to the actual uncertainty value. This method is also applied on the CMM under inspection for measuring a circle with using a ring gauge and the measurement uncertainty value of circle is equal to 0,309 microns without coverage factor.

Third method named as "Statistical Evaluation of Measurement Uncertainty by Designing Fractional Factorial Experiment" requires the most complicated evaluation of contributors. The main difference of this method from others is quantification the effects of contributors. Many measurement factors which effects the uncertainty such as sampling strategy, probe diameter, stylus length and measurement angle etc. are investigated with designing an experiment. The experimentation with actual measurements provides to see the worst measurement configuration and its magnitude.

Hybrid method containing the advantages of methods mentioned above consists of the evaluation of repeatability, geometric errors, probe and thermal effects. However, requirement for repeated measurement and time are the main disadvantages of this method.

Finally, recently developed simulation method is examined and software is designed at Visual Basic to mimic the actual measurement process and calculate uncertainty of different task specific measurement by using the Monte Carlo Simulation Method. The software eliminates the repeated measurements for each task and includes the thermal effects of the part and scales. On the other hand, the efficiency of the software is tested by using actual measurements on the CMM and some reference points.

Table 27 indicates the advantages and disadvantages of uncertainty analysis methods for measurement of CMM.

Table 27: Advantages and Disadvantages of Methods

	Uncertainty Budgeting	Comparison	Statistical Evaluation by Designing F.F. Experiment	Hybrid	Simulation
ADVANTAGES	Easy to implement.	A powerful technique to obtain feature specific measurement uncertainty, if an identical and calibrated part is available.	Effects of different contributors can be evaluated in detail. Results of method can guide the operators about choosing the measurement strategies.	This method includes effects of temperature, probing and geometric errors for uncertainty.	No need actual repeated measurement and calibrated artifact for each feature. Not feature task-specific. Includes temperature uncertainty. Save time.
DISADVANTAGES	Provide general evaluation. Many contributors can not be evaluated directly.	Feature - task specific. Necessity of a similar and calibrated artifact. Repeated measurements are required on the artifact in addition to those on the part.	Feature- task specific. Repeated measurements are required on the artifact by using different combination of contributors. Required a lot of time for measurement and statistical evaluation of results.	Repeated measurements are required on the artifacts by using different combination of contributors.	Need some assumptions about the mean value of point coordinates.

12.2.   Future Works

Although, this study covers all the methods about the measurement error and uncertainty analysis of CMMs, in order to improve it the following future works are recommended. These works can also be considered as the suggestions to achieve improvement of the CMMs measurement process.

1) Software can be improved with using different algorithm for constructing the features such as non-linear least square, min-max zone and chebyshev.

2) Features used in software increases in variety by analysing the measurement uncertainty of cylinder and cone. To do this, mathematical algorithm is constructed by using Matlab and converted to the COM Component. Afterwards, COM can be implemented in Visual Basic.

3) Software can be integrated to the actual measurement software and while measurement codes are constructed, it simulates the measurement strategy of operator and estimates the uncertainty of task specific measurements.

4) Together with the modelling of kinematic, geometric and thermal errors, the dynamic errors can be modelled with respect to the different structure types.

5) Real time error measurement and compensation system can be analysed and also this study may contain new positioning sensor system such as laser scales.

6) Structure of Nano-CMMs can be inspected from design point of view and evaluation.

REFERENCES

[1] Bosch J.A., *Coordinate measuring machines and systems*. New York, Marcel Dekker, 1995.

[2] ANSI/ASME B89.4.1. *Methods for performance evaluation of coordinate measuring machines*. New York, American Society of Mechanical Engineers, 1997.

[3] VDI/VDE 2617. *Accuracy of coordinate measuring machines*, Düsseldorf, Verein Deutscher Ingenieure (VDI/VDE), 1989.

[4] BS 6808. *British standard—coordinate measuring machines*. London, British Standards Institute, 1987.

[5] JIS B7440. Japanese industrial standard. Test code for accuracy of coordinate measuring machines. Tokyo: Japanese Standards Association; 1987.

[6] ISO 10360. *Coordinate metrology, parts 1–2*. Geneva: International Organization for Standardization (ISO); 1994.

[7] CMMA. *Accuracy specification for coordinate measuring machines*. London: Coordinate Measuring Machine Manufacturers Association.

[8] ISO. *Guide to the Expression of Uncertainty in Measurement (GUM).* Geneva: International Organization for Standardization (ISO), 1995.

[9] Wilhelm RG, Hocken R, Schwenke H. *Task specific uncertainty in coordinate measurement*. Ann CIRP 2001;**50**.

[10] Chapman M. *The benefits of laser systems that use remote interferometer optics for linear, angular and straightness measurements.* [Online] Available from: http://www.renishaw.com/media/doc/en/88d560afb5514343b356177179a1bea8.doc

[11] Balsamo A., Di Ciommo M., Mugno R., Rebaglia BI., Ricci E, Grella R. *Evaluation of CMM uncertainty through Monte Carlo simulations*. Ann CIRP 1999.

[12] Coleman H. W., *Experimentation and Uncertainty Analysis for Engineers*. New York:Wiley; 1991.

[13] Henrion A., Quantification of variance components in amount-ofsubstance measurements by the use of nested experimental design. In: Proceedings of 9th Metrologie Conference, Bordeaux, France; 1999.

[14] KoikeM, Ishida H. *Estimation of measurement uncertainty of Rockwell Hardness test using orthogonal array*. In: Proceedings of XV IMEKO World Congress, Osaka, Japan; 1999 June 21–27.

[15] Piratelli-Filho A, Giacomo BD. *Application of design of experiment techniques to estimate CMM measurement uncertainty*. In: Proceedings of American Society for Precision Engineering—ASPE Annual Meeting, Scottsdale, AZ, USA; 2000.

[16] Alexsander H.Slocum, *Precision Machine Design,* Prentice Hall, 1992

[17] Jaatinen, E., *Calculating CMM Measurement Uncertainty with OZSIM*. CTIP Technical Memorandum, 2001.

[18] Barakat, N.A., *Adaptive compensation of quasi-static errors for an intrinsic machine.* International Journal of Machine Tools and Manufacture, 2000. **40**: p. 2267-2291.

[19] Ertekin, Y.M , *Derivation of machine tool error models and error compensation procedure for three axes vertical machining center using rigid body kinematics.* International Journal of Machine Tools and Manufacture, 1999. **40**: p. 1199-1213.

[20] Weekers, W.G., *Compensation for dynamic errors of coordinate measuring machine.* Elsevier, 1997. **20**: p. 197-209.

[21] Romano, D., *Inspecting geometric tolerances: uncertainty analysis in position tolerances control on Coordinate Measuring Machines.* Springer, 2002.

[22] Dhanish, P.B.., *Effect of CMM point coordinate uncertainty on uncertainties in determination of circular features.* Elsevier, 2005.

[23] Dong, C., *Prediction and Compensation of Dynamic Errors for Coordinate Measuring.* Journal of Manufacturing Science and Engineering, 2002. **124**: p. 509 - 514.

[24] Savio, E., *An artifact for traceable freeform measurements on coordinate measuring machines.* Journal of the International Societies for Precision Engineering and Nanotechnology, 200. **26**: p. 58-68.

[25] Srivastava, A.K., *Modelling Geometric and Thermal Errors in a Five- Axis CNC Machine Tool.* Journal of Machine Tools Manufacturing 1995. **35**: p. 1321-1337.

[26] Valdes, R.A, *Synthesization of Thermally Induced Errors in Coordinate Measuring Machines.* Journal of the Brazil Society of Mechanical Science and Engineering, 2005. **27**: p. 172-175.

[27] Meng, Z., *The Direct-Error-Compensation method of measuring the error of a six -freedom-degree parallel mechanism CMM*. Journal of Materials Processing Technology, 2002. **129**: p. 574-578.

[28] Barakat, N.A., *Kinematic and Geometric Error Compensation of a Coordinate Measuring Machine* International Journal of Machine Tools and Manufacture 1999. **40**: p. 833-850.

[29] ISO 15530-2. Geometric Product Specifications (GPS) Coordinate Measuring Machines (CMMs): Techniques for evaluation of the uncertainty of measurements. Geneva: International Organization for Standardization (ISO), 2001.

[30] Manthey, D., *General Least Squares- Direct Solution and Bundle Adjustments*. 2005.

[31] Spath, H., *Least-Square Fitting with Spheres*. Journal of Optimization Theory and Application, 1998. **96**: p. 191-199.

[32] Cheraghi S. H., *Straightness and flatness tolerance evaluation: an optimization approach*. Elsevier.

[33] Çelebioğlu, H.E., *Developing a Computer Program for Evaluating Uncertainty of Some Typical Dimensional Measuring and Gauging Devices*, in *The Graduate School of Natural and Applied Science*. 2005, Middle East Technical University: Ankara. p. 128.

[34] Takamasu, K. (2002). International Standard Development of Virtual CMM (Coordinate Measuring Machine). Tokyo, NEDO International Joint Research Project.

[35] Feng, C.-X. (2004). "Design and analysis of experiments in CMM measurement uncertainty study." Precision Engineering **11**.

[36] Piratelli-Filho, A. (2003). "CMM uncertainty analysis with factorial design." Precision Engineering **27**: 283-288

[37] Cranfield Precision, High Precision Machine Tools [Online]. Available from: http://cranfieldprecision.com/precision-linear-drive.php [Accessed 29 April 2007]

[38] Heidenhain, Techinical Information [Online]. Available from: http://www.heidenhain.com/?/ca2238_177,Fundamentals778/ca778_177,Technical_Information-2498.html [Accessed 29 April 2007]

VOLUMETRIC ERROR MATRICES OF KINEMATIC MODEL

Table A1: Error Matrix at Z= -50 mm

	50	100	150	200	250	300	350	400	450	500	550	600	650	700	750	800	850
50	1,864	1,8673	1,8709	1,8745	1,8784	1,8824	1,8865	1,8908	1,8953	1,8999	1,9046	1,9095	1,9146	1,9198	1,9251	1,9306	1,9361
100	1,9418	1,9477	1,9538	1,8719	1,8751	1,8784	1,8818	1,8854	1,8892	1,8931	1,8971	1,9013	1,9057	1,9102	1,9149	1,9197	1,9247
150	1,9297	1,935	1,9403	1,9458	1,9515	1,9573	1,8802	1,8831	1,8861	1,8893	1,8927	1,8962	1,8999	1,9037	1,9077	1,9118	1,9161
200	1,9205	1,9251	1,9299	1,9347	1,9397	1,9448	1,95	1,9555	1,9611	1,8889	1,8916	1,8944	1,8974	1,9005	1,9038	1,9072	1,9108
250	1,9146	1,9184	1,9225	1,9267	1,931	1,9356	1,9401	1,9449	1,9498	1,9548	1,96	1,9654	1,898	1,9004	1,903	1,9057	1,9086
300	1,9117	1,9149	1,9182	1,9217	1,9254	1,9292	1,9332	1,9373	1,9416	1,9459	1,9505	1,9551	1,9599	1,9649	1,97	1,9073	1,9095
350	1,9119	1,9143	1,917	1,9198	1,9228	1,9259	1,9292	1,9326	1,9362	1,9399	1,9438	1,9479	1,952	1,9563	1,9608	1,9653	1,9701
400	1,975	1,917	1,9189	1,9211	1,9233	1,9257	1,9283	1,9311	1,934	1,937	1,9402	1,9436	1,947	1,9507	1,9545	1,9584	1,9625
450	1,9667	1,971	1,9756	1,9802	1,9271	1,9288	1,9307	1,9328	1,9349	1,9373	1,9398	1,9425	1,9453	1,9482	1,9514	1,9546	1,9581
500	1,9617	1,9653	1,9692	1,9732	1,9772	1,9816	1,986	1,9374	1,939	1,9405	1,9423	1,9443	1,9464	1,9487	1,9511	1,9537	1,9564
550	1,9593	1,9624	1,9656	1,9689	1,9724	1,976	1,9797	1,9836	1,9877	1,9919	1,9482	1,9495	1,9509	1,9525	1,9542	1,9561	1,9581
600	1,9604	1,9627	1,9652	1,9679	1,9707	1,9736	1,9768	1,98	1,9834	1,9869	1,9905	1,9944	1,9984	1,9593	1,9604	1,9616	1,9629
650	1,9644	1,9661	1,9679	1,9699	1,972	1,9743	1,9768	1,9793	1,9821	1,985	1,988	1,9912	1,9945	1,9979	2,0015	2,0053	1,9707
700	1,9716	1,9726	1,9737	1,975	1,9765	1,9781	1,9798	1,9817	1,9838	1,986	1,9884	1,9909	1,9936	1,9963	1,9993	2,0024	2,0056
750	2,009	2,0125	1,9825	1,9831	1,9839	1,9848	1,9859	1,9871	1,9885	1,99	1,9917	1,9935	1,9956	1,9977	2	2,0025	2,005
800	2,0077	2,0106	2,0136	2,0168	2,0201	1,9946	1,995	1,9956	1,9963	1,9971	1,9982	1,9993	2,0006	2,0021	2,0037	2,0055	2,0074
850	2,0095	2,0117	2,0141	2,0166	2,0192	2,0219	2,0249	2,028	2,0071	2,0073	2,0076	2,0081	2,0087	2,0096	2,0105	2,0116	2,0128
900	2,0142	2,0158	2,0175	2,0193	2,0214	2,0235	2,0258	2,0282	2,0307	2,0335	2,0363	2,0198	2,0197	2,0199	2,0201	2,0205	2,0212
950	2,0219	2,0228	2,0238	2,025	2,0263	2,0278	2,0294	2,0312	2,0331	2,0352	2,0374	2,0397	2,0422	2,0448	2,0326	2,0323	2,0323
1000	2,0323	2,0325	2,0329	2,0334	2,0341	2,0349	2,0358	2,037	2,0382	2,0397	2,0412	2,0429	2,0448	2,0467	2,0488	2,0511	2,0536

Table A2: Error Matrix at Z= -100 mm

	50	100	150	200	250	300	350	400	450	500	550	600	650	700	750	800	850
50	1,8217	1,8245	1,8274	1,8305	1,8338	1,8372	1,8408	1,8445	1,8484	1,8525	1,8567	1,861	1,8656	1,8703	1,875	1,88	1,8851
100	1,8903	1,8957	1,9012	1,8306	1,8331	1,8358	1,8386	1,8417	1,8449	1,8482	1,8517	1,8553	1,8591	1,8631	1,8672	1,8715	1,876
150	1,8805	1,8852	1,8901	1,895	1,9002	1,9055	1,8397	1,842	1,8445	1,8471	1,8498	1,8528	1,8559	1,8592	1,8626	1,8661	1,8699
200	1,8737	1,8778	1,882	1,8863	1,8907	1,8953	1,9001	1,905	1,9101	1,8494	1,8514	1,8536	1,856	1,8585	1,8612	1,8641	1,8671
250	1,8703	1,8736	1,8771	1,8807	1,8845	1,8885	1,8926	1,8968	1,9012	1,9056	1,9104	1,9152	1,8593	1,8611	1,8631	1,8652	1,8675
300	1,87	1,8726	1,8754	1,8783	1,8814	1,8847	1,888	1,8916	1,8954	1,8992	1,9032	1,9073	1,9116	1,9161	1,9207	1,8695	1,8711
350	1,8729	1,8747	1,8768	1,879	1,8814	1,884	1,8867	1,8895	1,8925	1,8957	1,899	1,9025	1,9061	1,9099	1,9138	1,9178	1,922
400	1,9264	1,8801	1,8814	1,883	1,8846	1,8864	1,8884	1,8906	1,8929	1,8953	1,8979	1,9007	1,9036	1,9067	1,91	1,9133	1,9169
450	1,9205	1,9243	1,9283	1,9325	1,8911	1,8922	1,8935	1,8949	1,8965	1,8983	1,9002	1,9023	1,9045	1,9068	1,9094	1,9121	1,9149
500	1,918	1,9211	1,9244	1,9278	1,9314	1,9352	1,9391	1,9023	1,9031	1,9042	1,9054	1,9067	1,9083	1,9099	1,9118	1,9138	1,9159
550	1,9182	1,9207	1,9233	1,9261	1,929	1,932	1,9352	1,9386	1,9421	1,9458	1,9139	1,9146	1,9154	1,9164	1,9175	1,9188	1,9202
600	1,9219	1,9236	1,9255	1,9276	1,9298	1,9322	1,9348	1,9374	1,9403	1,9432	1,9463	1,9496	1,9531	1,9259	1,9264	1,927	1,9277
650	1,9286	1,9297	1,9309	1,9323	1,9338	1,9355	1,9374	1,9394	1,9415	1,9439	1,9463	1,9489	1,9516	1,9545	1,9576	1,9608	1,9382
700	1,9384	1,9388	1,9393	1,94	1,9409	1,9419	1,9431	1,9444	1,9458	1,9475	1,9492	1,9512	1,9533	1,9555	1,9579	1,9604	1,963
750	1,9659	1,9689	1,9508	1,9508	1,951	1,9513	1,9517	1,9524	1,9532	1,9541	1,9552	1,9564	1,9579	1,9594	1,9611	1,963	1,965
800	1,9672	1,9694	1,9718	1,9745	1,9772	1,9638	1,9636	1,9636	1,9636	1,9639	1,9643	1,9648	1,9656	1,9664	1,9674	1,9687	1,97
850	1,9715	1,9731	1,9749	1,9768	1,9789	1,981	1,9835	1,986	1,9771	1,9767	1,9765	1,9763	1,9763	1,9766	1,9769	1,9774	1,978
900	1,9788	1,9798	1,9809	1,9822	1,9836	1,9851	1,9869	1,9887	1,9906	1,9928	1,9952	1,9906	1,99	1,9895	1,9892	1,989	1,989
950	1,9891	1,9894	1,9898	1,9904	1,9912	1,992	1,9931	1,9943	1,9956	1,9971	1,9987	2,0004	2,0024	2,0045	2,0043	2,0035	2,0028
1000	2,0022	2,0018	2,0016	2,0015	2,0016	2,0018	2,0021	2,0027	2,0033	2,0042	2,0052	2,0063	2,0075	2,0089	2,0104	2,0122	2,014

Table A3: Error Matrix at Z= -300 mm

	50	100	150	200	250	300	350	400	450	500	550	600	650	700	750	800	850
50	1,6776	1,6778	1,6781	1,6786	1,6792	1,6801	1,6811	1,6823	1,6837	1,6853	1,687	1,6889	1,6911	1,6934	1,6958	1,6984	1,7012
100	1,7041	1,7073	1,7106	1,6903	1,6902	1,6903	1,6905	1,6909	1,6915	1,6923	1,6933	1,6944	1,6957	1,6972	1,6988	1,7007	1,7027
150	1,7049	1,7072	1,7097	1,7124	1,7153	1,7184	1,7033	1,703	1,7028	1,7028	1,7029	1,7033	1,7038	1,7045	1,7054	1,7064	1,7077
200	1,709	1,7106	1,7124	1,7143	1,7164	1,7187	1,7211	1,7237	1,7265	1,7168	1,7162	1,7157	1,7155	1,7154	1,7155	1,7158	1,7162
250	1,7168	1,7176	1,7186	1,7198	1,7211	1,7226	1,7243	1,7261	1,7281	1,7302	1,7326	1,7352	1,7305	1,7296	1,7289	1,7284	1,7281
300	1,728	1,728	1,7282	1,7286	1,7291	1,7299	1,7308	1,7319	1,7332	1,7345	1,7361	1,7379	1,7398	1,7419	1,7442	1,7445	1,7434
350	1,7425	1,7417	1,7412	1,7408	1,7406	1,7405	1,7407	1,741	1,7415	1,7421	1,743	1,744	1,7451	1,7465	1,7479	1,7496	1,7515
400	1,7535	1,7588	1,7575	1,7563	1,7553	1,7545	1,7539	1,7534	1,7532	1,7531	1,7531	1,7534	1,7537	1,7543	1,7551	1,756	1,7571
450	1,7583	1,7597	1,7614	1,7631	1,7734	1,7719	1,7705	1,7693	1,7683	1,7674	1,7667	1,7662	1,7659	1,7657	1,7657	1,7658	1,7662
500	1,7667	1,7674	1,7682	1,7692	1,7703	1,7717	1,7733	1,7883	1,7865	1,7849	1,7835	1,7822	1,7811	1,7802	1,7795	1,7789	1,7784
550	1,7782	1,7781	1,7782	1,7785	1,7789	1,7795	1,7803	1,7812	1,7823	1,7836	1,8036	1,8016	1,7998	1,7981	1,7966	1,7953	1,7942
600	1,7932	1,7924	1,7917	1,7913	1,7909	1,7908	1,7909	1,791	1,7914	1,7919	1,7925	1,7934	1,7945	1,8192	1,817	1,8149	1,813
650	1,8113	1,8098	1,8084	1,8072	1,8062	1,8053	1,8046	1,8041	1,8037	1,8035	1,8035	1,8036	1,8039	1,8043	1,8049	1,8057	1,835
700	1,8326	1,8304	1,8283	1,8263	1,8246	1,823	1,8216	1,8203	1,8192	1,8183	1,8175	1,8169	1,8165	1,8162	1,8161	1,8162	1,8163
750	1,8168	1,8173	1,8511	1,8485	1,8461	1,8438	1,8416	1,8397	1,8379	1,8362	1,8347	1,8334	1,8323	1,8313	1,8305	1,8298	1,8293
800	1,829	1,8288	1,8287	1,8289	1,8293	1,8676	1,8648	1,8622	1,8596	1,8573	1,8551	1,8531	1,8512	1,8495	1,848	1,8466	1,8454
850	1,8444	1,8435	1,8428	1,8422	1,8418	1,8415	1,8415	1,8416	1,8844	1,8814	1,8785	1,8758	1,8732	1,8709	1,8686	1,8666	1,8646
900	1,8629	1,8613	1,8599	1,8586	1,8575	1,8566	1,8558	1,8551	1,8546	1,8544	1,8542	1,9013	1,8981	1,895	1,8921	1,8893	1,8868
950	1,8843	1,882	1,8799	1,8779	1,8762	1,8745	1,873	1,8717	1,8705	1,8695	1,8686	1,8679	1,8674	1,8671	1,9183	1,9149	1,9117
1000	1,9085	1,9056	1,9028	1,9001	1,8977	1,8953	1,8932	1,8912	1,8893	1,8876	1,8861	1,8847	1,8835	1,8824	1,8814	1,8807	1,8801

Table A4: Error Matrix at Z= -550 mm

	50	100	150	200	250	300	350	400	450	500	550	600	650	700	750	800	850
50	1,5641	1,5604	1,5568	1,5535	1,5503	1,5473	1,5446	1,542	1,5396	1,5373	1,5354	1,5335	1,5319	1,5306	1,5293	1,5282	1,5274
100	1,5267	1,5263	1,5261	1,5818	1,5779	1,5741	1,5705	1,5671	1,5639	1,5609	1,558	1,5554	1,5529	1,5507	1,5486	1,5468	1,5451
150	1,5436	1,5423	1,5412	1,5402	1,5396	1,539	1,5998	1,5956	1,5916	1,5878	1,5842	1,5808	1,5775	1,5744	1,5716	1,5688	1,5664
200	1,564	1,5619	1,56	1,5582	1,5567	1,5553	1,5541	1,5532	1,5524	1,6181	1,6138	1,6096	1,6055	1,6017	1,598	1,5945	1,5912
250	1,5881	1,5851	1,5824	1,5799	1,5775	1,5754	1,5733	1,5715	1,5699	1,5684	1,5672	1,5662	1,6366	1,632	1,6276	1,6234	1,6193
300	1,6154	1,6117	1,6082	1,6049	1,6016	1,5987	1,5959	1,5933	1,5909	1,5886	1,5866	1,5847	1,583	1,5815	1,5802	1,6554	1,6506
350	1,646	1,6415	1,6372	1,6331	1,6292	1,6255	1,6219	1,6185	1,6153	1,6123	1,6094	1,6068	1,6043	1,602	1,5998	1,5979	1,5962
400	1,5946	1,6744	1,6694	1,6646	1,6599	1,6554	1,6511	1,647	1,643	1,6392	1,6355	1,6321	1,6289	1,6258	1,6229	1,6202	1,6176
450	1,6153	1,6131	1,6111	1,6093	1,6937	1,6885	1,6834	1,6786	1,6739	1,6694	1,665	1,6608	1,6568	1,653	1,6493	1,6458	1,6426
500	1,6395	1,6365	1,6337	1,6311	1,6286	1,6265	1,6244	1,713	1,7077	1,7025	1,6974	1,6925	1,6878	1,6832	1,6788	1,6746	1,6705
550	1,6667	1,663	1,6595	1,6562	1,6529	1,6499	1,6471	1,6444	1,642	1,6397	1,7328	1,7273	1,7219	1,7166	1,7115	1,7066	1,7019
600	1,6973	1,6928	1,6885	1,6845	1,6806	1,6769	1,6733	1,6699	1,6666	1,6636	1,6607	1,658	1,6555	1,7527	1,747	1,7414	1,736
650	1,7307	1,7256	1,7207	1,7159	1,7113	1,7068	1,7025	1,6984	1,6945	1,6907	1,687	1,6836	1,6803	1,6772	1,6743	1,6716	1,7729
700	1,767	1,7612	1,7556	1,7501	1,7449	1,7397	1,7347	1,7299	1,7252	1,7208	1,7165	1,7123	1,7084	1,7045	1,7009	1,6973	1,694
750	1,6909	1,688	1,7932	1,7871	1,7812	1,7754	1,7698	1,7643	1,759	1,7538	1,7488	1,744	1,7393	1,7348	1,7305	1,7263	1,7222
800	1,7184	1,7146	1,7111	1,7078	1,7046	1,8138	1,8076	1,8015	1,7955	1,7897	1,7841	1,7786	1,7733	1,7681	1,763	1,7582	1,7535
850	1,7489	1,7446	1,7403	1,7362	1,7323	1,7286	1,725	1,7216	1,8347	1,8282	1,822	1,8159	1,8099	1,8041	1,7984	1,7929	1,7875
900	1,7823	1,7773	1,7723	1,7676	1,7631	1,7586	1,7543	1,7502	1,7462	1,7425	1,7389	1,8555	1,849	1,8426	1,8363	1,8301	1,8242
950	1,8183	1,8126	1,8071	1,8016	1,7964	1,7913	1,7864	1,7817	1,777	1,7726	1,7682	1,7641	1,7601	1,7563	1,8765	1,8698	1,8632
1000	1,8568	1,8505	1,8443	1,8383	1,8324	1,8267	1,8211	1,8158	1,8105	1,8054	1,8005	1,7956	1,791	1,7864	1,7821	1,7779	1,7739

APPENDIX B

VOLUMETRIC ERROR MATRICES OF KINEMATIC MODEL BY USING LASER ERROR DATA

Table B1: Error Matrix at Z= -50 mm

	50	100	150	200	250	300	350	400	450	500	550	600	650	700	750	800	850
50	1,9272	1,9303	1,9334	1,9373	1,9415	1,9443	1,9495	1,9526	1,9562	1,9593	1,9638	1,9699	1,9742	1,9762	1,9816	1,9859	1,9912
100	1,9987	2,0033	2,0075	1,8983	1,9014	1,9046	1,9086	1,9128	1,9157	1,921	1,924	1,9277	1,9308	1,9354	1,9416	1,9459	1,9479
150	1,9534	1,9578	1,9631	1,9707	1,9753	1,9796	1,8733	1,8765	1,8797	1,8837	1,888	1,8909	1,8963	1,8994	1,9031	1,9063	1,911
200	1,9171	1,9216	1,9236	1,9292	1,9336	1,9389	1,9466	1,9513	1,9557	1,8469	1,8501	1,8534	1,8575	1,8618	1,8647	1,8701	1,8732
250	1,877	1,8802	1,8849	1,8911	1,8956	1,8977	1,9032	1,9077	1,9131	1,9208	1,9255	1,9299	1,8179	1,8211	1,8244	1,8285	1,8328
300	1,8358	1,8412	1,8443	1,8481	1,8513	1,8561	1,8623	1,8668	1,8689	1,8745	1,879	1,8844	1,8921	1,8968	1,9013	1,7943	1,7976
350	1,8009	1,805	1,8094	1,8124	1,8179	1,8211	1,8249	1,8282	1,833	1,8393	1,8438	1,846	1,8516	1,8561	1,8616	1,8694	1,8742
400	1,8787	1,7698	1,7732	1,7766	1,7808	1,7852	1,7883	1,7938	1,7971	1,8009	1,8043	1,8092	1,8155	1,8201	1,8224	1,8281	1,8327
450	1,8382	1,8461	1,851	1,8555	1,7431	1,7464	1,7499	1,7541	1,7585	1,7616	1,7672	1,7705	1,7744	1,7778	1,7827	1,7891	1,7937
500	1,796	1,8017	1,8063	1,8119	1,8198	1,8247	1,8293	1,7174	1,7208	1,7244	1,7286	1,7332	1,7364	1,742	1,7454	1,7494	1,7529
550	1,7578	1,7643	1,7691	1,7714	1,7773	1,782	1,7877	1,7956	1,8006	1,8054	1,6947	1,6982	1,7017	1,706	1,7106	1,7138	1,7195
600	1,7229	1,7269	1,7304	1,7354	1,7419	1,7467	1,749	1,7549	1,7596	1,7653	1,7733	1,7783	1,7831	1,6703	1,6737	1,6772	1,6815
650	1,6861	1,6893	1,6949	1,6983	1,7023	1,7058	1,7108	1,7172	1,722	1,7243	1,7302	1,7349	1,7405	1,7485	1,7534	1,7581	1,6457
700	1,6491	1,6527	1,657	1,6616	1,6648	1,6705	1,6739	1,6779	1,6814	1,6864	1,6929	1,6977	1,7	1,7059	1,7106	1,7163	1,7242
750	1,7292	1,734	1,6213	1,6248	1,6284	1,6327	1,6373	1,6406	1,6463	1,6497	1,6537	1,6573	1,6623	1,6688	1,6736	1,676	1,6818
800	1,6866	1,6923	1,7002	1,7053	1,71	1,6	1,6036	1,6072	1,6116	1,6162	1,6195	1,6253	1,6288	1,6329	1,6364	1,6415	1,6481
850	1,6529	1,6554	1,6613	1,6661	1,6718	1,6798	1,6849	1,6897	1,5762	1,5798	1,5834	1,5879	1,5925	1,5959	1,6016	1,6052	1,6093
900	1,6129	1,618	1,6246	1,6294	1,6319	1,6378	1,6427	1,6484	1,6565	1,6616	1,6664	1,5503	1,554	1,5577	1,5623	1,567	1,5704
950	1,5763	1,58	1,5841	1,5879	1,5931	1,5998	1,6047	1,6073	1,6133	1,6183	1,6241	1,6323	1,6375	1,6424	1,5249	1,5286	1,5325
1000	1,5371	1,542	1,5455	1,5515	1,5553	1,5595	1,5634	1,5687	1,5755	1,5806	1,5833	1,5895	1,5945	1,6005	1,6088	1,6142	1,6192

Table B2: Error Matrix at Z= -300 mm

	50	100	150	200	250	300	350	400	450	500	550	600	650	700	750	800	850
50	1,9224	1,9257	1,9291	1,933	1,9372	1,9404	1,9452	1,9488	1,9525	1,9558	1,9605	1,9667	1,971	1,9731	1,9789	1,9832	1,9885
100	1,9956	2,0004	2,0048	1,8935	1,8969	1,9003	1,9043	1,9085	1,9117	1,9166	1,9203	1,9239	1,9273	1,932	1,9383	1,9427	1,9448
150	1,9506	1,955	1,9604	1,9675	1,9724	1,9768	1,8683	1,8717	1,8752	1,8792	1,8835	1,8868	1,8917	1,8954	1,8992	1,9026	1,9074
200	1,9137	1,9181	1,9203	1,9262	1,9306	1,9361	1,9433	1,9482	1,9527	1,8419	1,8454	1,8489	1,8529	1,8572	1,8605	1,8655	1,8693
250	1,873	1,8765	1,8813	1,8877	1,8921	1,8943	1,9003	1,9047	1,9102	1,9174	1,9224	1,927	1,8137	1,8171	1,8207	1,8247	1,8291
300	1,8324	1,8374	1,8412	1,845	1,8484	1,8533	1,8596	1,8641	1,8664	1,8723	1,8768	1,8823	1,8895	1,8945	1,8991	1,7901	1,7936
350	1,7972	1,8013	1,8057	1,8091	1,8141	1,818	1,8218	1,8253	1,8302	1,8366	1,8412	1,8435	1,8495	1,854	1,8596	1,8669	1,8719
400	1,8765	1,7657	1,7693	1,773	1,7772	1,7816	1,785	1,7902	1,7941	1,7979	1,8015	1,8065	1,813	1,8176	1,82	1,8261	1,8307
450	1,8363	1,8437	1,8488	1,8535	1,7396	1,7432	1,7469	1,7511	1,7555	1,759	1,7642	1,7681	1,772	1,7756	1,7806	1,7871	1,7918
500	1,7942	1,8003	1,8049	1,8106	1,8179	1,8231	1,8278	1,7133	1,717	1,7207	1,725	1,7295	1,7331	1,7383	1,7424	1,7464	1,7501
550	1,7552	1,7618	1,7665	1,769	1,7752	1,7799	1,7857	1,7932	1,7984	1,8033	1,6907	1,6944	1,6982	1,7025	1,7071	1,7106	1,7159
600	1,72	1,724	1,7277	1,7328	1,7394	1,7442	1,7467	1,7529	1,7577	1,7635	1,771	1,7762	1,7811	1,6672	1,6709	1,6746	1,6789
650	1,6835	1,687	1,6923	1,6963	1,7003	1,704	1,7091	1,7157	1,7204	1,7229	1,7291	1,7338	1,7396	1,747	1,7522	1,7571	1,6431
700	1,6468	1,6506	1,6549	1,6595	1,663	1,6683	1,6724	1,6764	1,6801	1,6852	1,6919	1,6966	1,6991	1,7053	1,71	1,7158	1,7233
750	1,7285	1,7334	1,6192	1,6229	1,6267	1,631	1,6356	1,6392	1,6445	1,6486	1,6526	1,6564	1,6615	1,6682	1,6729	1,6754	1,6817
800	1,6864	1,6922	1,6997	1,705	1,7098	1,5975	1,6012	1,6051	1,6095	1,6141	1,6178	1,6232	1,6273	1,6313	1,6351	1,6403	1,647
850	1,6518	1,6544	1,6607	1,6655	1,6713	1,6788	1,6842	1,6891	1,5741	1,5779	1,5818	1,5862	1,5909	1,5946	1,6	1,6041	1,6082
900	1,612	1,6172	1,624	1,6288	1,6314	1,6377	1,6425	1,6484	1,6559	1,6612	1,6662	1,5479	1,5518	1,5557	1,5602	1,565	1,5688
950	1,5743	1,5785	1,5827	1,5866	1,5919	1,5988	1,6037	1,6064	1,6128	1,6177	1,6237	1,6313	1,6368	1,6418	1,5218	1,5257	1,5298
1000	1,5344	1,5393	1,5432	1,5488	1,5532	1,5574	1,5615	1,5669	1,5739	1,579	1,5818	1,5883	1,5934	1,5995	1,6073	1,6128	1,618

Table B3: Error Matrix at Z= -400 mm

	50	100	150	200	250	300	350	400	450	500	550	600	650	700	750	800	850
50	1,9187	1,9222	1,9258	1,9297	1,9339	1,9373	1,9419	1,946	1,9496	1,9531	1,9579	1,9642	1,9685	1,9706	1,9767	1,981	1,9864
100	1,9932	1,9981	2,0026	1,8898	1,8933	1,897	1,9009	1,9051	1,9086	1,9132	1,9174	1,921	1,9246	1,9294	1,9357	1,9401	1,9423
150	1,9485	1,9528	1,9583	1,965	1,9701	1,9746	1,8644	1,8681	1,8717	1,8757	1,88	1,8836	1,8882	1,8924	1,8961	1,8997	1,9046
200	1,911	1,9154	1,9177	1,9239	1,9283	1,9339	1,9407	1,9458	1,9504	1,8381	1,8417	1,8454	1,8494	1,8537	1,8573	1,862	1,8663
250	1,87	1,8736	1,8786	1,885	1,8895	1,8918	1,898	1,9024	1,908	1,9149	1,92	1,9246	1,8104	1,8141	1,8178	1,8219	1,8262
300	1,8298	1,8345	1,8388	1,8425	1,8462	1,8511	1,8576	1,8621	1,8644	1,8706	1,8751	1,8807	1,8876	1,8927	1,8974	1,7869	1,7906
350	1,7943	1,7985	1,8028	1,8065	1,8113	1,8156	1,8194	1,8231	1,8281	1,8346	1,8391	1,8415	1,8478	1,8523	1,858	1,8649	1,8701
400	1,8749	1,7626	1,7664	1,7702	1,7744	1,7788	1,7825	1,7874	1,7917	1,7956	1,7994	1,8045	1,811	1,8156	1,8181	1,8245	1,8291
450	1,8348	1,8418	1,8471	1,8519	1,7369	1,7407	1,7446	1,7488	1,7532	1,757	1,7618	1,7662	1,7701	1,7739	1,779	1,7856	1,7902
500	1,7927	1,7991	1,8037	1,8095	1,8165	1,8218	1,8266	1,7101	1,714	1,7179	1,7222	1,7267	1,7306	1,7355	1,74	1,744	1,7479
550	1,7531	1,7598	1,7645	1,7671	1,7736	1,7783	1,7842	1,7913	1,7967	1,8016	1,6877	1,6915	1,6955	1,6998	1,7043	1,7082	1,7132
600	1,7177	1,7217	1,7256	1,7308	1,7375	1,7423	1,7449	1,7514	1,7561	1,762	1,7691	1,7746	1,7795	1,6648	1,6687	1,6726	1,6769
650	1,6814	1,6853	1,6902	1,6947	1,6987	1,7026	1,7078	1,7145	1,7192	1,7217	1,7282	1,7329	1,7388	1,7458	1,7512	1,7561	1,6411
700	1,645	1,6489	1,6532	1,6578	1,6617	1,6667	1,6712	1,6752	1,6791	1,6843	1,691	1,6957	1,6983	1,7048	1,7095	1,7154	1,7225
750	1,7279	1,7328	1,6175	1,6214	1,6254	1,6297	1,6343	1,6381	1,6432	1,6477	1,6517	1,6557	1,6609	1,6676	1,6724	1,675	1,6815
800	1,6862	1,6921	1,6992	1,7046	1,7096	1,5955	1,5994	1,6035	1,6078	1,6125	1,6164	1,6215	1,6261	1,6301	1,6341	1,6394	1,6462
850	1,651	1,6536	1,6602	1,6649	1,6709	1,678	1,6835	1,6885	1,5725	1,5765	1,5805	1,5849	1,5896	1,5935	1,5986	1,6033	1,6073
900	1,6113	1,6166	1,6234	1,6282	1,6309	1,6375	1,6423	1,6482	1,6554	1,6609	1,6659	1,546	1,55	1,5542	1,5587	1,5634	1,5674
950	1,5727	1,5774	1,5815	1,5856	1,591	1,598	1,6029	1,6056	1,6123	1,6172	1,6233	1,6305	1,6362	1,6413	1,5194	1,5235	1,5278
1000	1,5324	1,5372	1,5414	1,5467	1,5515	1,5558	1,56	1,5656	1,5726	1,5777	1,5806	1,5874	1,5924	1,5986	1,606	1,6118	1,617

Table B4: Error Matrix at Z= -550 mm

	50	100	150	200	250	300	350	400	450	500	550	600	650	700	750	800	850
50	1,9149	1,9186	1,9223	1,9262	1,9304	1,9341	1,9384	1,9429	1,9466	1,9502	1,9551	1,9615	1,9658	1,968	1,9744	1,9787	1,9842
100	1,9905	1,9957	2,0003	1,8859	1,8897	1,8935	1,8974	1,9016	1,9054	1,9097	1,9143	1,918	1,9217	1,9266	1,933	1,9374	1,9397
150	1,9461	1,9504	1,956	1,9624	1,9676	1,9723	1,8605	1,8642	1,8681	1,8721	1,8764	1,8802	1,8846	1,8892	1,8929	1,8967	1,9017
200	1,9082	1,9126	1,915	1,9214	1,9258	1,9315	1,9379	1,9432	1,9479	1,8341	1,8379	1,8418	1,8458	1,8501	1,854	1,8584	1,8631
250	1,8668	1,8706	1,8756	1,8821	1,8866	1,889	1,8955	1,8999	1,9056	1,9121	1,9174	1,9222	1,807	1,8109	1,8148	1,8188	1,8231
300	1,827	1,8315	1,8362	1,8399	1,8438	1,8488	1,8553	1,8598	1,8622	1,8687	1,8732	1,8789	1,8854	1,8907	1,8955	1,7835	1,7874
350	1,7913	1,7954	1,7998	1,8037	1,8082	1,813	1,8168	1,8207	1,8258	1,8324	1,8369	1,8394	1,846	1,8505	1,8562	1,8628	1,8682
400	1,873	1,7593	1,7633	1,7673	1,7714	1,7759	1,7799	1,7844	1,7893	1,7931	1,7971	1,8022	1,8089	1,8135	1,816	1,8227	1,8273
450	1,8331	1,8397	1,8452	1,8501	1,7341	1,7381	1,7421	1,7463	1,7507	1,7547	1,7593	1,7642	1,7681	1,7721	1,7772	1,7839	1,7885
500	1,7911	1,7978	1,8024	1,8082	1,8149	1,8204	1,8253	1,7068	1,7109	1,715	1,7192	1,7238	1,7279	1,7326	1,7375	1,7415	1,7456
550	1,7508	1,7576	1,7623	1,765	1,7718	1,7765	1,7824	1,7892	1,7948	1,7998	1,6844	1,6885	1,6926	1,6969	1,7015	1,7056	1,7103
600	1,7152	1,7192	1,7233	1,7286	1,7354	1,7402	1,7428	1,7496	1,7543	1,7603	1,7671	1,7727	1,7777	1,6623	1,6663	1,6704	1,6747
650	1,6792	1,6833	1,688	1,693	1,6969	1,701	1,7063	1,713	1,7178	1,7204	1,7271	1,7318	1,7378	1,7445	1,7501	1,7551	1,6389
700	1,643	1,6471	1,6514	1,656	1,6601	1,6648	1,6698	1,6738	1,6779	1,6831	1,69	1,6947	1,6974	1,7041	1,7088	1,7148	1,7215
750	1,7271	1,7321	1,6156	1,6197	1,6239	1,6282	1,6328	1,6369	1,6416	1,6466	1,6506	1,6547	1,6601	1,6669	1,6716	1,6743	1,6811
800	1,6858	1,6918	1,6985	1,7041	1,7091	1,5933	1,5975	1,6017	1,606	1,6107	1,6148	1,6196	1,6247	1,6287	1,6329	1,6382	1,6451
850	1,6499	1,6526	1,6595	1,6642	1,6703	1,677	1,6827	1,6878	1,5707	1,5749	1,5791	1,5835	1,5881	1,5923	1,5971	1,6022	1,6063
900	1,6105	1,6158	1,6227	1,6275	1,6303	1,6371	1,6419	1,6479	1,6547	1,6604	1,6655	1,5439	1,5481	1,5525	1,5569	1,5617	1,566
950	1,5709	1,576	1,5802	1,5845	1,5899	1,597	1,6018	1,6047	1,6116	1,6165	1,6227	1,6296	1,6354	1,6406	1,5168	1,5211	1,5256
1000	1,5301	1,535	1,5394	1,5445	1,5497	1,554	1,5584	1,564	1,5712	1,5762	1,5792	1,5862	1,5913	1,5976	1,6046	1,6105	1,6158

FLATNESS DATA POINT

Table C1: Flatness Data Point

Example 1			Example 2			Example 3		
X	*Y*	Z	*X*	*Y*	Z	*X*	*Y*	Z
-2	1	5	0,2	0,2	-0,0645	0,3846	0,2416	-0,0828
-1	1	4	0,2	0,4	-0,06438	1,5008	0,2922	-0,0821
0	1	1	0,2	0,6	0,008761	2,3107	0,3289	-0,0787
1	1	2	0,2	0,8	-0,01117	2,9817	0,3593	-0,0789
2	1	2	0,2	1	-0,06237	3,6964	0,3917	-0,076
-2	0	4	0,4	0,2	-0,03829	3,6743	0,8794	-0,0785
-1	0	3	0,4	0,4	0,0655	3,1195	0,8543	-0,0735
0	0	3	0,4	0,6	0,06357	2,3552	0,8196	-0,0745
1	0	2	0,4	0,8	0,02849	1,5875	0,7849	-0,0714
2	0	2	0,4	1	-0,006113	0,5573	0,7382	-0,074
-2	-1	3	0,6	0,2	-0,09525	0,5413	1,0921	-0,073
-1	-1	4	0,6	0,4	-0,01154	1,22205	1,1229	-0,0727
0	-1	2	0,6	0,6	-0,02406	2,1673	1,1658	-0,0716
1	-1	1	0,6	0,8	0,03515	3,0881	1,2076	-0,0749
2	-1	2	0,6	1	-0,01997	3,8459	1,2419	-0,0799
			0,8	0,2	0,054	3,8305	1,5796	-0,0848
			0,8	0,4	-0,01324	3,2057	1,5514	-0,041
			0,8	0,6	-0,02225	2,423	1,5159	-0,0759
			0,8	0,8	0,0771	1,671	1,4819	-0,0746
			0,8	1	-0,0003596	0,5263	1,43	-0,0745
			1	0,2	0,05773			
			1	0,4	-0,0562			
			1	0,6	0,09206			
			1	0,8	0,06536			
			1	1	-0,02121			

MATLAB FUNCTION OF KINEMATIC ERROR MODELLING

----
function [S1, J1, T1, S2, J2, T2, S3, J3, T3, Tactual, T_ideal,Error_Place, VolError, ErrorX, ErrorY, ErrorZ] = ...
      Models_Differences_Vol3den (T, Alfa1, Beta1, Theta1, a1, b1, c1, TEC1, del_a1, del_b1, del_c1, Alfa2, Beta2, Theta2, a2, b2, c2, TEC2, del_a2, del_b2, del_c2, Alfa3, Beta3, Theta3, a3, b3, c3, TEC3, del_a3, del_b3, del_c3)
% 'INPUTS
% 'TEC = Thermal Expansion Coefficient of machine parts
% 'T is homogeneous machine temperature
% 'a,b,c are the length of the links.
% 'del_a,del_b,del_c are the error of the links.
% 'Alfa is the roll error .
% 'Beta is the pitch error.
% 'Theta is the yaw error.
% 'OUTPUTS
% 'S1,S2... are the link error matrices.
% 'J1,J2... are the joint error matrices.
% 'T1,T2... are the axis error matrices.
% 'Tactual is actual coordinate matrix with errors.
% 'T_ideal is ideal coordinate matrix. Error values are assumed zero.
% 'VolError, ErrorX, ErrorY, ErrorZ are error matrices and scalar error values
% of each axis.

Figure 69: Inputs and Outputs of Matlab Modelling Function

APPENDIX E

SPECIFICATIONS OF RENISHAW TP7M PROBE

Table E1: Specifications of Renishaw TP7M Probe

		Sensitivity Level	Value
1	Unidirectional Repeatability		
		Level 1	0,25 µm
		Level 2	0,25 µm
2	3D (XYZ) Pretravel variation		
		Level 1	0,5 µm
		Level 2	1 µm
3	2D (XY) Pretravel variation		
		Level 1	0,25 µm
		Level 2	0,5 µm
4	Typical pretravel before trigger		
		Level 1	2 µm
		Level 2	4 µm
5	Stylus force at trigger		
	Min X,Y Plane		0,02 N
	Max Z Axis		0,15 N
6	Stylus overtravel limit		
	XY axes		$\pm 16^0$
	$\pm$ Zaxis		$\pm$ 5 mm
7	Full overtravel force		
	XY axes		0,49 N
	$\pm$ Zaxis		2,84 N
8	Trigger rate		Max. 3 triggers per second
9	Allowable probing speed range		0.5 to 40 mm/sec (±10%)

APPENDIX F

LINEAR SENSORS OF CMM USED IN THESIS

Table F1: Specifications of Linear Sensors

AXIS	SCALE MODEL	PROPERTIES
X	Heidenhain LS 703	Glass Scale with Diadur Grating Thermal Expansion Coefficient=$11*10^{-6}$ / ^{0}C
Y	Heidenhain LS 707	Glass Scale with Diadur Grating Thermal Expansion Coefficient=$11*10^{-6}$ / ^{0}C
Z	Heidenhain LS 403	Glass Scale with Diadur Grating Thermal Expansion Coefficient=$11*10^{-6}$ / ^{0}C
S	Heidenhain LB 326	Steel Scale with Aurodur Grating Thermal Expansion Coefficient=$10*10^{-6}$ / ^{0}C

APPENDIX G

CALIBRATION CERTIFICATE OF RING GAUGE USED IN THESIS

TÜRKAK
TÜRK AKREDİTASYON KURUMU
TURKISH ACCREDITATION AGENCY
tarafından akredite edilmiş

EGEMET
Kalibrasyon-Ölçüm Tic. Ltd. Şti.
172 Sokak No: 8 Işıkkent – İZMİR
Tel : 0(232) 472 06 04 (Pbx) Fax : 0(232) 472 05 04
E-Mail : info@egemet.com.tr http//www.egemet.com.tr

35001-01
110981
11- 06

Kalibrasyon Sertifikası
Calibration Certificate

Cihazın Sahibi / *Customer name/address*	:	
İstek Numarası / *Order No.*	:	SE064330
Makine/Cihaz / *Instrument/Device*	:	Halka Mastar 2.7430"
İmalatçı / *Manufacturer*	:	Federal
Tip / *Type*	:	Referans Etalon
Seri Numarası / *Serial Number*	:	MG 942 (1427)
Kalibrasyon Tarihi / *Date of Calibration*	:	18.11.2006
Sertifikanın Sayfa Sayısı / *Number of Pages of the Certificate*	:	2

Bu kalibrasyon sertifikası, Uluslararası Birimler Sisteminde (SI) tanımlanmış birimleri realize eden ulusal ölçüm standardlarına izlenebilirliği belgeler.
This calibration certificate documents the traceability to national standards, which realize the unit of measurement according to the International System of Units (SI).
Ölçüm sonuçları, genişletilmiş ölçüm belirsizlikleri ve kalibrasyon metodları bu sertifikanın tamamlayıcı kısmı olan takib eden sayfalarda verilmiştir.
The measurements, the uncertainties with confidence probability and calibration methods are given on the following pages which are part of this certificate.

Mühür / *Seal*	**Tarih** / *Date*	**Kalibrasyonu Yapan** / *Calibrated by*	**Laboratuvar Müdürü** / *Head of Calibration Laboratory*
	20.11.2006	Erbil ACAY	Barbaros CİHANGİR

Bu sertifika, laboratuvarın yazılı izni olmadan kısmen kopyalanıp çoğaltılamaz.
İmzasız ve mühürsüz sertifikalar geçersizdir.
This certificate shall not be reproduced other than in full except with the permission of the Laboratory.
Calibration certificates without signature and seal are not valid.

Figure 70: Calibration Certificate of Ring Gauge Used in Thesis Studies (Page 1)

154

EGEMET
Kalibrasyon-Ölçüm Tic. Ltd. Şti.

35001-01	
110981	
11- 06	

Makine/Cihaz : Halka Mastar 2.7430"
Instrument/Device

Cihazın laboratuvara kabul tarihi : 15.11.2006
Date of receipt of Device

Prosedür : Kalibrasyon işlemi, VDI / VDE / DGQ 2618 Bölüm 4, 4.1 - DIN 7162, 7163, 7168,
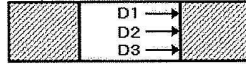*Procedures* DIN 2259 standardına ve T504.111 nolu kalibrasyon talimatına uygun olarak
yapılmıştır.

Ölçüm Şartları :
Measurement Conditions

Ölçümde kullanılan cihazlar	İzlenebilirlikler
Üniversal uzunluk ölçüm makinası, SIP 302 M, No 2501, Sertifika No:2007	UME - PTB - DKD
Referans Halka Etalon No: 42814, Sertifika No:G2BF-0156	UME

Çevre Şartları : Sıcaklık 20.0 °C ±1.0, Nem oranı %50 ±10
Environmental Conditions *Temperature 20.0 °C ±1.0, Humidity %50 ±10*

Ölçüm Sonuçları :
Measurement Results

REFERANS YÜZEYİ

D1 →
D2 →
D3 →

ÇAP (")	
D1 :	2,74299
D2 :	2,74298
D3 :	2,74298

OVALLİK (")
0,00001

Ölçüm Belirsizliği : ± 0,5 E-4 inç
Measurement Uncertainty Beyan edilen genişletilmiş ölçüm belirsizliği, standart belirsizliğin, k=2 olarak
alınan genişletme katsayısı ile çarpımı sonucunda bulunan değerdir ve %95
oranında güvenilirlik sağlamaktadır.
The reported expanded uncertainty of measurement is stated as the standard
uncertainty of measurement multiplied by the coverage factor k=2, which for a
normal distribution corresponds to a coverage probability of approximately 95%.

Fiziksel Kontrol Sonucu : Halka Mastar da herhangi bir hasar ve eksiklik gözlenmemiştir.
Result of Physical Control *There is not any demage on the object that affects function.*

Kalibrasyon Sonucu : Ölçüm sonuçlarına bakınız.
Result of Calibration *See measurement results.*

**Figure 71: Calibration Certificate of Ring Gauge Used in Thesis Studies
(Page 2)**

APPENDIX H

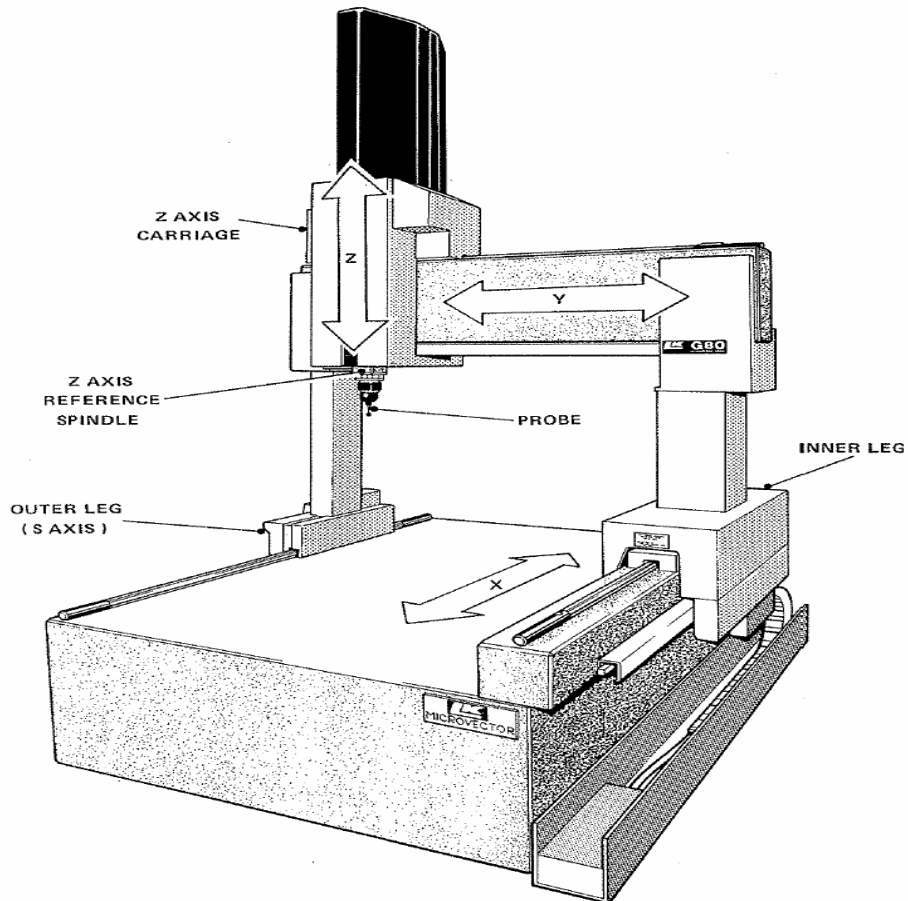## SPECIFICATIONS OF CMM UNDER INSPECTION

Figure 72: The structure of CMM used in this study

The properties of CMM;

    X Axis: 1000 mm

    Y Axis: 900 mm

    Z Axis: 600 mm

    Certificate Accuracy: 1.2μm+ L/400 (L = Distance)

    Probe: Renishaw TP7M Enhanced Performance.